Dark Energy, Anthropic Selection Effects, Entropy and Life

Chas Astro Egan

A thesis submitted for the degree of

Doctor of Philosophy

of The University of New South Wales

UNSW
THE UNIVERSITY OF NEW SOUTH WALES

School of Physics
The University of New South Wales
Sydney NSW
Australia

28th of August, 2009

To Tonga, may your coconuts grow.

Statement of Originality

I hereby declare that this submission is my own work and to the best of my knowledge it contains no materials previously published or written by another person, or substantial proportions of material which have been accepted for the award of any other degree or diploma at UNSW or any other educational institution, except where due acknowledgement is made in the thesis. Any contribution made to the research by others, with whom I have worked at UNSW or elsewhere, is explicitly acknowledged in the thesis. I also declare that the intellectual content of this thesis is the product of my own work, except to the extent that assistance from others in the project's design and conception or in style, presentation and linguistic expression is acknowledged.

(Signed) .....

(Date) .....

CONTENTS

LIST OF FIGURES

LIST OF TABLES

Abstract

According to the standard ΛCDM model, the matter and dark energy densities (ρ_m and ρ_{DE}) are only comparable for a brief time. Using the temporal distribution of terrestrial planets inferred from the cosmic star formation history, we show that the observation $\rho_m \sim \rho_{DE}$ is expected for terrestrial-planet-bound observers under ΛCDM, or under any model of dark energy consistent with observational constraints. Thus we remove the coincidence problem as a factor motivating dark energy models.

We compare the Sun to representative stellar samples in 11 properties plausibly related to life. We find the Sun to be most anomalous in mass and galactic orbital eccentricity. When the 11 properties are considered together we find that the probability of randomly selecting a star more typical than the Sun is only $29 \pm 11\%$. Thus the observed "anomalies" are consistent with statistical noise. This contrasts with previous work suggesting anthropic explanations for the Sun's high mass.

The long-term future of dissipative processes (such as life) depends on the continued availability of free energy to dissipate thereby increasing entropy. The entropy budget of the present observable Universe is dominated by supermassive black holes in galactic cores. Previous estimates of the total entropy in the observable Universe were between $\sim 10^{101}\ k$ and $\sim 10^{103}\ k$. Using recent measurements of the supermassive black hole mass function we find the total entropy in the observable Universe to be $S_{obs} = 3.1^{+3.0}_{-1.7} \times 10^{104}\ k$, at least an order of magnitude higher than previous estimates. We compute the entropy in 3 new subdominant components and report a new entropy budget of the Universe with quantified uncertainties. We evaluate upper bounds on the entropy of a comoving volume (normalized to the present observable Universe). Under the assumption that energy in matter is constant in a comoving volume, the availability of free energy is found to be finite and the future entropy in the volume is limited to a constant of order $10^{123}k$. Through this work we uncover a number of unresolved questions with implications for the ultimate fate of the Universe.

Acknowledgments

I want to thank my unofficial supervisor, Charles Lineweaver, for the years of inspiration and guidance. Charley has an enthusiasm for getting to the bottom of fundamental scientific issues which is not dissuaded by dogma or conventional disciplinary borders.

Secondly, to the Research School of Astronomy and Astrophysics at the Australian National University, thank you for generously hosting me for the majority of my candidature. Mount Stromlo is steeped in academic heritage. It is a wonderful and inspiring place to work. The drive up the mountain is always a delight.

I would like to thank my official supervisor, John Webb and others in the School of Physics at the University of New South Wales for making it possible for me to carry out my candidature remotely.

A warm gracias my most excellent academic brother Jose Robles for turning me into a mac user. It was a pleasure coding with you. To Shane, my office-mate and pepsi lover, and to Josh, the gentoo guru, to Leith my mediocre table tennis partner, to Brad for organizing all the great events, and to Dan and Grant for those mellow days at the beach, thanks for all the good times.

I am indebted to my big family at the Woden Fish Market for always making me feel close to the ocean.

Mum, Dad and Hayley, thank you for 27 years of love and support.

Finally and most importantly, Anna, my soulmate, you have given me more than it is fair to ask of anyone. Every day with you is grand no matter where we are. Thanks for supporting this dream of mine. I love you forever.

Preface

The contents of this thesis are based on research articles that I have published during the course of my PhD candidature. Although I use the first person plural throughout, all of the work presented in this thesis is my own unless explicitly stated here, or in section 1.5 of the Introduction.

- **C. H. Lineweaver & C. A. Egan, 2007**, "The Cosmic Coincidence as a Temporal Selection Effect Produced by the Age Distribution of Terrestrial Planets in the Universe", ApJ, v671, 853–860.

- **C. A. Egan & C. H. Lineweaver, 2008**, "Dark Energy Dynamics Required to Solve the Cosmic Coincidence", Phys. Rev. D., v78(8), 083528.

- **J. A. Robles, C. H. Lineweaver, D. Grether, C. Flynn, C. A. Egan, M. Pracy, J. Holmberg & E. Gardner, 2008**, "A comprehensive comparison of the Sun to other stars: searching for self-selection effects", ApJ, v684, 691–706.

- **J. A. Robles, C. A. Egan & C. H. Lineweaver, 2009**, "Statistical Analysis of Solar and Stellar Properties", Australian Space Science Conference Series: 8th Conference Proceedings NSSA Full Referreed Proceedings CD, (ed) National Space Society of Australia Ltd, edt. W. Short, conference held in Canberra, Australia September 23–25, 2008, ISBN 13: 978-0-9775740-2-5.

- **C.A. Egan & C.H. Lineweaver, 2010**, "A Larger Estimate of the Entropy of the Universe", ApJ, v710, 1825-1834.

- **C.A. Egan & C.H. Lineweaver, 2010**, "The Cosmological Heat Death", in preparation.

I have attached as appendix A a publication that is predominantly the work of my supervisor, Charles. H. Lineweaver, but to which I made minor contributions.

- **C.H. Lineweaver & C.A. Egan, 2008**, "Life, gravity and the second law of thermodynamics." Physics of Life Reviews, v5, 225–242.

CHAPTER 1

INTRODUCTION

I may be reckless, may be a fool,
but I get excited when I get confused.

- Fischerspooner, "The Best Revenge"

1.1. Copernicanism and Anthropic Selection

The Copernican idea, that we perceive the Universe from an entirely mediocre vantage point, is deeply embedded in the modern scientific world view. Before the influences of Copernicus, Galileo and Newton in the 16th and 17th centuries the prevalent world view was anthropocentric: we and the Earth were at the center of the Universe, and the heavenly bodies lived on spherical planes around us. The paradigm shift to a Copernican world view was ferociously resisted by theologians and philosophers, but was eventually adopted because of its ability to explain mounting physical and astronomical observations.

It is with great esteem that we remember these pioneers of modern science, who taught us that observational evidence trumps philosophical aesthetics. However, upon pedantic inspection, the Copernican idea leads to untrue predictions. For example, if we did occupy a mediocre vantage point then the density of our immediate environment would be $\sim 10^{-30}\ g\ cm^{-3}$. However the density of our

actual environment is $\sim 1\ g\ cm^{-3}$. A napkin calculation considering the density and size of collapsed objects suggest the chance of us living in an environment as dense or denser by pure chance is around 1 in 10^{30} – a significant signal.

There are selection effects connected with being an observer. They determine, to some degree, where and when we observe the Universe. At the cost of strict Copernicanism we must make considerations for anthropic selection as a class of observational selection effect (Dicke, 1961; Carter, 1974; Barrow and Tipler, 1986; Bostrom, 2002), and we *must* take the appropriate steps to remove anthropic selection effects from our data.

1.2. The Cosmic Coincidence Problem

Recent cosmological observations including observations of the cosmic microwave background temperature fluctuations, the luminosity-redshift relation from supernova light-curves and the matter power spectrum measured in the large scale structure and Lyman-Alpha forests of quasar spectra, have converged on a cosmological model which is expanding, and whose energy density is dominated by a mysterious component referred to generally as dark energy ($\sim 73\%$) but contains a comparable amount of matter ($\sim 27\%$) and some radiation ($\sim 5 \times 10^{-5}\%$). See e.g. (Seljak et al., 2006) and references therein.

The energy in these components drives the expansion of the Universe via the Friedmann equation, and in turn responds to the expansion via their equations of state: radiation dilutes as a^{-4}, matter dilutes as a^{-3} the dark energy density remains constant (assuming that dark energy is Einstein's cosmological constant) where a is the scalefactor of the Universe (Carroll, 2004).

Since matter and dark energy dilute at different rates during cosmic expansion, these two components only have comparable densities for a brief interval during cosmic history. Thus we are faced with the "cosmic coincidence problem": Why, just now, do the matter and dark energy densities happen to be of the same order (Weinberg, 1989; Carroll, 2001b)? Ad-hoc dynamic dark energy (DDE) models have been designed to solve the cosmic coincidence problem by arranging that the dark energy density is similar to the matter density for significant fractions of the age of the Universe.

Whether or not there is a coincidence problem depends on the range of times during which the Universe may be observed. In Chapter 2, we quantify the severity of the coincidence problem under ΛCDM by using the temporal distribution of terrestrial planets as a basis for the probable times of observation.

In Chapter 3 we generalize this approach to quantify the severity of the coincidence problem for all models of dark energy (using a standard parameterization). The two possible outcomes of this line of investigation are both valuable. One the one hand finding a significant coincidence problem for otherwise observationally allowed dark energy models would rule them out, complementing observational constraints on dark energy. On the other hand, finding that the coincidence problem vanishes for all observationally allowed models would remove the cosmic coincidence problem as a factor motivating dark energy models.

1.3. Searching for Life Tracers Amongst the Solar Properties

If the origin and evolution of terrestrial-planet-bound observers depend on anomalous properties of the planet's host star, then the stars that host such observers (including the Sun) are anthropically selected to have those properties.

Gonzalez (1999a,b) found that the Sun was more massive than $\sim 91\%$ of stars, and suggested that this may be explained if observers may develop preferentially around very massive stars. A star's mass determines, in large part, its lifetime, luminosity, temperature and the location of the terrestrial habitable zone, all of which may influence the probability of that star hosting observers. But the statistical significance of this "anomalous" mass depends on the number of other solar properties, also plausibly related to life, from which mass was selected. Thus while Gonzalez's proposition is plausible, it is unclear how strongly it is supported by the data.

In Chapter 4 of this thesis we compare the Sun to representative samples of stars in 11 independent parameters plausibly related to life (including mass), with the aim of quantifying the overall typicality of the Sun and potentially identifying statistically significant anomalous properties - potential tracers of life in the Universe.

1.4. The Entropy of the Present and Future Universe

One feature that we can count on as being important to all life in the Universe is the availability of free energy. Indeed we can only be sure of this because *all* irreversible processes in the Universe consume free energy and contribute to the increasing total entropy of the Universe.

The current entropy of the observable Universe was estimated by Frampton et al. (2008) to be $\sim 10^{102}\ k$ of a maximum possible value of $\sim 10^{123}\ k$. The current entropy of the observable Universe is dominated by the entropy in supermassive black holes at the centers of galaxies, followed distantly by the cosmic microwave background, neutrino background and other components.

If the entropy of the Universe reaches a value from which it could not be further increased, then all dissipative processes would cease. The idea that the future of the universe could end in such a state of thermodynamic equilibrium (a so-called heat death) was written about by Thomson (1852), and later revived within the context of an expanding Universe by Eddington (1931). Scientific and popular science literature over the past three decades is ambiguous about whether or not there will be a heat death, and if so, in what form.

In Chapter 5 we present an improved budget of the entropy of the observable Universe using new measurements of the supermassive black hole mass function. In Chapter 6 we compare the growing entropy of the Universe to upper bounds that have been proposed, and draw conclusions about the future heat death.

1.5. About the Papers Presented in this Thesis

Chapter 2 was published as Lineweaver and Egan (2007). The text was co-written with Charles Lineweaver, who is also to be credited for the original idea. However, the work presented in the paper is predominantly mine: details of the method, quantitative analyses, the preparation of all figures. For these reasons, and with Dr. Lineweaver's endorsement, it has been included here verbatim.

Chapter 3 is my own and was published as Egan and Lineweaver (2008).

In Chapter 4 I describe work published in Robles et al. (2008b), Robles et al. (2008a) and the erratum, Robles et al. (2008c). I was a co-author of this work, which was lead by Jose Robles, and I contributed in part to the collection of data (age; see figure 4.2), data analysis (advice on, and implementation of statistical, methods, as well as coding other parts of the analysis pipeline), interpretation and presentation of the results (contributing to figures and published articles). This chapter summarizes the main results paper, Robles et al. (2008b), in words that are my own. The figures are taken, with permission, from Robles et al. (2008b).

Chapter 5 is my own and has been submitted for publication to ApJ as Egan and Lineweaver (2010a).

Chapter 6 is my own and will contribute towards an article currently in preparation, which we refer to as Egan and Lineweaver (2010b).

Appendix A has been published as Lineweaver and Egan (2008). The text, and most of the work presented in that paper is that of my supervisor. My contributions include the contribution of the preparation of Figure A.4. The paper is included in the appendix of this thesis as it is referred to several times, and motivates the work presented in Chapters 5 and 6.

CHAPTER 2

THE COSMIC COINCIDENCE AS A TEMPORAL SELECTION EFFECT PRODUCED BY THE AGE DISTRIBUTION OF TERRESTRIAL PLANETS IN THE UNIVERSE

Late at night, stars shining bright
on me, down by the sea.
And when I see them in the sky
constantly I'm asking why
I was stranded here.
I wish I could be out in space.

- S.P.O.C.K, "Out in Space"

2.1. Is the Cosmic Coincidence Remarkable or Insignificant?

2.1.1. Dicke's argument

Dirac (1937) pointed out the near equality of several large fundamental dimensionless numbers of the order 10^{40}. One of these large numbers varied with time since it depended on the age of the Universe. Thus there was a limited time during which this near equality would hold. Under the assumption that observers could exist at any time during the history of the Universe, this large number coincidence could not be explained in the standard cosmology. This problem motivated Dirac (1938) and Jordan (1955) to construct an ad hoc new cosmology. Alternatively, Dicke (1961) proposed that our observations of the Universe could only be made during a time interval after carbon had been produced in the Universe and before the last stars stop shining. Dicke concluded that this temporal observational selection effect – even one so loosely delimited – could explain Dirac's large number coincidence without invoking a new cosmology.

Here, we construct a similar argument to address the cosmic coincidence: Why just now do we find ourselves in the relatively brief interval during which $\Omega_m \sim \Omega_\Lambda$. The temporal constraints on observers that we present are more empirical and specific than those used in Dicke's analysis, but the reasoning is similar. Our conclusion is also similar: a temporal observational selection effect can explain the apparent cosmic coincidence. That is, given the evolution of Ω_Λ and Ω_m in our Universe, most observers in our Universe who have emerged on terrestrial planets will find $\Omega_\Lambda \sim \Omega_m$. Rather than being an unusual coincidence, it is what one should expect.

There are two distinct problems associated with the cosmological constant (Weinberg, 2000a; Garriga and Vilenkin, 2001; Steinhardt, 2003). One is the coincidence problem that we address here. The other is the smallness problem and has to do with the observed energy density of the vacuum, ρ_Λ. Why is ρ_Λ so small compared to the $\sim 10^{120}$ times larger value predicted by particle physics? Anthropic solutions to this problem invoke a multiverse and argue that galaxies would not form and there would be no life in a Universe, if ρ_Λ were larger than ~ 100 times its observed value (Weinberg, 1987; Martel et al., 1998; Garriga and Vilenkin, 2001; Pogosian and Vilenkin, 2007). Such explanations for the smallness of ρ_Λ do not explain the temporal coincidence between the time of our observation and the time of the near-equality of Ω_m and Ω_Λ. Here we address this temporal coincidence in our Universe, not the smallness problem in

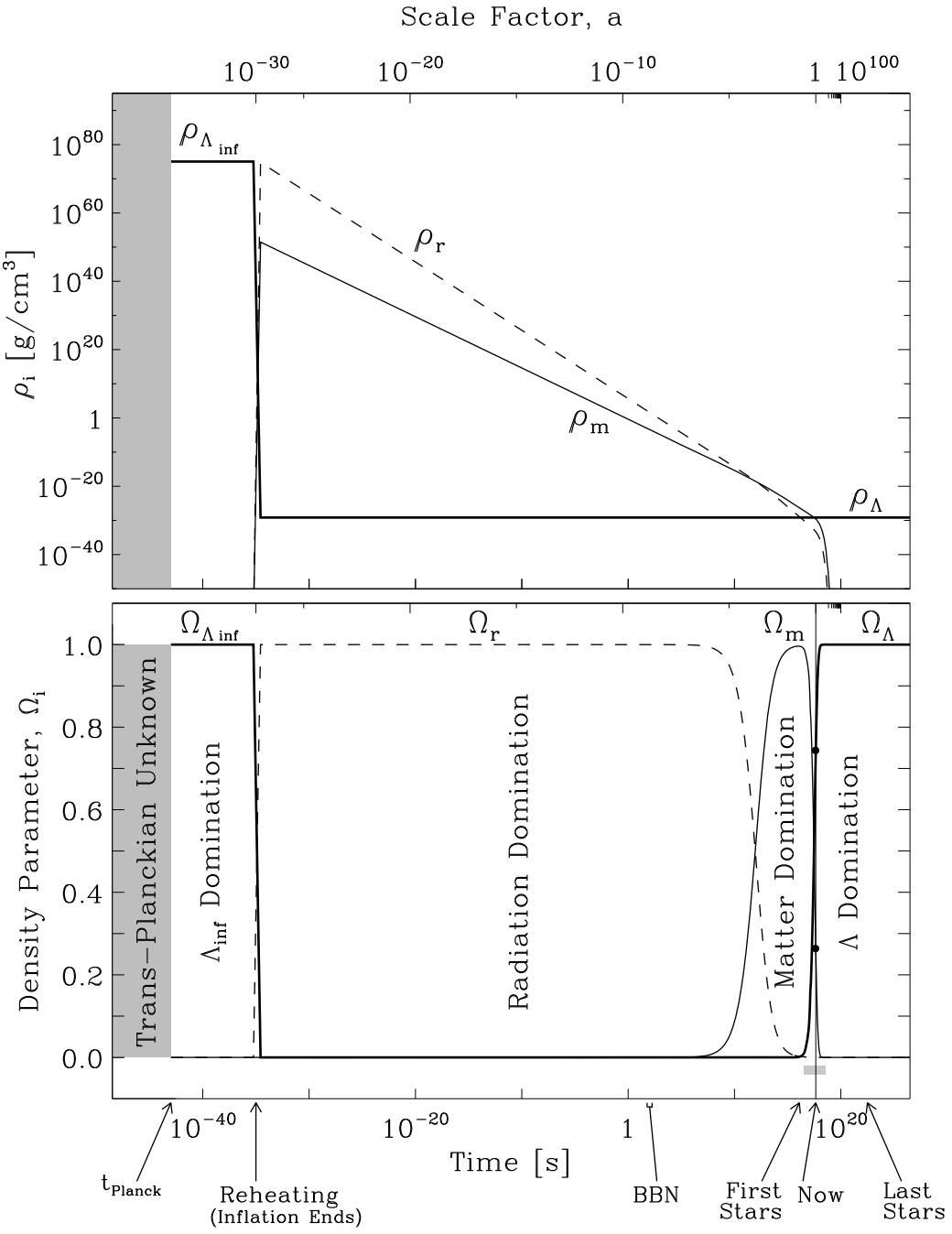

Figure 2.1 The time dependence of the densities of the major components of the Universe. Given the observed Hubble constant, H_o and energy densities in the Universe today, Ω_{r_o}, Ω_{m_o}, Ω_{Λ_o} (radiation, matter and cosmological constant), we use the Friedmann equation to plot the temporal evolution of the components of the Universe in g/cm^3 (top panel), or normalized to the time-dependent critical density $\rho_{crit} = \frac{3H(t)^2}{8\pi G}$ (bottom panel). We assume an epoch of inflation at $\sim 10^{-35}$ seconds after the big bang and a false vacuum energy density $\rho_{\Lambda_{\mathrm{inf}}}$ between the Planck scale and t_{GUT}. See Table 2.1 and Appendix A for details.

a multiverse.

2.1.2. Evolution of the Energy Densities

Given the currently observed values for H_o and the energy densities Ω_{r_o}, Ω_{m_o} and Ω_{Λ_o} in the Universe (Spergel et al., 2006; Seljak et al., 2006), the Friedmann equation tells us the evolution of the scale factor a, and the evolution of these energy densities. These are plotted in Fig. 2.1. The history of the Universe can be divided chronologically into four distinct periods each dominated by a different form of energy: initially the false vacuum energy of inflation dominates, then radiation, then matter, and finally vacuum energy. Currently the Universe is making the transition from matter domination to vacuum energy domination. In an expanding Universe, with an initial condition $\Omega_m > \Omega_\Lambda > 0$, there will be some epoch in which $\Omega_m \sim \Omega_\Lambda$, since ρ_m is decreasing as $\propto 1/a^3$ while ρ_Λ is a constant (see top panel of Fig. 2.1 and Appendix A). Figure 2.1 also shows that the transition from matter domination to vacuum energy domination is occurring now. When we view this transition in the context of the time evolution of the Universe (Fig. 2.2) we are presented with the cosmic coincidence problem: Why just now do we find ourselves at the relatively brief interval during which this transition happens? Carroll (2001b,a) and Dodelson et al. (2000) find this coincidence to be a remarkable result that is crucial to understand. The cosmic coincidence problem is often regarded as an important unsolved problem whose solution may help unravel the nature of dark energy (Turner 2001; Carroll 2001a). The coincidence problem is one of the main motivations for the tracker potentials of quintessence models (Caldwell et al., 1998; Steinhardt et al., 1999; Zlatev et al., 1999; Wang et al., 2000; Dodelson et al., 2000; Armendariz-Picon et al., 2001; Guo and Zhang, 2005). In these models the cosmological constant is replaced by a more generic form of dark energy in which Ω_m and Ω_Λ are in near-equality for extended periods of time. It is not clear that these models successfully explain the coincidence without fine-tuning (see Weinberg 2000a; Bludman 2004).

The interpretation of the observation $\Omega_{m_o} \sim \Omega_{\Lambda_o}$ as a remarkable coincidence in need of explanation depends on some assumptions that we quantify to determine how surprising this apparent coincidence is. We begin this quantification by introducing a time-dependent proximity parameter,

$$r = \min\left[\frac{\Omega_\Lambda}{\Omega_m}, \frac{\Omega_m}{\Omega_\Lambda}\right] \tag{2.1}$$

which is equal to one when $\Omega_m = \Omega_\Lambda$ and is close to zero when $\Omega_m >> \Omega_\Lambda$ or $\Omega_m << \Omega_\Lambda$. The current value is $r_o \approx 0.4$. In Figure 2.2 we plot r as a function of log(scale factor) in the upper panel and as a function of log(time) in the

lower panel. These logarithmic axes allow a large dynamic range that makes our existence at a time when $r \sim 1$, appear to be an unlikely coincidence. This appearance depends on the implicit assumption that we could make cosmological observations at any time with equal likelihood. More specifically, the implicit assumption is that the *a priori* probability distribution P_{obs}, of the times we could have made our observations, is uniform in $\log t$, or $\log a$, over the interval shown.

Our ability to quantify the significance of the coincidence depends on whether we assume that P_{obs} is uniform in time, log(time), scale factor or log(scale factor). That is, our result depends on whether we assume: $P_{obs}(t) = constant$, $P_{obs}(\log t) = constant$, $P_{obs}(a) = constant$ or $P_{obs}(\log a) = constant$. These are the most common possibilities, but there are others. For a discussion of the relative merits of log and linear time scales and implicit uniform priors see Section 2.3.3 and Jaynes (1968).

In Fig. 2.3 we plot $r(t)$ on an axis linear in time where the implicit assumption is that the *a priori* probability distribution of our existence is uniform in t over the intervals $[0, 100]$ Gyr (top panel) and $[0, 13.8]$ Gyr (bottom panel). The bottom panel shows that the observation $r > 0.4$ could have been made anytime during the past 7.8 Gyr. Thus, our current observation that $r_o \approx 0.4$, does not appear to be a remarkable coincidence. Whether this most recent 7.8 Gyr period is seen as "brief" (in which case there is an unlikely coincidence in need of explanation) or "long" (in which case there is no coincidence to explain) depends on whether we view the issue in log time (Fig. 2.2) or linear time (Fig. 2.3).

A large dynamic range is necessary to present the fundamental changes that occurred in the very early Universe, e.g., the transitions at the Planck time, inflation, baryogenesis, nucleosynthesis, recombination and the formation of the first stars. Thus a logarithmic time axis is often preferred by early Universe cosmologists because it seems obvious, from the point of view of fundamental physics, that the cosmological clock ticks logarithmically. This defensible view and the associated logarithmic axis gives the impression that there is a coincidence in need of an explanation. The linear time axis gives a somewhat different impression. Evidently, deciding whether a coincidence is of some significance or only an accident is not easy (Peebles and Vilenkin, 1999). We conclude that although the importance of the cosmic coincidence problem is subjective, it is important enough to merit the analysis we perform here.

The interpretation of the observation $\Omega_{m_o} \sim \Omega_{\Lambda_o}$ as a coincidence in need of explanation depends on the *a priori* (not necessarily uniform) probability distribution of our existence. That is, it depends on when cosmological observers can exist. We propose that the cosmic coincidence problem can be more constructively evaluated by replacing these uninformed uniform priors with the

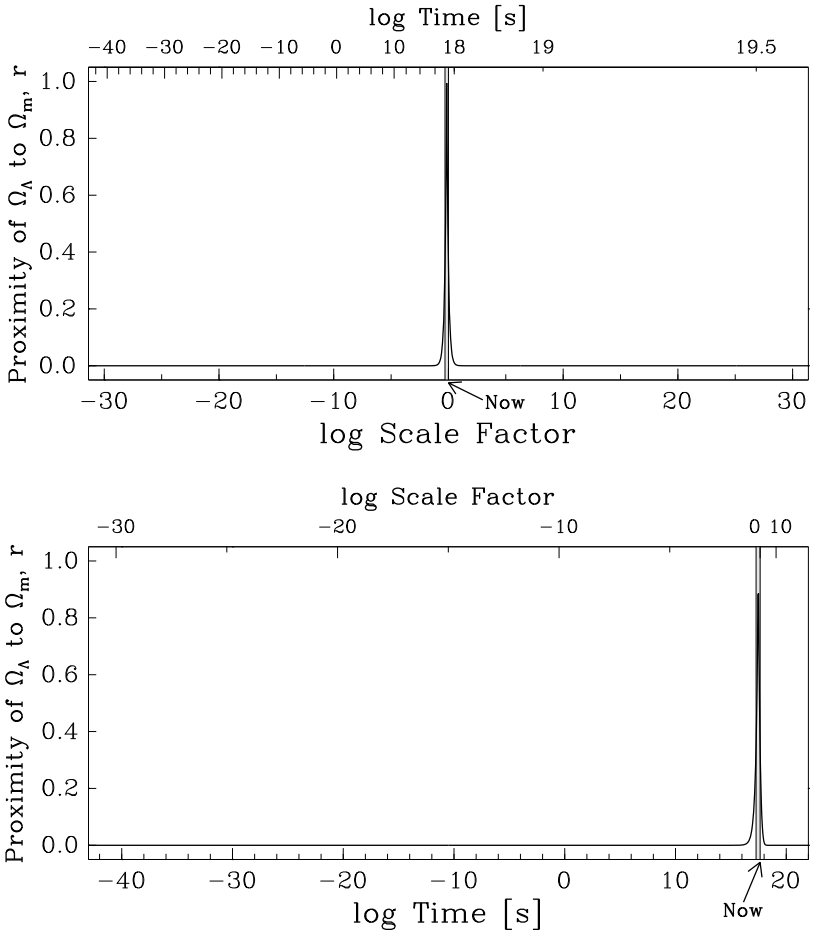

Figure 2.2 Plot of the proximity factor r (see Eq. 2.1). When the matter and vacuum energy densities of the Universe are the same, $\Omega_m = \Omega_\Lambda$, we have $r = 1$. We currently observe $\Omega_{m_o} \sim \Omega_{\Lambda_o}$ and thus, $r \sim 1$. Our existence now when $r \sim 1$ appears to be an unlikely cosmic coincidence when the x axis is logarithmic in the scale factor (top panel) or logarithmic in time (bottom panel). In the top panel, following Carroll (2001b), we have chosen a range of scale factors with "Now" midway between the scale factor at the Planck time and the scale factor at the inverse Planck time [$a_{Planck} < a < a_{Planck}^{-1}$]. The brief epoch shown in grey between the thin vertical lines is the epoch during which $r > r_o$ (where $r_o \approx 0.4$ is the currently observed value). In the bottom panel the range shown on the x axis is [$t_{Planck} < t < 10^{22}$] seconds. The Planck time and Planck scale provide reasonably objective lower time limits. The upper limits are somewhat arbitrary but contribute to the impression that $r \approx 0.4 \sim 1$ is an unlikely coincidence.

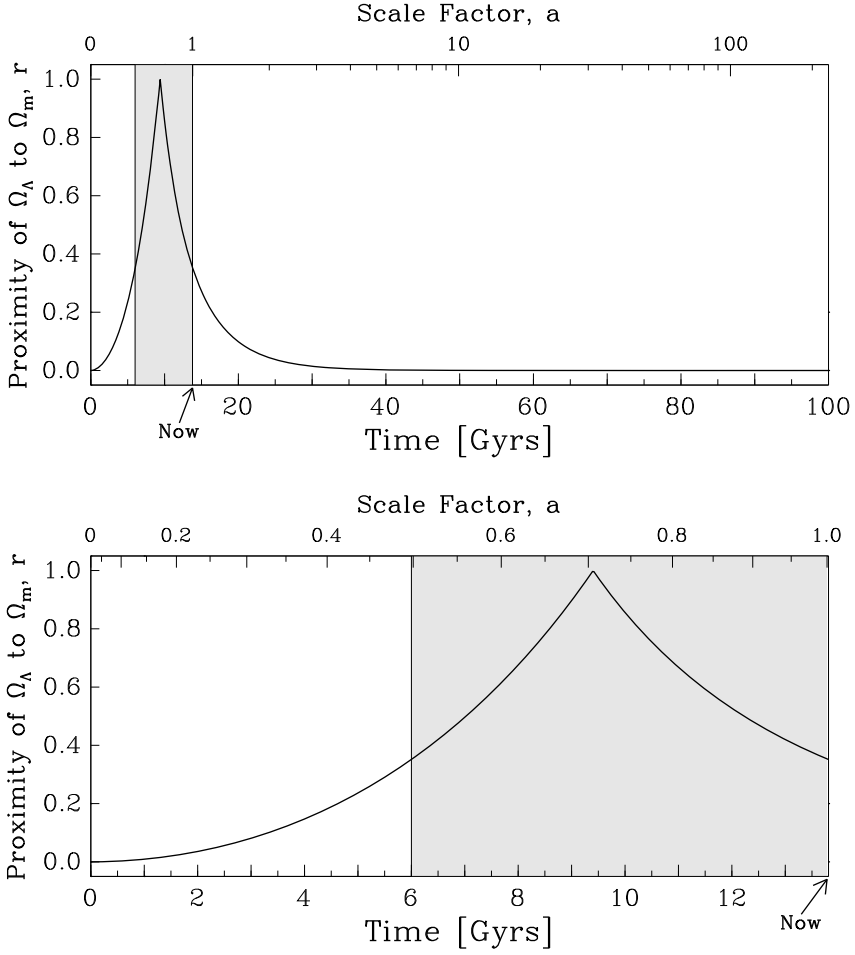

Figure 2.3 Plot of the proximity factor r, as in the previous figure, but plotted here with a linear rather than a logarithmic time axis. The condition $r > r_o \approx 0.4$ does not seem as unlikely as in the previous figure. The range of time plotted also affects this appearance; with the $[0, 100]$ Gyr range of the top panel, the time interval highlighted in grey where $r > r_o$, appears narrow and relatively unlikely. In contrast, the $[0, 13.8]$ Gyr range of the bottom panel seems to remove the appearance of $r > r_o$ being an unlikely coincidence in need of explanation; for the first ~ 6 Gyrs we have $r < r_o$ while in the subsequent 7.8 Gyr we have $r > r_o$. How can $r > r_o$ be an unlikely coincidence when it has been true for most of the history of the Universe?

more realistic assumption that observers capable of measuring cosmological parameters are dependent on the emergence of high density regions of the Universe called terrestrial planets, which require non-trivial amounts of time to form – and that once these planets are in place, the observers themselves require non-trivial amounts of time to evolve.

In this paper we use the age distribution of terrestrial planets estimated by Lineweaver (2001) to constrain when in the history of the Universe, observers on terrestrial planets can exist. In Section 2.2, we briefly describe this age distribution (Fig. 2.4) and show how it limits the existence of such observers to an interval in which $\Omega_m \sim \Omega_\Lambda$ (Fig. 2.5). Using this age distribution as a temporal selection function, we compute the probability of an observer on a terrestrial planet observing $r \geq r_o$ (Fig. 2.6). In Section 2.3 we discuss the robustness of our result and find (Fig. 2.7) that this result is relatively robust if the time it takes an observer to evolve on a terrestrial planet is less than ~ 10 Gyr. In Section 2.4 we discuss and summarize our results, and compare it to previous work to resolve the cosmic coincidence problem (Garriga and Vilenkin, 2000; Bludman and Roos, 2001).

2.2. How We Compute the Probability of Observing $\Omega_m \sim \Omega_\Lambda$

2.2.1. The Age Distribution of Terrestrial Planets and New Observers

The mass histogram of detected extrasolar planets peaks at low masses: $dN/dM \propto M^{-1.7}$, suggesting that low mass planets are abundant (Lineweaver and Grether, 2003). Terrestrial planet formation may be a common feature of star formation (Wetherill 1996; Chyba 1999; Ida and Lin 2005). Whether terrestrial planets are common or rare, they will have an age distribution proportional to the star formation rate – modified by the fact that in the first ~ 2 billion years of star formation, metallicities are so low that the material for terrestrial planet formation will not be readily available. Using these considerations, Lineweaver (2001) estimated the age distribution of terrestrial planets – how many Earths are produced by the Universe per year, per Mpc^3 (Figure 2.4). If life emerges rapidly on terrestrial planets (Lineweaver and Davis, 2002) then this age distribution is the age distribution of biogenesis in the Universe. However, we are not just interested in any life; we would like to know the distribution in time of when independent observers first emerge and are able to measure Ω_m and Ω_Λ, as we

are able to do now. If life originates and evolves preferentially on terrestrial planets, then the Lineweaver (2001) estimate of the age distribution of terrestrial planets is an *a priori* input which can guide our expectations of when we (as members of a hypothetical group of terrestrial-planet-bound observers) could have been present in the Universe. It takes time (if it happens at all) for life to emerge on a new terrestrial planet and evolve into cosmologists who can observe Ω_m and Ω_Λ. Therefore, to obtain the age distribution of new independent observers able to measure the composition of the Universe for the first time, we need to shift the age distribution of terrestrial planets by some characteristic time, Δt_{obs} required for observers to evolve. On Earth, it took $\Delta t_{obs} \sim 4$ Gyr for this to happen. Whether this is characteristic of life elsewhere in the Universe is uncertain (Carter 1983; Lineweaver and Davis 2003). For our initial analysis we use $\Delta t_{obs} = 4$ Gyr as a nominal time to evolve observers. In Section 2.3.1 we allow Δt_{obs} to vary from 0-12 Gyr to see how sensitive our result is to these variations. Fig. 2.4 shows the age distribution of terrestrial planet formation in the Universe shifted by $\Delta t_{obs} = 4$ Gyr. This curve, labeled "P_{obs}" is a crude prior for the temporal selection effect of when independent observers can first measure r. Thus, if the evolution of biological equipment capable of doing cosmology takes about $\Delta t_{obs} \sim 4$ Gyr, the "P_{obs}" in Fig. 2.4 shows the age distribution of the first cosmologists on terrestrial planets able to look at the Universe and determine the overall energy budget, just as we have recently been able to do.

2.2.2. The Probability of Observing $\Omega_m \sim \Omega_\Lambda$.

In Fig. 2.5 we zoom into the portion of Fig. 2.1 containing the relatively narrow window of time in which $\Omega_m \sim \Omega_\Lambda$. We plot $r(t)$ to show where $r \sim 1$ and we also plot the age distribution of planets and the age distribution of recently emerged cosmologists from Fig. 2.4. The white area under the thick $P_{obs}(t)$ curve provides an estimate of the time distribution of new observers in the Universe. We interpret $P_{obs}(t)$ as the probability distribution of the times at which new, independent observers are able to measure r for the first time.

Lineweaver (2001) estimated that the Earth is relatively young compared to other terrestrial planets in the Universe. It follows under the simple assumptions of our analysis that most terrestrial-planet-bound observers will emerge earlier than we have. We compute the fraction f of observers who have emerged earlier than we have,

$$f = \frac{\int_0^{t_o} P_{obs}(t)\, dt}{\int_0^{\infty} P_{obs}(t)\, dt} \approx 68\% \tag{2.2}$$

and find that 68% emerge earlier while 32% emerge later. These numbers are indicated in Fig. 2.5.

2.2.3. Converting $P_{obs}(t)$ to $P_{obs}(r)$

We have an estimate of the distribution in time of observers, $P_{obs}(t)$, and we have the proximity parameter $r(t)$. We can then convert these to a probability $P_{obs}(r)$, of observed values of r. That is, we change variables and convert the $t-$dependent probability to an $r-$dependent probability: $P_{obs}(t) \rightarrow P_{obs}(r)$. We want the probability distribution of the r values first observed by new observers in the Universe. Let the probability of observing r in the interval dr be $P_{obs}(r)dr$. This is equal to the probability of observing t in the interval dt, which is $P_{obs}(t)dt$

Thus,

$$P_{obs}(r)\, dr = P_{obs}(t)\, dt \tag{2.3}$$

or equivalently

$$P_{obs}(r) = \frac{P_{obs}(t)}{dr/dt} \tag{2.4}$$

where $P_{obs}(t) = PFR(t-\Delta t_{obs})$ is the temporally shifted age distribution of terrestrial planets and dr/dt is the slope of $r(t)$. Both are shown in Fig. 2.5. The distribution $P_{obs}(r)$ is shown in Fig. 2.6 along with the upper and lower confidence limits on $P_{obs}(r)$ obtained by inserting the upper and lower confidence limits of $P_{obs}(t)$ (denoted "P^+" and "P^-" in Fig. 2.4), into Eq. 2.4 in place of $P_{obs}(t)$.

The probability of observing $r > r_o$ is,

$$P(r > r_o) = \int_{r_o}^{1} P_{obs}(r)\, dr = \int_{t'}^{t_o} P_{obs}(t)\, dt \approx 68\% \tag{2.5}$$

where t' is the time in the past when r was equal to its present value, i.e., $r(t') = r(t_o) = r_o \approx 0.4$. We have $t' = 6$ Gyr and $t_o = 13.8$ Gyr (see bottom panel of Fig. 2.3). This integral is shown graphically in Fig. 2.6 as the hatched area underneath the "$P_{obs}(r)$" curve, between $r = r_o$ and $r = 1$. We interpret this as follows: of all observers that have emerged on terrestrial planets, 68% will emerge when $r > r_o$ and thus will find $r > r_o$. The 68% from Eq. 2.2 is only the same as the 68% from Eq. 2.5 because all observers who emerge earlier than we did, did so more recently than 7.8 billion years ago and thus, observe $r > r_o$ (Fig. 2.5).

We obtain estimates of the uncertainty on this 68% estimate by computing analogous integrals underneath the curves labeled P^+ and P^- in Fig. 2.6. These yield 82% and 59% respectively. Thus, under the assumptions made here, 68^{+14}_{-10}%

of the observers in the Universe will find Ω_Λ and Ω_m even closer to each other than we do. This suggests that a temporal selection effect due to the constraints on the emergence of observers on terrestrial planets provides a plausible solution to the cosmic coincidence problem. If observers in our Universe evolve predominantly on Earth-like planets (see the "principle of mediocrity" in Vilenkin (1995b)), we should not be surprised to find ourselves on an Earth-like planet and we should not be surprised to find $\Omega_{\Lambda_o} \sim \Omega_{m_o}$.

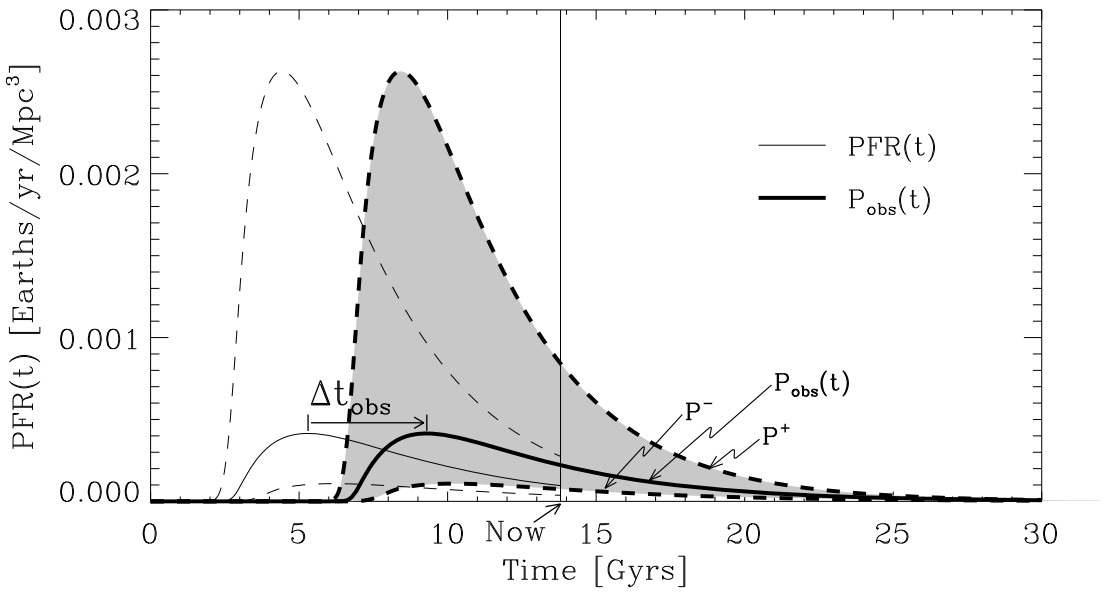

Figure 2.4 The terrestrial planet formation rate $PFR(t)$, derived in Lineweaver (2001) is an estimate of the age distribution of terrestrial planets in the Universe and is shown here as a thin solid line. Estimated uncertainty is given by the thin dashed lines. To allow time for the evolution of observers on terrestrial planets, we shift this distribution by Δt_{obs} to obtain an estimate of the age distribution of observers: $P_{obs}(t) = PFR(t - \Delta t_{obs})$ (thick solid line). The grey band represents the error estimate on $P_{obs}(t)$ which is the shifted error estimates on $PFR(t)$. In the case shown here Δt_{obs} = 4 Gyr, which is how long it took life on Earth to emerge, evolve and be able to measure the composition of the Universe. To obtain the numerical values on the y axis, we have followed Lineweaver (2001) and assumed that one out of one hundred stars is orbited by a terrestrial planet. We have smoothly extrapolated the $PFR(t)$ of Lineweaver (2001) into the future. This time dependence and our subsequent analysis does not depend on whether the probability for terrestrial planets to produce observers is high or low.

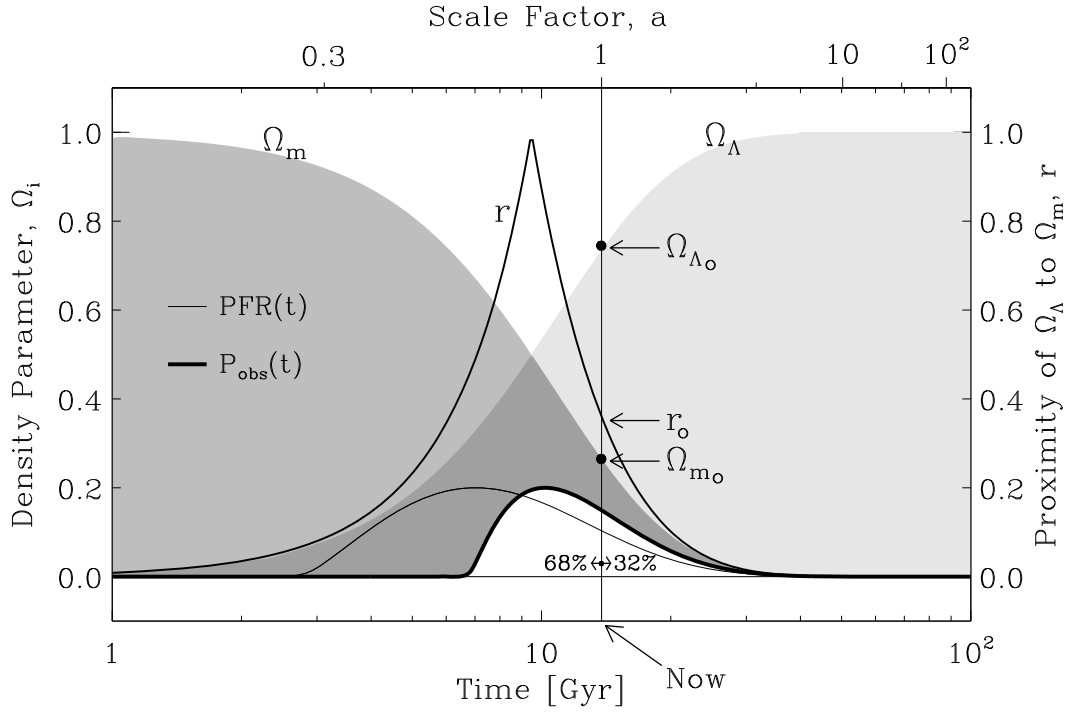

Figure 2.5 Zoom-in of the portion of Fig. 2.1 between 1 and 100 billion years after the big bang, containing the relatively narrow window of time in which $\Omega_m \sim \Omega_\Lambda$. The 99 Gyr time interval displayed here is indicated in Fig. 2.1 by the small grey rectangle above the "Now" label. The proximity parameter $r(t)$ (Eq. 2.1, Figs. 2.2 & 2.3) is superimposed. The thin solid line shows the age distribution of terrestrial planets in the Universe while the thick solid line is the lateral displacement of this distribution by Δt_{obs} = 4 Gyr. These distributions were presented in Fig. 2.4, but here the time axis is logarithmic. We interpret P_{obs} as the frequency distribution of new observers able to measure Ω_m and Ω_Λ for the first time. Since $r(t)$ peaks at about the same time as $P_{obs}(t)$, large values of r will be observed more often than small values.

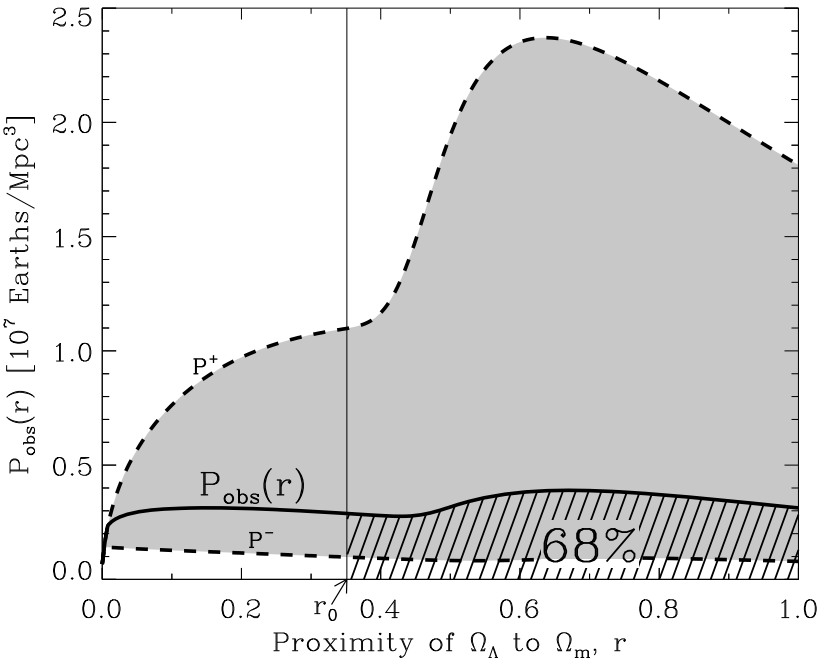

Figure 2.6 Probability of new observers on terrestrial planets observing a given r (Eq. 2.4). Given our estimate of the age distribution of new cosmologists in the Universe $P_{obs}(t)$, the probability of observing Ω_m and Ω_Λ as close together as they are, or closer, is the integral given in Eq. (2.5), shown here as the hashed area labeled 68%. The dashed lines labeled P^+ and P^- are from replacing $P_{obs}(t)$ in Eq. 2.4 with the curves labeled P^+ and P^- in Fig. 2.4.

2.3. How Robust is this 68% Result?

2.3.1. Dependence on the timescale for the evolution of observers

A necessary delay, required for the biological evolution of observing equipment – e.g. brains, eyes, telescopes, makes the observation of recent biogenesis unobservable (Lineweaver and Davis, 2002, 2003). That is, no observer in the Universe can wake up to observerhood and find that their planet is only a few hours old. Thus, the timescale for the evolution of observers, $\Delta t_{obs} > 0$.

Our 68^{+14}_{-10}% result was calculated under the assumption that evolution from a new terrestrial planet to an observer takes $\Delta t_{obs} \sim 4$ Gyr. To determine how robust our result is to variations in Δt_{obs}, we perform the analysis of Sec. 2.2 for $0 < \Delta t_{obs} < 12$ Gyr. The results are shown in Fig. 2.7. Our 68^{+14}_{-10}% result is the data point plotted at $\Delta t_{obs} = 4$ Gyr. If life takes ~ 0 Gyr to evolve to observerhood, once a terrestrial planet is in place, $P_{obs}(t) \approx PFR(t)$ and 55% of new cosmologists would observe an r value larger than the $r_o \approx 0.4$ that we actually observe today. If observers typically take twice as long as we did to evolve ($\Delta t_{obs} \sim 8$ Gyr), there is still a large chance (~ 30%) of observing $r > r_o$. If $\Delta t_{obs} > 11$ Gyr, $P_{obs}(t)$ in Fig. 2.5 peaks substantially after $r(t)$ peaks, and the percentage of cosmologists who see $r > r_o$, is close to zero (Eq. 2.5). Thus, if the characteristic time it takes for life to emerge and evolve into cosmologists is $\Delta t_{obs} \lesssim 10$ Gyr, our analysis provides a plausible solution to the cosmic coincidence problem.

The Sun is more massive than 94% of all stars. Therefore 94% of stars live longer than the $t_\odot \approx 10$ Gyr main sequence lifetime of the Sun. This is mildly anomalous and it is plausible that the Sun's mass has been anthropically selected. For example, perhaps stars as massive as the Sun are needed to provide the UV photons to jump start and energize the molecular evolution that leads to life. If so, then ~ 10 Gyr is a rough upper limit to the amount of time a terrestrial planet with simple life has to produce observers. Even if the characteristic time for life to evolve into observers is much longer than 10 Gyr, as concluded by Carter (1983), this UV requirement that life-hosting stars have main sequence lifetimes $\lesssim 10$ Gyr would lead to the extinction of most extraterrestrial life before it can evolve into observers. This would lead to observers waking to observerhood to find the age of their planet to be a large fraction of the main sequence lifetime of their star; the time they took to evolve would satisfy $\Delta t_{obs} \lesssim 10$ Gyr, and they would observe that $r \sim 1$ and that other observers are very rare. Such is our situation.

If we assume that we are typical observers (Vilenkin, 1995a,b, 1996a,b) and that the coincidence problem must be resolved by an observer selection effect (Bostrom, 2002), then we can conclude that the typical time it takes observers to evolve on terrestrial planets is less than 10 Gyr ($\Delta t_{obs} < 10$ Gyr).

2.3.2. Dependence on the age distribution of terrestrial planets

The $P_{obs}(t)$ used here (Fig. 2.5) is based on the star formation rate (SFR) computed in Lineweaver (2001). There is general agreement that the SFR has been declining since redshifts $z \sim 2$. Current debate centers around whether that decline has only been since $z \sim 2$ or whether the SFR has been declining from a much higher redshift (Lanzetta et al. 2002; Hopkins 2006; Nagamine et al. 2006; Thompson et al. 2006). Since Lineweaver (2001) assumed a relatively high value for the SFR at redshifts above 2, this led to a relatively high estimate of the metallicity of the Universe at $z \sim 2$, which corresponds to a relatively short delay (~ 2 Gyr) between the big bang and the first terrestrial planets. For the purposes of this analysis, the early-SFR-dependent uncertainty in the ~ 2 Gyr delay is degenerate with, but much smaller than, the uncertainty of Δt_{obs}. Thus the variations of Δt_{obs} discussed above subsume the SFR-dependent uncertainty in $P_{obs}(t)$.

2.3.3. Dependence on Measure

In Figs. 2.2 & 2.3 we illustrated how the importance of the cosmic coincidence depends on the range over which one assumes that the observation of r could have occurred. This involved choosing the range Δx shown on the x axis in Figs. 2.2 & 2.3. We also showed how the apparent significance of the coincidence depended on how one expressed that range, i.e., logarithmic in Fig. 2.2 and linear in Fig. 2.3. The coincidence seems most compelling when Δx is the largest and the problem is presented on a logarithmic x axis. This dependence is a specific example of a "measure" problem (Aguirre and Tegmark 2005; Aguirre et al. 2007).

The measure problem is illustrated in Fig. 2.8, where we plot four different uniform distributions of observers on a linear time axis. In Panel *a*) $P_{obs}(t)$ = constant. That is, we assume that observers could find themselves anywhere between $t_{rec} = 380,000$ yr and 100 Gyr after the big bang, with uniform probability (dark grey). In *b*), we make the different assumption that observers are distributed uniformly in log(t) over the same range in time. This means for example that the probability of finding yourself between 0.1 and 1 Gyr is the same as between 1 and 10 Gyr. We plot this as a function of linear time and find that the distribution

of observers (dark grey) is highest towards earlier times.

To quantify and explore these dependencies further, in Table 2.2, we take the duration when $r > r_o$ (call this interval Δx_r) and divide it by various larger ranges Δx (a range of time or scale factor). Thus, when the probability $P(r > r_o) = \frac{\Delta x_r}{\Delta x}$ is << 1, there is a low probability that one would find oneself in the interval Δx_r and the cosmic coincidence is compelling. However, when $P(r > r_o) \sim 1$ the coincidence is not significant.

In the four panels *a,b,c* and *d* of Fig. 2.8 the probability of us observing $r \geq r_o$ (finding ourselves in the light grey area) is respectively $8\%, 7\%, 0.2\%$ and 6%. These values are given in the first row of Table 2.2 along with analogous values when 11 other ranges for Δx are considered. Probabilities corresponding to the four panels of Figs. 2.2 & 2.3 are shown in bold in Table 2.2. Our conclusion is that this simple ratio method of measuring the significance of a coincidence yields results that can vary by many orders of magnitude depending on the range (Δx) and measure (e.g. linear or logarithmic) chosen. The use of the non-uniform $P_{obs}(t)$ shown in Fig. 2.4 is not subject to these ambiguities in the choice of range and measure.

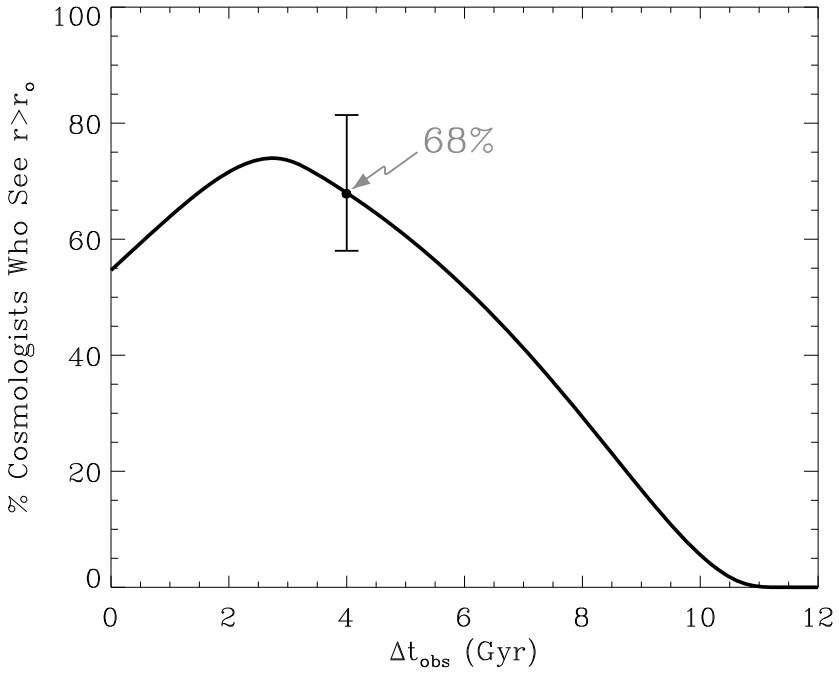

Figure 2.7 Percentage of cosmologists who see $r > r_o$ as a function of the time Δt_{obs}, it takes observers to evolve on a terrestrial planet. Since we have only vague notions about how long it takes observers to evolve on a planet, we vary Δt_{obs} between 0 and 12 billion years and show how the probability $P(r > r_o)$ of observing $r > r_o$ (Eq. 2.5) varies as a function of Δt_{obs}. The 68^{+14}_{-10}% point plotted is the result from Fig. 2.6 where $\Delta t_{obs} = 4$ Gyr. If $\Delta t_{obs} = 0$, we use the thin solid line in Fig. 2.5 as $P_{obs}(t)$ rather than the thick solid line and we obtain 55%.

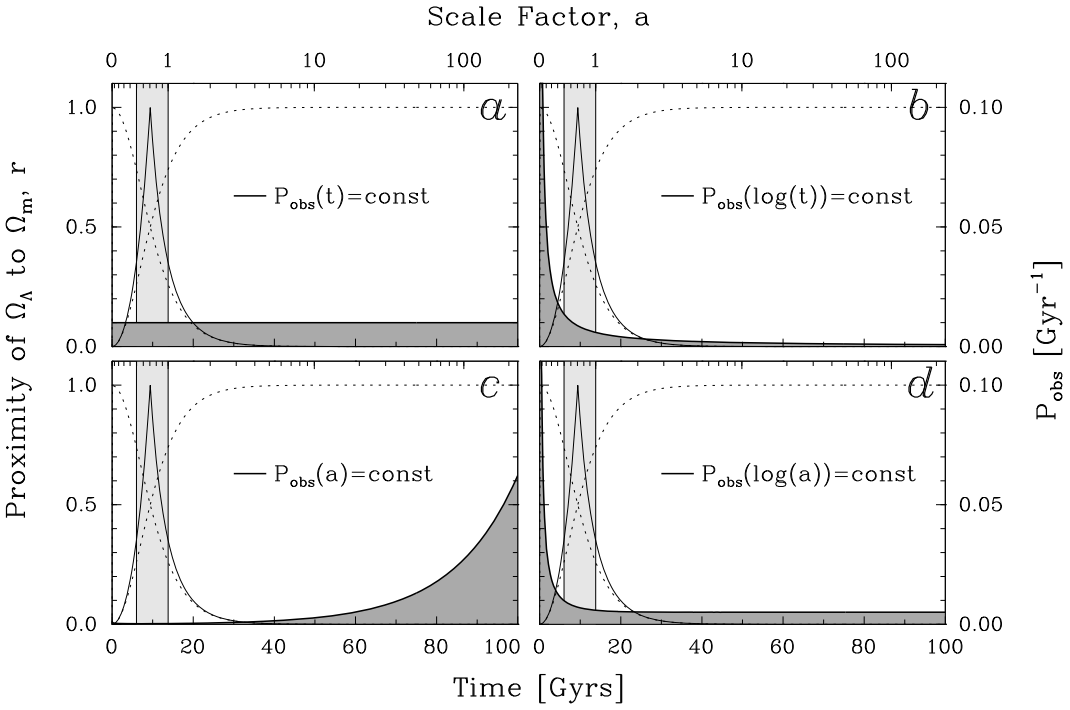

Figure 2.8 The expected observed value of r depends strongly on the assumed distribution of observers over time t. This figure demonstrates a variety of uniform observer distributions P_{obs} which, if used, result in the cosmic coincidence problem that the observed value of r is unexpectedly high. The P_{obs} that are functions of $log(a)$ or $log(t)$ have been normalized to the interval t_{rec} to 100 Gyr. Panel *a*) is the same as the top panel of Fig. 2.3. The probabilities that an observer would fall within the vertical light grey band ($r > r_o$) in Panels *a,b,c* and *d* are 8%, 7%, 0.2% and 6% respectively, and are given in the first row of Table 2.2.

2.4. Discussion & Summary

Anthropic arguments to resolve the coincidence problem include Garriga and Vilenkin (2000) and Bludman and Roos (2001). Both use a semi-analytical formalism (Gunn and Gott 1972; Press and Schechter 1974; Martel et al. 1998) to compute the number density of objects that collapse into large galaxies. This is then used as a measure of the number density of intelligent observers. Our work complements these semi-analytic models by using observations of the star formation rate to constrain the possible times of observation. Our work also extends this previous work by including the effect of Δt_{obs}, the time it takes observers to evolve on terrestrial planets. This inclusion puts an important limit on the validity of anthropic solutions to the coincidence problem.

Garriga and Vilenkin (2000) is probably the work most similar to ours. They take ρ_Λ as a random variable in a multiverse model with a prior probability distribution. For a wide range of ρ_Λ (prescribed by a prior based on inflation theory) they find approximate equality between the time of galaxy formation t_G, the time when Λ starts to dominate the energy density of the Universe t_Λ and now t_o. That is, they find that, within one order of magnitude, $t_G \sim t_\Lambda \sim t_o$. Their analysis is more generic but approximate in that it addresses the coincidence for a variety of values of ρ_Λ to an order of magnitude precision. Our analysis is more specific and empirical in that we condition on our Universe and use the Lineweaver (2001) star-formation-rate-based estimate of the age distribution of terrestrial planets to reach our main result (68%).

To compare our result to that of Garriga and Vilenkin (2000), we limit their analysis to the ρ_Λ observed in our Universe ($\rho_\Lambda = 6.7 \times 10^{-30} g/cm^3$) and differentiate their cumulative number of galaxies which have assembled up to a given time (their Eq. 9). We find a broad time-dependent distribution for galaxy formation which is the analog of our more empirical and narrower (by a factor of 2 or 3) $P_{obs}(t)$.

We have made the most specific anthropic explanation of the cosmic coincidence using the age distribution of terrestrial planets in our Universe and found this explanation fairly robust to the largely uncertain time it takes observers to evolve. Our main result is an understanding of the cosmic coincidence as a temporal selection effect if observers emerge preferentially on terrestrial planets in a characteristic time $\Delta t_{obs} < 10$ Gyr. Under these plausible conditions, we, and any observers in the Universe who have evolved on terrestrial planets, should not be surprised to find $\Omega_{m_o} \sim \Omega_{\Lambda_o}$.

Acknowledgements We would like to thank Paul Francis and Charles Jenkins for

helpful discussions. CE acknowledges a UNSW School of Physics post graduate fellowship.

Appendix A: Evolution of Densities

Recent cosmological observations have led to the new standard ΛCDM model in which the density parameters of radiation, matter and vacuum energy are currently observed to be $\Omega_{r_o} \approx 4.9 \pm 0.5 \times 10^{-5}$, $\Omega_{m_o} \approx 0.26 \pm 0.03$ and $\Omega_{\Lambda_o} \approx 0.74 \pm 0.03$ respectively and Hubble's constant is $H_o = 71 \pm 3\ kms^{-1}Mpc^{-1}$ (Spergel et al., 2006; Seljak et al., 2006).

The energy densities in relativistic particles ("radiation" i.e., photons, neutrinos, hot dark matter), non-relativistic particles ("matter" i.e., baryons,cold dark matter) and in vacuum energy scale differently (Peacock, 1999),

$$\rho_i \propto a^{-3(w_i+1)}. \tag{2.6}$$

Where the different equations of state are, $\rho_i = w_i\ p$ where $w_{radiation} = 1/3$, $w_{matter} = 0$ and $w_\Lambda = -1$ (Linder, 1997). That is, as the Universe expands, these different forms of energy density dilute at different rates.

$$\rho_r \propto a^{-4} \tag{2.7}$$
$$\rho_m \propto a^{-3} \tag{2.8}$$
$$\rho_\Lambda \propto a^{0} \tag{2.9}$$

Given the currently observed values for Ω_r, Ω_m and Ω_Λ, the Friedmann equation for a standard flat cosmology tells us the evolution of the scale factor of the Universe, and the history of the energy densities:

$$\left(\frac{\dot{a}}{a}\right)^2 = \frac{8\pi G}{3}(\rho_r + \rho_m + \rho_\Lambda) \tag{2.10}$$
$$= \frac{8\pi G}{3}(\rho_{r_o}a^{-4} + \rho_{m_o}a^{-3} + \rho_\Lambda a^0) \tag{2.11}$$
$$= (\Omega_{r_o}a^{-4} + \Omega_{m_o}a^{-3} + \Omega_{\Lambda_o}a^0) \tag{2.12}$$

where we have $\rho_{crit} = \frac{3H(t)^2}{8\pi G}$ and $\Omega_i = \frac{\rho_i}{\rho_{crit}}$. The upper panel of Fig. 2.1 illustrates these different dependencies on scale factor and time in terms of densities while

the lower panel shows the corresponding normalized density parameters. A false vacuum energy $\rho_{\Lambda_{inf}}$ is assumed between the Planck scale and the GUT scale. In constructing this density plot and setting a value for $\Omega_{\Lambda_{inf}}$ we have used the constraint that at the GUT scale, all the energy densities add up to $\rho_{\Lambda_{inf}}$ which remains constant at earlier times.

Appendix B: Tables

Event	Symbol	Time after Big Bang	
		seconds	Gyr
Planck time, beginning of time	t_{Planck}	5.4×10^{-44}	1.7×10^{-60}
end of inflation, reheating, origin of matter, thermalization	t_{reheat}	$[10^{-43}, 10^{-33}]$	$[10^{-60}, 10^{-50}]$
energy scale of Grand Unification Theories (GUT)	t_{GUT}	10^{-33}	10^{-50}
matter-anti-matter annihilation, baryogenesis	$t_{baryogenesis}$	$[10^{-33}, 10^{-12}]$	$[10^{-50}, 10^{-29}]$
electromagnetic and weak nuclear forces diverge	$t_{electroweak}$	10^{-12}	10^{-29}
light atomic nuclei produced	t_{BBN}	$[100, 300]$	$[3, 9] \times 10^{-15}$
radiation-matter equality[1]	t_{r-m}	8.9×10^{11}	2.8×10^{-5}
recombination[1] (first chemistry)	t_{rec}	1.2×10^{13}	0.38×10^{-3}
first thermal disequilibrium	$t_{1sttherm-dis}$	1.2×10^{13}	0.38×10^{-3}
first stars, Pop III, reionization[1]	$t_{1ststars}$	1×10^{16}	0.4
first terrestrial planets[2]	$t_{1stEarths}$	8×10^{16}	2.5
last time r had same value as today	t_{rnow}	1.9×10^{17}	6.1
formation of the Sun, Earth[3]	t_{Sun},t_{Earth}	2.9×10^{17}	9.1
matter-Λ equality[1]	$t_{m-\Lambda}$	3.0×10^{17}	9.4
now	t_o	4.4×10^{17}	13.8
last stars die[4]	$t_{laststars}$	10^{22}	10^{6}
protons decay[4]	$t_{protondecay}$	10^{45}	10^{29}
super massive black holes consume matter[4]	$t_{blackholes}$	10^{107}	10^{91}
maximum entropy (no gradients to drive life)[4]	$t_{heatdeath}$	10^{207}	10^{191}

Table 2.1 Important Times in the History of the Universe. References:
(1) Spergel et al. 2006, http://map.gsfc.nasa.gov/
(2) Lineweaver 2001
(3) Allègre et al. 1995
(4) Adams and Laughlin 1997

Range Δx [a]		$P(r > r_o)$ [%]			
x_{min}	x_{max}	t	$\log(t)$	a	$\log(a)$
t_{rec}	100 Gyr [b]	**8** [c]	7	0.2	6
t_{Planck}	$t_{laststars}$	8×10^{-4}	**0.6** [d]	10^{-10^4}	10^{-3}
t_{Planck}	t_o	**60** [c]	0.6	50	1
t_{Planck}	t_{Planck}^{-1}	30	0.3	30	**0.5** [d]
t_{Planck}	$t_{heatdeath}$	10^{-188}	0.1	$10^{-10^{189}}$	10^{-188}
t_{rec}	$t_{protondecay}$	10^{-26}	1	$10^{-10^{27}}$	10^{-26}
t_{rec}	$t_{blackholes}$	10^{-88}	0.4	$10^{-10^{89}}$	10^{-88}
t_{rec}	$t_{heatdeath}$	10^{-188}	0.2	$10^{-10^{189}}$	10^{-188}
$t_{1ststars}$	$t_{laststars}$	8×10^{-4}	6	10^{-10^4}	10^{-3}
$t_{1ststars}$	$t_{protondecay}$	10^{-26}	1	$10^{-10^{27}}$	10^{-26}
$t_{1ststars}$	$t_{blackholes}$	10^{-88}	0.4	$10^{-10^{89}}$	10^{-88}
$t_{1ststars}$	$t_{heatdeath}$	10^{-188}	0.2	$10^{-10^{189}}$	10^{-188}

Table 2.2 The probability $P(r > r_o)$ of observing $r > r_o$ assuming a uniform distribution of observers P_{obs} in linear time, log(time), scale factor and log(scale factor) within the range Δx listed.

[a] See Table 1 for the times corresponding to columns 1 and 2.

[b] The four values in the top row correspond to Fig. 2.8.

[c] The two values shown in bold in the t column correspond to the two panels of Fig. 2.3.

[d] These values correspond to the two panels of Fig.2.2.

CHAPTER 3

DARK ENERGY DYNAMICS REQUIRED TO SOLVE THE COSMIC COINCIDENCE

Tonight I have a date on Mars.
Tonight I'm gonna get real far.
I'll be leaving Earth behind me.

- Encounter, "Date on Mars"

3.1. Introduction

In 1998, using supernovae Ia as standard candles, Riess et al. (1998) and Perlmutter et al. (1999) revealed a recent and continuing epoch of cosmic acceleration - strong evidence that Einstein's cosmological constant Λ, or something else with comparable negative pressure $p_{de} \sim -\rho_{de}$, currently dominates the energy density of the universe (Lineweaver, 1998). Λ is usually interpreted as the energy of zero-point quantum fluctuations in the vacuum (Zel'Dovich, 1967; Durrer and Maartens, 2007) with a constant equation of state $w \equiv p_{de}/\rho_{de} = -1$. This necessary additional energy component, construed as Λ or otherwise, has become generically known as "dark energy" (DE).

A plethora of observations have been used to constrain the free parameters of the new standard cosmological model, ΛCDM , in which Λ *does* play the role of the dark energy. Hinshaw et al. Hinshaw (2006) find that the universe is expanding at a rate of $H_0 = 71 \pm 4\ km/s/Mpc$; that it is spatially flat and therefore critically dense ($\Omega_{tot0} = \frac{\rho_{tot0}}{\rho_{crit0}} = \frac{8\pi G}{3H_0^2}\rho_{tot0} = 1.01 \pm 0.01$); and that the total density is comprised of contributions from vacuum energy ($\Omega_{\Lambda 0} = 0.74 \pm 0.02$), cold dark matter (CDM; $\Omega_{CDM0} = 0.22 \pm 0.02$), baryonic matter ($\Omega_{b0} = 0.044 \pm 0.003$) and radiation ($\Omega_{r0} = 4.5 \pm 0.2 \times 10^{-5}$). Henceforth we will assume that the universe is flat ($\Omega_{tot0} = 1$) as predicted by inflation and supported by observations.

Two problems have been influential in moulding ideas about dark energy, specifically in driving interest in alternatives to ΛCDM . The first of these problems is concerned with the smallness of the dark energy density (Zel'Dovich, 1967; Weinberg, 1989; Cohn, 1998). Despite representing more than 70% of the total energy of the universe, the current dark energy density is ∼ 120 orders of magnitude smaller than energy scales at the end of inflation (or ∼ 80 orders of magnitude smaller than energy scales at the end of inflation if this occurred at the GUT rather than Planck scale) (Weinberg, 1989). Dark energy candidates are thus challenged to explain why the observed DE density is so small. The standard idea, that the dark energy is the energy of zero-point quantum fluctuations in the true vacuum, seems to offer no solution to this problem.

The second cosmological constant problem Weinberg (2000b); Carroll (2001a); Steinhardt (2003) is concerned with the near coincidence between the current cosmological matter density ($\rho_{m0} \approx 0.26 \times \rho_{crit0}$) and the dark energy density ($\rho_{de0} \approx 0.74 \times \rho_{crit0}$). In the standard ΛCDM model, the cosmological window during which these components have comparable density is short (just 1.5 e-folds of the cosmological scalefactor a) since matter density dilutes as $\rho_m \propto a^{-3}$ while vacuum density ρ_{de} is constant (Lineweaver and Egan, 2007). Thus, even if one explains why the DE density is much less than the Planck density (the smallness problem) one must explain why we happen to live during the time when $\rho_{de} \sim \rho_m$.

The likelihood of this coincidence depends on the range of times during which we suppose we might have lived. In works addressing the smallness problem, Weinberg (1987, 1989, 2000a) considered a multiverse consisting of a large number of big bangs, each with a different value of ρ_{de}. There he asked, suppose that we could have arisen in any one of these universes; What value of ρ_{de} should we expect our universe to have? While Weinberg supposed we could have arisen in another universe, we are simply supposing that we could have arisen in another time. We ask, what time t_{obs}, and corresponding densities $\rho_{de}(t_{obs})$ and $\rho_m(t_{obs})$ should we expect to observe? Weinberg's key realization was that

not every universe was equally probable: those with smaller ρ_{de} contain more Milky-Way-like galaxies and are therefore more hospitable (Weinberg, 1987, 1989). Subsequently, he, and other authors used the relative number of Milky-Way-like galaxies to estimate the distribution of observers as a function of ρ_{de}, and determined that our value of ρ_{de} was indeed likely (Efstathiou, 1995; Martel et al., 1998; Pogosian and Vilenkin, 2007). Our value of ρ_{de} could have been found to be unlikely and this would have ruled out the type of multiverse being considered. Here we apply the same reasoning to the cosmic coincidence problem. Our observerhood could not have happened at any time with equal probability (Lineweaver and Egan, 2007). By estimating the temporal distribution of observers we can determine whether the observation of $\rho_{de} \sim \rho_m$ was likely. If we find $\rho_{de} \sim \rho_m$ to be unlikely while considering a particular DE model, that will enable us to rule out that DE model.

In a previous paper (Lineweaver and Egan, 2007), we tested ΛCDM in this way and found that $\rho_{de} \sim \rho_m$ is expected. In the present paper we apply this test to dynamic dark energy models to see what dynamics is required to solve the coincidence problem when the temporal distribution of observers is being considered.

The smallness of the dark energy density has been anthropically explained in multiverse models with the argument that in universes with much larger DE components, DE driven acceleration starts earlier and precludes the formation of galaxies and large scale structure. Such universes are probably devoid of observers (Weinberg, 1987; Martel et al., 1998; Pogosian and Vilenkin, 2007). A solution to the coincidence problem in this scenario was outlined by Garriga et al. (1999) who showed that if ρ_{de} is low enough to allow galaxies to form, then observers in those galaxies will observe $r \sim 1$.

To quantify the time-dependent proximity of ρ_m and ρ_{de}, we define a proximity parameter,

$$r \equiv \min\left[\frac{\rho_{de}}{\rho_m}, \frac{\rho_m}{\rho_{de}}\right], \tag{3.1}$$

which ranges from $r \approx 0$, when many orders of magnitude separate the two densities, to $r = 1$, when the two densities are equal. The presently observed value of this parameter is $r_0 = \frac{\rho_{m0}}{\rho_{de0}} \approx 0.35$. In terms of r, the coincidence problem is as follows. If we naively presume that the time of our observation t_{obs} has been drawn from a distribution of times $P_t(t)$ spanning many decades of cosmic scalefactor, we find that the expected proximity parameter is $r \approx 0 \ll 0.35$. In the top panel of Fig. 3.1 we use a naive distribution for t_{obs} that is constant in $\log(a)$ to illustrate how observing r as large as $r_0 \approx 0.35$ seems unexpected.

In Lineweaver and Egan (2007) we showed how the apparent severity of the

coincidence problem strongly depends upon the distribution $P_t(t)$ from which t_{obs} is hypothesized to have been drawn. Naive priors for t_{obs}, such as the one illustrated in the top panel of Fig. 3.1, lead to naive conclusions. Following the reasoning of Weinberg (1987, 1989, 2000a) we interpret $P_t(t)$ as the temporal distribution of observers. The temporal and spatial distribution of observers has been estimated using large ($10^{11} M_{\odot}$) galaxies (Weinberg, 1987; Efstathiou, 1995; Martel et al., 1998; Garriga et al., 1999) and terrestrial planets (Lineweaver and Egan, 2007) as tracers. The top panel of Fig. 3.1 shows the temporal distribution of observers $P_t(t)$ from Lineweaver and Egan (2007).

A possible extension of the concordance cosmological model that may explain the observed smallness of ρ_{de} is the generalization of dark energy candidates to include dynamic dark energy (DDE) models such as quintessence, phantom dark energy, k-essence and Chaplygin gas. In these models the dark energy is treated as a new matter field which is approximately homogenous, and evolves as the universe expands. DDE evolution offers a mechanism for the decay of $\rho_{de}(t)$ from the expected Planck scales (10^{93} g/cm^3) in the early universe (10^{-44} s) to the small value we observe today (10^{-30} g/cm^3). The light grey shade in the bottom panel of Fig. 3.1 represents contemporary observational constraints on the DDE density history. Many DDE models are designed to solve the coincidence problem by having $\rho_{de}(t) \sim \rho_m(t)$ for a large fraction of the history/future of the universe (Amendola, 2000a; Dodelson et al., 2000; Sahni and Wang, 2000; Chimento et al., 2000; Zimdahl et al., 2001; Sahni, 2002; Chimento et al., 2003; Ahmed et al., 2004; França and Rosenfeld, 2004; Mbonye, 2004; del Campo et al., 2005; Guo and Zhang, 2005; Olivares et al., 2005; Pavón and Zimdahl, 2005; Scherrer, 2005; Zhang, 2005; del Campo et al., 2006; França, 2006; Feng et al., 2006; Nojiri and Odintsov, 2006; Amendola et al., 2006, 2007; Olivares et al., 2007; Sassi and Bonometto, 2007). With $\rho_{de} \sim \rho_m$ for extended or repeated periods the hope is to ensure that $r \sim 1$ is expected.

Our main goal in this paper is to take into account the temporal distribution of observers to determine when, and for how long, a DDE model must have $\rho_{de} \sim \rho_m$ in order to solve the coincidence problem? Specifically, we extend the work of Lineweaver and Egan (2007) to find out for which cosmologies (in addition to ΛCDM) the coincidence problem is solved when the temporal distribution of observers is considered. In doing this we answer the question, Does a dark energy model fitting contemporary constraints on the density ρ_{de} and the equation of state parameters, necessarily solve the cosmic coincidence? Both positive and negative answers have interesting consequences. An answer in the affirmative will simplify considerations that go into DDE modeling: any DDE model in agreement with current cosmological constraints has $\rho_{de} \sim \rho_m$ for a significant fraction of observers. An answer in the negative would yield a new

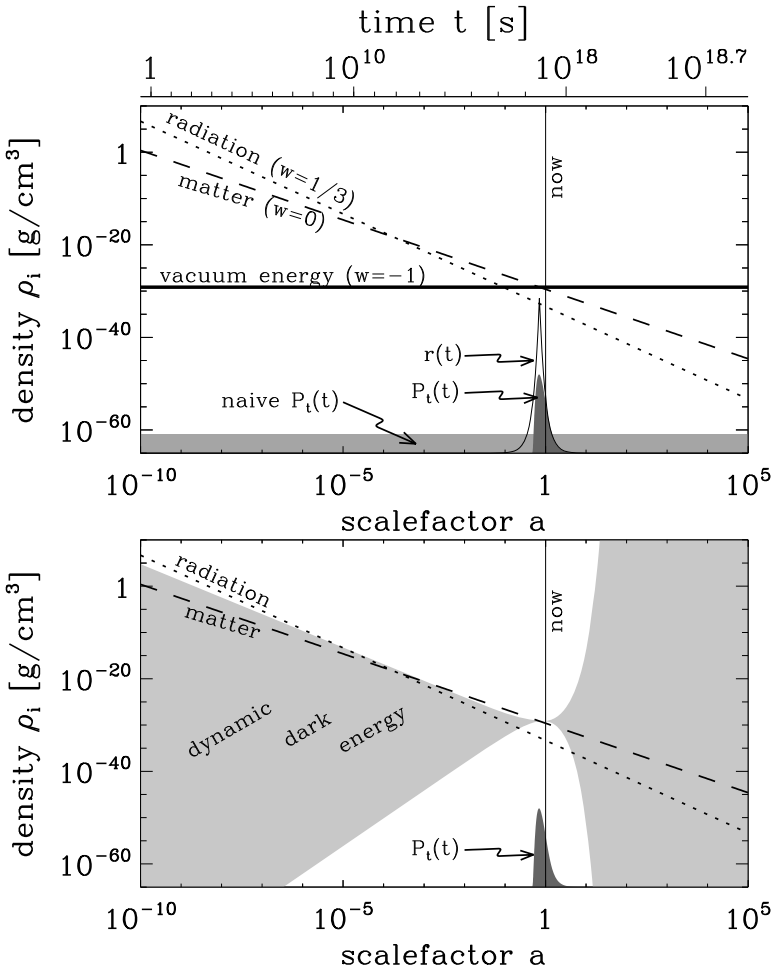

Figure 3.1 **(Top)** The history of the energy density of the universe according to standard ΛCDM . The dotted line shows the energy density in radiation (photons, neutrinos and other relativistic modes). The radiation density dilutes as a^{-4} as the universe expands. The dashed line shows the density in ordinary non-relativistic matter, which dilutes as a^{-3}. The thick solid line shows the energy of the vacuum (the cosmological constant) which has remained constant since the end of inflation. The thin solid peaked curve shows the proximity r of the matter density to the vacuum energy density (see Eq. 3.1). The proximity r is only ~ 1 for a brief period in the $log(a)$ history of the cosmos. Whether or not there is a coincidence problem depends on the distribution $P_t(t)$ for t_{obs}. If one naively assumes that we could have observed any epoch with equal probability (the light grey shade) then we should not expect to observe r as large as we do. If, however, $P_t(t)$ is based on an estimate of the temporal distribution of observers (the dark grey shade) then $r_0 \approx 0.35$ is not surprising, and the coincidence problem is solved under ΛCDM (Lineweaver and Egan, 2007). **(Bottom)** The dark energy density history is modified in DDE models. Observational constraints on the dark energy density history are represented by the light grey shade (details in Section 3.3).

opportunity to constrain the DE equation of state parameters *more strongly* than contemporary cosmological surveys.

A different coincidence problem arises when the time of observation is conditioned on and the parameters of a model are allowed to slide. The tuning of parameters and the necessity to include ad-hoc physics are large problems for many current dark energy models. This paper does not address such issues, and the interested reader is referred to Hebecker and Wetterich (2001), Bludman (2004) and Linder (2006b). In the coincidence problem addressed here we let the time of observation vary to see if $r(t_{obs}) \geq 0.35$ is unlikely according to the model.

In Section 3.2 we present several examples of DDE models used to solve the coincidence problem. An overview of observational constraints on DDE is given in Section 3.3. In Section 3.4 we estimate the temporal distribution of observers. Our main analysis is presented in Section 3.5. Our main result - that the coincidence problem is solved for all DDE models fitting observational constraints - is illustrated in Fig. 3.7. Finally, in Section 3.6, we end with a discussion of our results, their implications and potential caveats.

3.2. Dynamic Dark Energy Models in the Face of the Cosmic Coincidence

Though it is beyond the scope of this article to provide a complete review of DDE (see Copeland et al. (2006); Szydłowski et al. (2006)), here we give a few representative examples in order to set the context and motivation of our work. Fig. 3.2 illustrates density histories typical of tracker quintessence, tracking oscillating energy, interacting quintessence, phantom dark energy, k-essence, and Chaplygin gas. They are discussed in turn below.

3.2.1. Quintessence

In quintessence models the dark energy is interpreted as a homogenous scalar field with Lagrangian density $\mathcal{L}(\phi, X) = \frac{1}{2}\dot{\phi}^2 - V(\phi)$ (Özer and Taha, 1987; Ratra and Peebles, 1988; Ferreira and Joyce, 1998; Caldwell et al., 1998; Steinhardt et al., 1999; Zlatev et al., 1999; Dalal et al., 2001). The evolution of the quintessence field and of the cosmos depends on the postulated potential $V(\phi)$ of the field and on any postulated interactions. In general, quintessence has a time-varying equation of state $w = \frac{p_{de}}{\rho_{de}} = \frac{\dot{\phi}^2/2 - V(\phi)}{\dot{\phi}^2/2 + V(\phi)}$. Since the kinetic term $\dot{\phi}^2/2$ cannot be negative, the

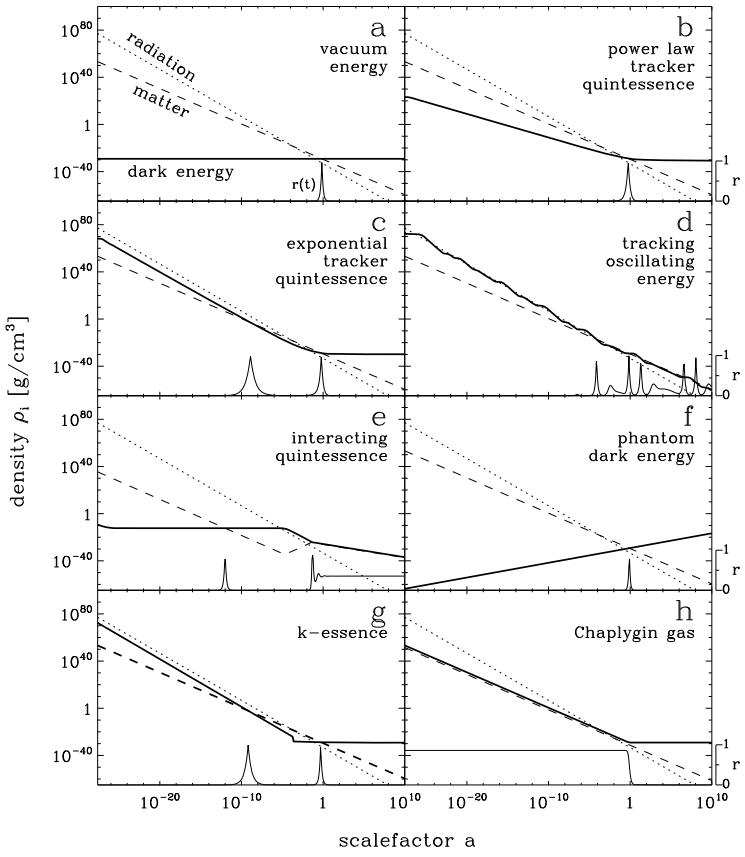

Figure 3.2 The energy density history of the universe according to ΛCDM (panel a), and seven DDE models selected from the literature (see text for references). In each panel the radiation and matter densities are the dotted and dashed lines respectively. The DE density is given by the thick black line. The proximity parameter r is given by the thin black line at the base of each panel. Of the DDE models shown here, tracker quintessence and k-essence (panels b, c and g) have $r \sim 1$ for a small fraction of the life of the universe (whether the abscissa is t, $\log(t)$, a, $\log(a)$, or any other of a large number of measures). On the other hand, tracking oscillating energy, interacting quintessence, phantom DE and Chaplygin gas (panels d, e, f and h) exhibit $r \sim 1$ for a large fraction of the life of the universe. For the phantom DE example (panel f) this is true in t, but not in a or $\log(a)$. In phantom models the future universe grows super-exponentially to $a = \infty$ (a "big-rip") shortly after matter-DE equality. Thus the universe spends a large fraction of *time* with $r \sim 1$, however this is is not seen in $\log(a)$-space. For each of the models in this figure, numerical values for free parameters were chosen to crudely fit observational constraints and are given in Appendix 3.6.

equation of state is restricted to values $w \geq -1$. Moreover, if the potential $V(\phi)$ is non-negative then w is also restricted to values $w \leq +1$.

If the quintessence field only interacts gravitationally then energy density evolves as $\frac{\delta\rho_{de}}{\rho_{de}} = -3(w+1)\frac{\delta a}{a}$ and the restrictions $-1 \leq w \leq +1$ mean ρ_{de} decays (but never faster than a^{-6}) or remains constant (but never increases).

Tracker Quintessence

Particular choices for $V(\phi)$ lead to interesting attractor solutions which can be exploited to make ρ_{de} scale ("track") sub-dominantly with $\rho_r + \rho_m$.

The DE can be forced to transit to a Λ-like ($w \approx -1$) state at any time by fine-tuning $V(\phi)$. In the Λ-like state ρ_{de} overtakes ρ_m and dominates the recent and future energy density of the universe. We illustrate tracker quintessence in Fig. 3.2 using a power law potential $V(\phi) = M\phi^{-\alpha}$ (panel b) (Ratra and Peebles, 1988; Caldwell et al., 1998; Zlatev et al., 1999) and an exponential potential $V(\phi) = M\exp(1/\phi)$ (panel c) (Dodelson et al., 2000).

The tracker paths are attractor solutions of the equations governing the evolution of the field. If the tracker quintessence field is initially endowed with a density off the tracker path (e.g. an equipartition of the energy available at reheating) its density quickly approaches and joins the tracker solution.

Oscillating Dark Energy

Dodelson et al. (2000) explored a quintessence potential with oscillatory perturbations $V(\phi) = M\exp(-\lambda\phi)\left[1 + A\sin(\nu\phi)\right]$. They refer to models of this type as tracking oscillating energy. Without the perturbations (setting $A = 0$) this potential causes exact tracker behaviour: the quintessence energy decays as $\rho_r + \rho_m$ and never dominates. With the perturbations the quintessence energy density oscillates about $\rho_r + \rho_m$ as it decays (Fig. 3.2d). The quintessence energy dominates on multiple occasions and its equation of state varies continuously between positive and negative values. One of the main motivations for tracking oscillating energy is to solve the coincidence problem by ensuring that $\rho_{de} \sim \rho_m$ or $\rho_{de} \sim \rho_r$ at many times in the past or future.

It has yet to be seen how such a potential might arise from particle physics. Phenomenologically similar cosmologies have been discussed in Ahmed et al. (2004); Yang and Wang (2005); Feng et al. (2006).

Interacting Quintessence

Non-gravitational interactions between the quintessence field and matter fields might allow energy to transfer between these components. Such interactions are not forbidden by any known symmetry Amendola (2000b). The primary motivation for the exploration of interacting dark energy models is to solve the coincidence problem. In these models the present matter/dark energy density proximity r may be constant (Amendola, 2000a; Zimdahl et al., 2001; Amendola and Quercellini, 2003; França and Rosenfeld, 2004; Guo and Zhang, 2005; Olivares et al., 2005; Pavón and Zimdahl, 2005; Zhang, 2005; França, 2006; Amendola et al., 2006, 2007; Olivares et al., 2007) or slowly varying (del Campo et al., 2005, 2006).

We plot a density history of the interacting quintessence model of Amendola (2000a) in Fig. 3.2e. This model is characterized by a DE potential $V(\phi) = A\exp[B\phi]$ and DE-matter interaction term $Q = -C\rho_m\dot{\phi}$, specifying the rate at which energy is transferred to the matter fields. The free parameters were tuned such that radiation domination ends at $a = 10^{-5}$ and that $r_{t\to\infty} = 0.35$.

3.2.2. Phantom Dark Energy

The analyses of Riess et al. (2004) and Wood-Vasey et al. (2007) have mildly ($\sim 1\sigma$) favored a dark energy equation of state $w_{de} < -1$. These values are unattainable by standard quintessence models but can occur in phantom dark energy models (Caldwell, 2002), in which kinetic energies are negative. The energy density in the phantom field *increases* with scalefactor, typically leading to a future "big rip" singularity where the scalefactor becomes infinite in finite time. Fig. 3.2f shows the density history of a simple phantom model with a constant equation of state $w = -1.25$. The big rip ($a = \infty$ at $t = 57.5$ Gyrs) is not seen in $\log(a)$-space.

Caldwell et al. (2003) and Scherrer (2005) have explored how phantom models may solve the coincidence problem: since the big rip is triggered by the onset of DE domination, such cosmologies spend a significant fraction of their total time with r large. For the phantom model with $w = -1.25$ (Fig. 3.2f) Scherrer (2005) finds $r > 0.1$ for 12% of the total lifetime of the universe. Whether this solves the coincidence or not depends upon the prior probability distribution $P_t(t)$ for the time of observation. Caldwell et al. (2003) and Scherrer (2005) implicitly assume that the temporal distribution of observers is constant in time (i.e. $P_t(t)$ = constant). For this prior the coincidence problem *is* solved because the chance of observing $r \geq 0.1$ is large (12%). Note that for the "naive $P_t(t)$" prior shown in Fig. 3.1, the solution of Caldwell et al. (2003) and Scherrer (2005)

fails because $r > 0.1$ is brief in $\log(a)$-space. It fails in this way for many other choices of $P_t(t)$ including, for example, distributions constant in a or $\log(t)$.

3.2.3. K-Essence

In k-essence the DE is modeled as a scalar field with non-canonical kinetic energy (Chiba et al., 2000; Armendariz-Picon et al., 2000, 2001; Malquarti et al., 2003). Non-canonical kinetic terms can arise in the effective action of fields in string and supergravity theories. Fig. 3.2g shows a density history typical of k-essence models. This particular model is from Armendariz-Picon et al. (2001) and Steinhardt (2003). During radiation domination the k-essence field tracks radiation sub-dominantly (with $w_{de} = w_r = 1/3$) as do some of the other models in Fig. 3.2. However, no stable tracker solution exists for $w_{de} = w_m (= 0)$. Thus after radiation-matter equality, the field is unable to continue tracking the dominant component, and is driven to another attractor solution (which is generically Λ-like with $w_{de} \approx -1$). The onset of DE domination was recent in k-essence models because matter-radiation equality prompts the transition to a Λ-like state. K-essence thereby avoids fine-tuning in any particular numerical parameters, but the Lagrangian has been constructed ad-hoc.

3.2.4. Chaplygin Gas

A special fluid known as Chaplygin gas motivated by braneworld cosmology may be able to play the role of dark matter *and* the dark energy (Bento et al., 2002; Kamenshchik et al., 2001). Generalized Chaplygin gas has the equation of state $p_{de} = -A\rho_{de}^{-\alpha}$ which behaves like pressureless dark matter at early times ($w_{de} \approx 0$ when ρ_{de} is large), and like vacuum energy at late times ($w_{de} \approx -1$ when ρ_{de} is small). In Fig. 3.2h we show an example with $\alpha = 1$.

3.2.5. Summary of DDE Models

Two broad classes of DDE models emerge from our comparison:

1. In ΛCDM , tracker quintessence and k-essence models, the dark energy density is vastly different from the matter density for most of the lifetime of the universe (panels a, b, c, g of Fig. 3.2). The coincidence problem can only be solved if the probability distribution $P_t(t)$ for the time of observation is narrow, and overlaps significantly with an $r \sim 1$ peak. If $P_t(t)$ is wide,

e.g. constant over the life of the universe in t or $\log(t)$, then observing $r \sim 1$ would be unlikely in these models and the coincidence problem *is not* resolved.

2. Tracking oscillating energy, interacting quintessence, phantom models and Chaplygin gas models (panels d, e, f, h of Fig. 3.2) employ mechanisms to ensure that $r \sim 1$ for large fractions of the life of the universe. In these models the coincidence problem may be solved for a wider range of $P_t(t)$ including, depending on the DE model, distributions that are constant over the whole life of the universe in t, $\log(t)$, a or $\log(a)$.

The importance of an estimate of the distribution $P_t(t)$ is highlighted: such an estimate will either rule out models of the first category because they do not solve the coincidence problem, or demotivate models of the second because their mechanisms are unnecessary to solve the coincidence problem. This analysis does not address the problems associated with fine-tuning, initial conditions or ad hoc mechanisms of many DDE models (Hebecker and Wetterich, 2001; Bludman, 2004; Linder, 2006b).

We leave this line of enquiry temporarily to discuss contemporary *observational* constraints on the dark energy density history, because we wish to test what DE dynamics are required to solve the coincidence, beyond those which models must exhibit to satisfy standard cosmological observations.

3.3. Current Observational Constraints on Dynamic Dark Energy

3.3.1. Supernovae Ia

Observationally, possible dark energy dynamics is explored almost solely using measurements of the cosmic expansion history. Recent cosmic expansion is directly probed by using type Ia supernova (SNIa) as standard candles (Riess et al., 1998; Perlmutter et al., 1999). Each observed SNIa provides an independent measurement of the luminosity distance d_l to the redshift of the supernova z_{SN}. The luminosity distance to z_{SN} is given by

$$d_l(z_{SN}) = (1 + z_{SN}) \frac{c}{H_0} \int_{z=0}^{z_{SN}} \frac{dz}{E(z)} \tag{3.2}$$

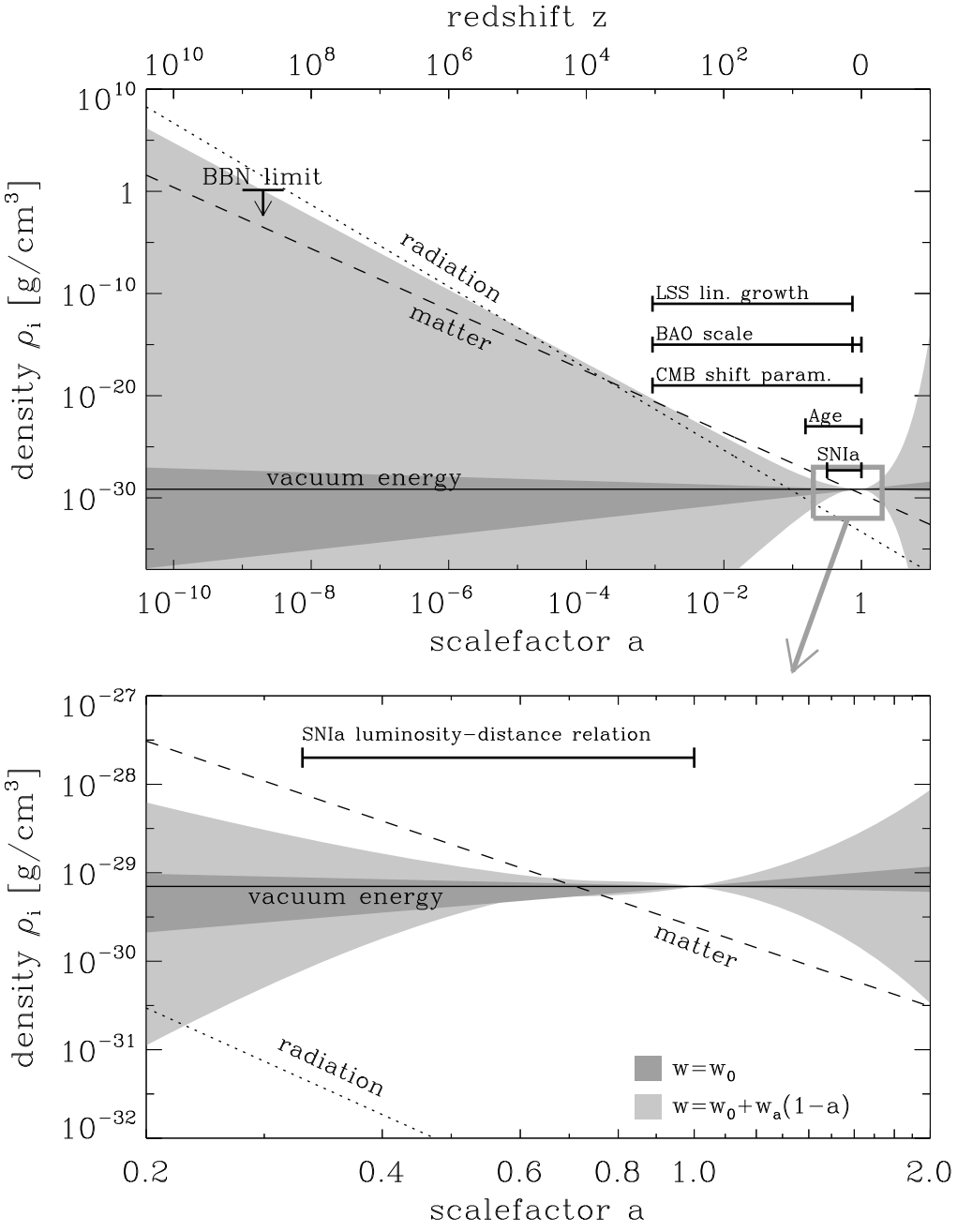

Figure 3.3 The energy densities of radiation ρ_r, matter ρ_m and the cosmological constant ρ_Λ are shown as a function of scalefactor, by the dotted, dashed, and solid lines respectively. Cosmological probes of dark energy include SNIa, CMB, BAO, the LSS linear growth factor and constraints from BBN (see text). Each of these probes is sensitive to the effects of dark energy over different redshift intervals, as indicated. The light grey band envelopes w_0-w_a-parameterized DDE models allowed at $< 2\sigma$ by Davis et al. (2007) (the contour in $w_0 - w_a$ space is shown explicitly in Fig. 3.7). The dark grey band envelopes w_0-parameterized DDE models ($w_a = 0$ assumed) allowed at $< 2\sigma$ by Wood-Vasey et al. (2007). The constraint is $w = -1.09 \pm 0.16$ at 2σ.

where

$$E(z) = \frac{H(z)}{H_0} = \left[\Omega_{r0}(1+z)^4 + \Omega_{m0}(1+z)^3 + \Omega_{de0}\frac{\rho_{de}(z)}{\rho_{de0}}\right]^{\frac{1}{2}} \quad (3.3)$$

and thus depends on H_0, Ω_{m0}, and the evolution of the dark energy $\rho_{de}(z)/\rho_{de0}$. The radiation term, irrelevant at low redshifts, can be dropped from Equation 3.3. Ω_{de0} is a dependent parameter due to flatness ($\Omega_{de0} = 1 - \Omega_{m0}$). Contemporary datasets include $\sim$ 200 supernovae at redshifts $z_{SN} \leq 2.16$ ($a \geq 0.316$) (Astier et al., 2006; Riess et al., 2007; Wood-Vasey et al., 2007) and provide an effective continuum of constraints on the expansion history over that range (Wang and Tegmark, 2005; Wang and Mukherjee, 2006). The redshift range probed by SNIa is indicated in both panels of Fig. 3.3.

3.3.2. Cosmic Microwave Background

The first peak in the cosmic microwave background (CMB) temperature power spectrum corresponds to density fluctuations on the scale of the sound horizon at the time of recombination. Subsequent peaks correspond to higher-frequency harmonics. The locations of these peaks in l-space depend on the comoving scale of the sound horizon at recombination, and the angular distance to recombination. This is summarized by the so-called CMB shift parameter R (Efstathiou and Bond, 1999; Elgarøy and Multamäki, 2007) which is related to the cosmology by

$$R = \sqrt{\Omega_{m0}} \int_{z=0}^{z_{rec}} \frac{dz}{E(z)} \quad (3.4)$$

where $z_{rec} \approx 1089$ (Spergel et al., 2006) is the redshift of recombination. The 3-year WMAP data gives a shift parameter $R = 1.71 \pm 0.03$ (Davis et al., 2007; Spergel et al., 2006). Since the dependence of Equation 3.4 on H_0 and Ω_{m0} differs from that of Equation 3.2, measurements of the CMB shift parameter can be used to break degeneracies between H_0, Ω_{m0} and DE evolution in the analysis of SNIa. In the top panel of Fig. 3.3 we represent the CMB observations using a bar from $z = 0$ to z_{rec}.

3.3.3. Baryonic Acoustic Oscillations and Large Scale Structure

As they imprinted acoustic peaks in the CMB, the baryonic oscillations at recombination were expected to leave signature wiggles - baryonic acoustic

oscillations (BAO) - in the power spectrum of galaxies (Eisenstein and Hu, 1998). These were detected with significant confidence in the SDSS luminous red galaxy power spectrum (Eisenstein et al., 2005). The expected BAO scale depends on the scale of the sound horizon at recombination, and on transverse and radial scales at the mean redshift z_{BAO}, of galaxies in the survey. Eisenstein et al. (2005) measured the quantity

$$A(z_{BAO}) = \frac{\sqrt{\Omega_{m0}}}{E(z_{BAO})^{\frac{1}{3}}} \left[\frac{1}{z_{BAO}} \int_{z=0}^{z_{BAO}} \frac{dz}{E(z)} \right]^{\frac{2}{3}} \tag{3.5}$$

to have a value $A(z_{BAO} = 0.35) = 0.469 \pm 0.017$, thus constraining the matter density and the dark energy evolution parameters in a configuration which is complomentary to the CMB shift parameter and the SNIa luminosity distance relation. Ongoing BAO projects have been designed specifically to produce stronger constraints on the dark energy equation of state parameter w. For example, WIGGLEZ (Glazebrook et al., 2007) will use a sample of high-redshift galaxies to measure the BAO scale at $z_{BAO} \approx 0.75$. As well as reducing the effects of non-linear clustering, this redshift is at a larger angular distance, making the observed scale more sensitive to w. Constraints from the BAO scale depend on the evolution of the universe from z_{rec} to z_{BAO} to set the physical scale of the oscillations. They also depend on the evolution of the universe from z_{BAO} to $z = 0$, since the observed angular extent of the oscillations depends on this evolution. The bar representing BAO scale observations in the top panel of Fig. 3.3 indicates both these regimes.

The amplitude of the BAOs - the amplitude of the large scale structure (LSS) power spectrum - is determined by the amplitude of the power spectrum at recombination, and how much those fluctuations have grown (the transfer function) between z_{rec} and z_{BAO}. By comparing the recombination power spectrum (from CMB) with the galaxy power spectrum, the LSS linear growth factor can be measured and used to constrain the expansion history of the universe (independently of the BAO scale) over this redshift range. In practice, biases hinder precise normalization of the galaxy power spectrum, weakening this technique. The range over which this technique probes the DE is indicated in Fig. 3.3.

3.3.4. Ages

Cosmological parameters from SN1a, CMB, LSS, BAO and other probes allow us to calculate the current age of the universe to be 13.8 ± 0.1 (Hinshaw, 2006) assuming ΛCDM . Uncertainties on the age calculated in this way grow dramatically if we drop the assumption that the DE is vacuum energy ($w = -1$).

An independent lower limit on the current age of the universe is found by estimating the ages of the oldest known globular clusters (Hansen et al., 2004). These observations rule out models which predict the universe to be younger than 12.7 ± 0.7 Gyrs (2σ confidence):

$$\begin{aligned} t_0 &= H_0^{-1} \int_{z=0}^{\infty} \frac{dz}{(1+z)E(z)} \\ &\gtrsim 12.7 \pm 0.7 \text{ Gyrs.} \end{aligned} \tag{3.6}$$

Other objects can also be used to set this age limit Lineweaver (1999), but generally less successfully due to uncertainties in dating techniques.

Assuming ΛCDM , an age of 12.7 Gyrs corresponds to a redshift of $z \approx 5.5$. Contemporary age measurements are sensitive to the dark energy content from $z \approx 5.5$ to $z = 0$. In the top panel of Fig. 3.3 we show this redshift interval. The evolution and energy content of the universe before 12.7 Gyrs ago is not probed by these age constraints.

3.3.5. Nucleosynthesis

In addition to the constraints on the expansion history (SN1a, CMB, BAO and t_0) we know that $\rho_{de}/\rho_{tot} < 0.045$ (at 2σ confidence) during Big Bang Nucleosynthesis (BBN) (Bean et al., 2001). Larger dark energy densities imply a higher expansion rate at that epoch ($z \sim 6 \times 10^8$) which would result in a lower neutron to proton ratio, conflicting with the measured helium abundance, $Y_{\rm He}$.

3.3.6. Dark Energy Parameterization

Because of the variety of proposed dark energy models, it has become usual to summarize observations by constraining a parameterized time-varying equation of state. Dark energy models are then confronted with observations in this parameter space. The unique zeroth order parameterization of w is $w = w_0$ (a constant), with $w = -1$ characterizing the cosmological constant model. The observational data can be used to constrain the first derivative of w. This additional dimension in the DE parameter space may be useful in distinguishing models which have the same w_0. From an observational standpoint, the obvious choice of 1st order parameterization is $w(z) = w_0 + \frac{dw}{dz} z$ (di Pietro and Claeskens, 2003). This is rarely used today since currently considered DDE models are poorly portrayed by this functional form. The most popular parameterization is $w(a) = w_0 + w_a(1-a)$ Albrecht et al. (2006); Linder (2006a), which does not diverge at high redshift.

Linder and Huterer (2005) have argued that the extension of this approach to second order, e.g. $w(a) = w_0 + w_a(1-a) + w_{aa}(1-a)^2$, is not motivated by current DDE models. Moreover, they have shown that next generation observations are unlikely to be able to distinguish the quadratic from a linear expansion of w. Riess et al. (2007) have illustrated this recently using new SN1a.

An alternative technique for exploring the history of dark energy is to constrain $w(z)$ or $\rho_{de}(z)$ in independent redshift bins. This technique makes fewer assumptions about the specific shape of $w(z)$. In the absence of any strongly motivated parameterization of $w(z)$ this bin-wise method serves as a good reminder of how little we actually know from observation. Using luminosity distance measurements from SNIa, DE evolution has been constrained in this way in $\Delta z \sim 0.5$ bins out to redshift $z_{SN} \sim 2$ (Wang and Tegmark, 2004; Huterer and Cooray, 2005; Riess et al., 2007). In the future, BAO measurements at various redshifts may contribute to these constraints, however z_{BAO} will probably never be larger than z_{SN}. Moreover, because the recombination redshift $z_{rec} \approx 1089$ is fixed, only the cumulative effect (from $z = z_{rec}$ to $z = 0$) of the DE can be measured with the CMB and LSS linear growth factor. With only this single data point above z_{SN}, the bin-wise technique effectively degenerates to a parameterized analysis at $z > z_{SN}$.

3.3.7. Summary of Current DDE Constraints

If one assumes the popular $w_0 - w_a$ parameterization until last scattering, then all cosmological probes can be combined to constrain w_0 and w_a. In a recent analysis of SN1a, CMB and BAO observations, Davis et al. (2007) found $w_0 = -1.0 \pm 0.4$ and $w_a = -0.4 \pm 1.8$ at 2σ confidence (the contour is shown in Fig. 3.7). Using the same observations, Wood-Vasey et al. (2007) assumed $w_a = 0$ and found $w = w_0 = -1.09 \pm 0.16$ (2σ).

The evolution of ρ_{de} is related to w by covariant energy conservation (Carroll, 2004)

$$\frac{\delta \rho_{de}}{\rho_{de}} = -3\,(w(a) + 1)\,\frac{\delta a}{a}. \tag{3.7}$$

The dark energy density corresponding to the $w_0 - w_a$ parameterization of w is thus given by

$$\rho_{de}(z) = \rho_{de0}\; e^{3w_a(a-1)}\; a^{-3(1+w_0+w_a)}. \tag{3.8}$$

The cosmic energy density history is illustrated in Fig. 3.3. Radiation and matter densities steadily decline as the dotted and dashed lines. With the DE equation of state parameterized as $w(a) = w_0 + w_a(1-a)$, its density history is constrained

to the light-grey area (Davis et al., 2007). If the evolution of w is negligible, i.e. we condition on $w_a \approx 0$, then $w(a) \approx w_0$ and the DE density history lies within the dark-grey band (Wood-Vasey et al., 2007). If the dark energy is pure vacuum energy (or Einstein's cosmological constant) then $w = -1$ and its density history is given by the horizontal solid black line.

3.4. The Temporal Distribution of Observers

The energy densities ρ_r, ρ_m and ρ_{de}, and the proximity parameter r we imagine we might have observed, depend on the distribution $P_t(t)$ from which we imagine our time of observation t_{obs} has been drawn. What we can expect to observe must be restricted by the conditions necessary for our presence as observers (Carter, 1974). Thus, for example, it is meaningless to suppose we might have lived during inflation, or during radiation domination, or before the first atoms (Dicke, 1961).

We can, however, suppose that we are randomly selected cosmology-discovering observers, and we can expect our observations of ρ_m and ρ_{de} to be typical of observations made by such observers. This is Vilenkin's principle of mediocrity Vilenkin (1995b). Accordingly, the distribution $P_t(t)$ for the time of observation t_{obs} is proportional to the temporal distribution of cosmology-discovering observers (referred to henceforth as simply "observers"). Thus to solve the coincidence problem one must show that the proximity parameter we measure, r_0, is typical of those measured by other observers.

The most abundant elements in the cosmos are hydrogen, helium, oxygen and carbon (Pagel, 1997). In the past decade > 200 extra solar planets have been observed via doppler, transit or microlensing methods. Extrapolation of current patterns in planet mass and orbital period are consistent with the idea that planetary systems like our own are common in the universe (Lineweaver and Grether, 2003). All this does not necessarily imply that observers are common, but it does support the idea that terrestrial-planet-bound carbon-based observers, even if rare, may be the *most common* observers. In the following estimation of $P_t(t)$ we consider only observers bound to terrestrial planets.

3.4.1. First the Planets...

Lineweaver (2001) estimated the terrestrial planet formation rate (PFR) by making a compilation of measurements of the cosmic star formation rate (SFR) and

suppressing a fraction of the early stars $f(t)$ to correct for the fact that the metallicity was too low for those early stars to host terrestrial planetary systems,

$$PFR(t) = const \times SFR(t) \times f(t). \tag{3.9}$$

In Fig. 3.4 we plot the PFR reported by Lineweaver (2001) as a function of redshift, $z = \frac{1}{a} - 1$. As illustrated in the figure, there is large uncertainty in the normalization of the formation history. Our analysis will not depend on the normalization of this function so this uncertainty *will not* propagate into our analysis. There are also uncertainties in the location of the turnover at high redshift, and in the slope of the formation history at low redshift - both of these *will* affect our results.

The conversion from redshift to time depends on the particular cosmology, through the Friedmann equation,

$$\begin{aligned} \left(\frac{da}{dt}\right)^2 &= H(a)^2 a^2 \\ &= H_0^2 \Big[\Omega_{r0} a^{-2} + \Omega_{m0} a^{-1} + \\ &\quad \Omega_{de0} \ \exp[3w_a(a-1)] \ a^{-3w_0 - 3w_a - 1} \Big]. \end{aligned} \tag{3.10}$$

In Fig. 3.5 we plot the PFR from Fig. 3.4 as a function of time assuming the best fit parameterized DDE cosmology.

3.4.2. ... then First Observers

After a star has formed, some non-trivial amount of time Δt_{obs} will pass before observers, if they arise at all, arise on an orbiting rocky planet. This time allows planets to form and cool and, possibly, biogenesis and the emergence observers. Δt_{obs} is constrained to be shorter than the life of the host star. If we consider that our Δt_{obs} has been drawn from a probability distribution $P_{\Delta t_{obs}}(t)$. The observer formation rate (OFR) would then be given by the convolution

$$OFR(t) = const \times \int_0^\infty PFR(\tau) P_{\Delta t_{obs}}(t - \tau) d\tau. \tag{3.11}$$

In practice we know very little about $P_{\Delta t_{obs}}(t)$. It must be very nearly zero below about $\Delta t_{obs} \sim 0.5$ Gyrs - this is the amount of time it takes for terrestrial planets to cool and the bombardment rate to slow down. Also, it must be near zero above the lifetime of a small ($0.1 M_\odot$) star (above ~ 500 Gyrs). If we assume that

our Δt_{obs} is typical, then $P_{\Delta t_{obs}}(t)$ has significant weight around Δt_{obs} = 4 Gyrs - the amount of time it has taken for us to evolve here on Earth.

A fiducial choice, where *all* observers emerge 4 Gyrs after the formation of their host planet, is $P_{\Delta t_{obs}}(t) = \delta(t - 4 \text{ Gyrs})$. This choice results in an OFR whose shape is the same as the PFR, but is shifted 4 Gyrs into the future,

$$OFR(t) = const \times PFR(t - 4 \text{ Gyrs}) \tag{3.12}$$

(see the lower panel of Fig. 3.5). Even for non-standard w_0 and w_a values, this fiducial OFR aligns closely with the $r(t)$ peak and the effect of a wider $P_{\Delta t_{obs}}$ is generally to increase the severity of the coincidence problem by spreading observers outside the $r(t)$ peak. Hence using our fiducial $P_{\Delta t_{obs}}$ (which is the narrowest possibility) will lead to conclusions which are conservative in that they underestimate the severity of the cosmic coincidence. If another choice for $P_{\Delta t_{obs}}$ could be justified, the cosmic coincidence would be more severe than estimated here. We will discuss this choice in Section 3.6.

The OFR is then extrapolated into the future using a decaying exponential with respect to t (the dashed segment in the lower panel of Fig. 3.5). The observed SFH is consistent with a decaying exponential. We have tested other choices (linear & polynomial decay) and our results do not depend strongly on the shape of the extrapolating function used.

The temporal distribution of observers $P_t(t)$ is proportional to the observer formation rate,

$$P_t(t) = const \times OFR(t). \tag{3.13}$$

This observer distribution is similar to the one used by Garriga et al. (1999) to treat the coincidence problem in a multiverse scenario. By comparison, our $OFR(t)$ distribution starts later because we have considered the time required for the build up of metallicity, and because we have included an evolution stage of 4 Gyrs. Our distribution also decays more quickly than theirs does. Some of our cosmologies suffer big-rip singularities in the future. In these cases we truncate $P_t(t)$ at the big-rip.

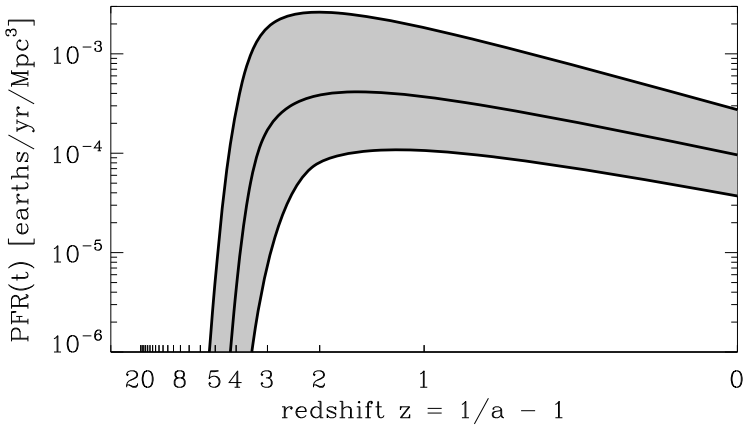

Figure 3.4 The terrestrial planet formation rate as estimated by Lineweaver (2001). It is based on a compilation of SFR measurements and has been corrected for the low metallicity of the early universe, which prevents the terrestrial planet formation rate from rising as quickly as the stellar formation rate at $z \gtrsim 4$.

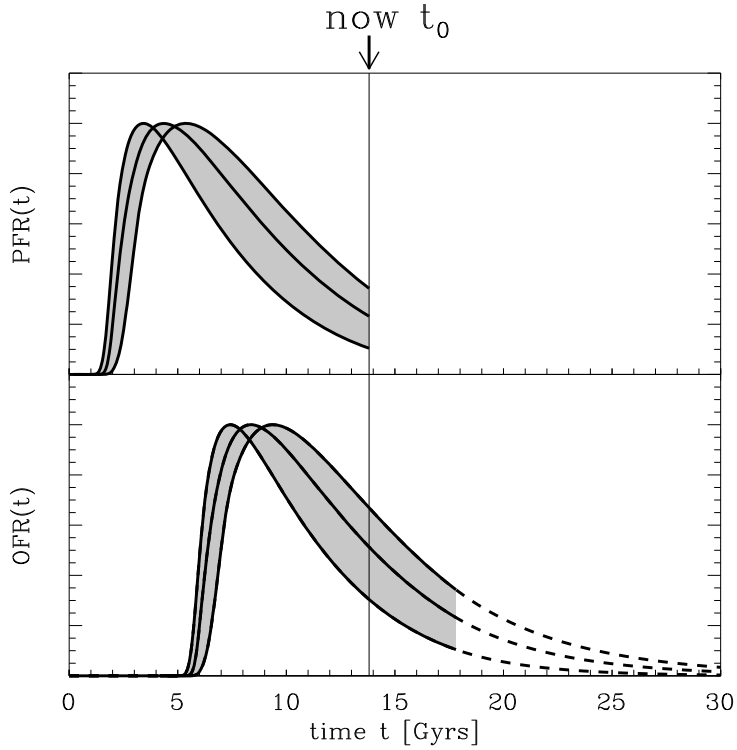

Figure 3.5 The terrestrial planet formation from Fig. 3.4 is shown here as a function of time. The transformation from redshift to time is cosmology dependent. To create this figure we have used best-fit values for the DDE parameters, $w_0 = -1.0$ and $w_a = -0.4$ (Davis et al., 2007). The y-axis is linear (c.f. the logarithmic axis in Fig. 3.4) and the family of curves have been re-normalized to highlight the sources of uncertainty important for this analysis: uncertainty in the width of the function, and in the location of its peak. The observer formation rate (OFR) is calculated by shifting the planet formation rate by some amount Δt_{obs} (= 4 Gyrs) to allow the planet to cool, and the possible emergence of observers. These distributions are closed by extrapolating exponentially in t.

3.5. Analysis and Results: Does fitting contemporary constraints necessarily solve the cosmic coincidence?

For a given model the proximity parameter observed by a typical observer is described by a probability distribution $P_r(r)$ calculated as

$$P_r(r) = \sum \frac{dt}{dr} P_t(t(r)). \tag{3.14}$$

The summation is over contributions from all solutions of $t(r)$ (typically, any given value of r occurs at multiple times during the lifetime of the Universe). In Fig. 3.6 we plot $P_r(r)$ for the $w_0 = -1.0$, $w_a = -0.4$ cosmology. In this case, observers are distributed over a wide range of r values, with 71% seeing $r > r_0$, and 29% seeing $r < r_0$.

We define the severity S of the cosmic coincidence problem as the probability that a randomly selected observer measures a proximity parameter r lower than we do:

$$S = P(r < r_0) = 1 - P(r > r_0) = \int_{r=0}^{r_0} P_r(r) dr. \tag{3.15}$$

For the $w_0 = -1.0$, $w_a = -0.4$ cosmology of Figs. 3.5 and 3.6, the severity is $S = 0.29 \pm 0.09$. This model does not suffer a coincidence problem since 29% of observers would see r lower than we do. If the severity of the cosmic coincidence would be near 0.95 (0.997) in a particular model, then that model would suffer a 2σ (3σ) coincidence problem and the value of r we observe really would be unexpectedly high.

We calculated the severities S for cosmologies spanning a large region of the $w_0 - w_a$ plane and show our results in Fig. 3.7 using contours of equal S. The severity of the coincidence problem is low (e.g. $S \lesssim 0.7$) for most combinations of w_0 and w_a shown. There is a coincidence problem, where the severity is high ($S \gtrsim 0.8$), in two regions of this parameter space. These are indicated in Fig. 3.7.

Some features in Fig. 3.7 are worth noting:

- Dominating the left of the plot, the severity of the coincidence increases towards the bottom left-hand corner. This is because as w_0 and w_a become more negative, the r peak becomes narrower, and is observed by fewer observers.
- There is a strong vertical dipole of coincidence severity centered at ($w_0 = 0, w_a = 0$). For ($w_0 \approx 0, w_a > 0$) there is a large coincidence problem because

in such models we would be currently witnessing the very closest approach between DE and matter, with $\rho_{de} \gg \rho_m$ for all earlier and later times (see Fig. 3.8c). For $(w_0 \approx 0, w_a < 0)$ there is an anti-coincidence problem because in those models we would be currently witnessing the DDE's furthest excursion from the matter density, with ρ_{de} and ρ_m in closer proximity for all relevant earlier and later times, i.e., all times when $P_t(t)$ is non-negligible.

- There is a discontinuity in the contours running along $w_a = 0$ for phantom models ($w_0 < -1$). The distribution $P_t(t)$ is truncated by big-rip singularities in strongly phantom models (provided they remain phantom; $w_a > 0$). This truncation of late-time observers means that early observers who witness large values of r represent a greater fraction of the total population.

To illustrate these features, Fig. 3.8 shows the density histories and observer distributions for four specific examples selected from the $w_0 - w_a$ plane of Fig. 3.7.

We find that *all* observationally allowed combinations of w_0 and w_a result in low severities ($S < 0.4$), i.e., there are large ($> 60\%$) probabilities of observing the matter and vacuum density to be at least as close to each other as we observe them to be.

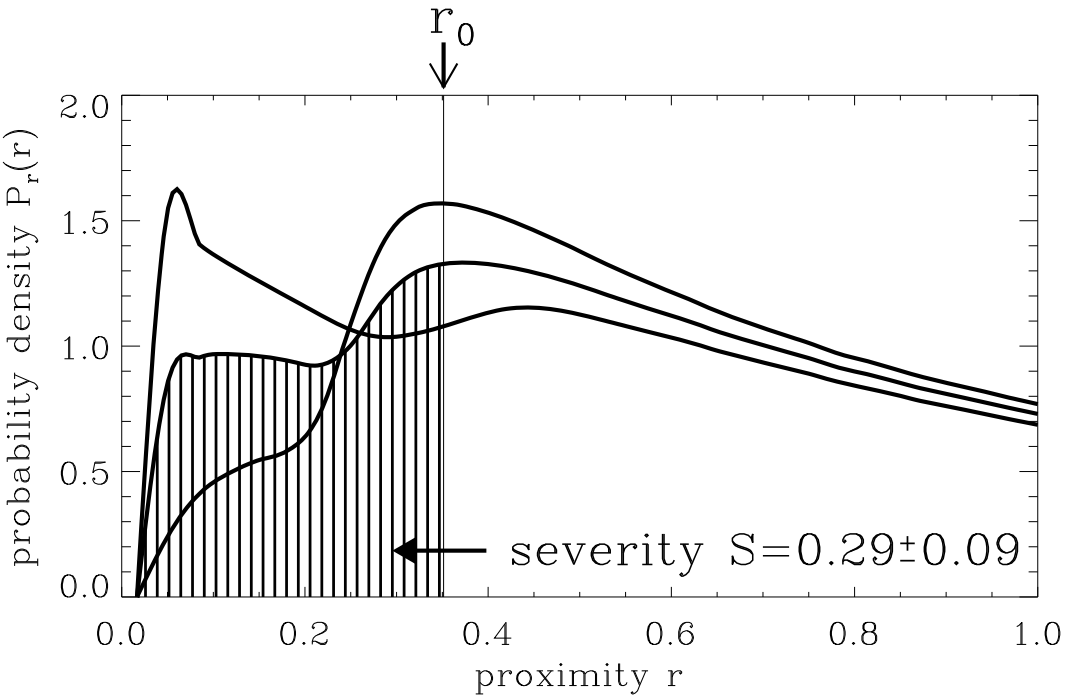

Figure 3.6 The predicted distribution of observations of r is plotted for the parameterized DDE model which best-fits cosmological observations: $w_0 = -1.0$ and $w_a = -0.4$. The proximity parameter we observe $r_0 = \frac{\rho_{m0}}{\rho_{de0}} \approx 0.35$ is typical in this cosmology since only 29% of observers (vertical striped area) observe $r < 0.35$. The upper and lower limits on this value resulting from uncertainties in the SFR are 38% and 20% respectively. Thus the severity of the cosmic coincidence in this model is $S = 0.29 \pm 0.09$. This model does not suffer a coincidence problem.

3.6. Discussion

It was not clear what DDE dynamics were required to solve the coincidence problem. Our analysis might have resulted in new constraints on the values of w_0 and w_a, by simply demanding that we do not live during a special time in which $r \sim 1$. There are regions of $w_0 - w_a$ parameter space that can be ruled out in this manner (see Fig. 3.7) however those points are already strongly excluded by observational constraints on w_0 and w_a. Therefore, the cosmic coincidence problem can not be used as a tool to further constrain DDE since the problem is solved for all DDE models satisfying observational constraints on w_0 and w_a.

The main result of our analysis is that any DDE model in agreement with current cosmological constraints has $\rho_{de} \sim \rho_m$ for a significant fraction of observers.

Interacting quintessence models in which the proximity parameter asymptotes to a constant at late times (Amendola, 2000a; Zimdahl et al., 2001; Amendola and Quercellini, 2003; França and Rosenfeld, 2004; Guo and Zhang, 2005; Olivares et al., 2005; Pavón and Zimdahl, 2005; Zhang, 2005; França, 2006; Amendola et al., 2006, 2007; Olivares et al., 2007) have been proposed as a solution to the coincidence problem. More recently, del Campo et al. (2005, 2006) have argued for a broader class of interacting quintessence models that "soften" the coincidence problem by predicting a very slowly varying (though not constant) proximity parameter. Our analysis finds that r need not asymptote to a constant, nor evolve particularly slowly, partially undermining the motivations for these interacting quintessence models.

Caldwell et al. (2003) and Scherrer (2005) have proposed that the coincidence problem may be solved by phantom models in which there is a future big-rip singularity because such cosmologies spend a significant fraction of their lifetimes in $r \sim 1$ states. In our work $P_t(t)$ is terminated by big-rip singularities in ripping models. In non-ripping models, however, the distribution is effectively terminated by the declining star formation rate. Therefore the big-rip gives phantom models only a marginal advantage over other models. This marginal advantage manifests as the discontinuity along $w_a = 0$ on the left side of Fig. 3.7.

We could improve our analysis, in the sense of getting tighter coincidence constraints (larger severities), if we used a less conservative $P_{\Delta t_{obs}}$. We used the most conservative choice - a delta function - because the present understanding of the time it takes to evolve into observers is too poorly developed to motivate any other form of $P_{\Delta t_{obs}}$. Another possible improvement is the DE equation of state parameterization. We used the current standard, $w = w_0 + w_a(1 - a)$, which may not parameterize some models well for very small or very large values of a.

We conclude that DDE models need not be fitted with exact tracking or oscillatory behaviors specifically to solve the coincidence by generating long or repeated periods of $\rho_{de} \sim \rho_m$. Also, particular interactions guaranteeing $\rho_{de} \sim \rho_m$ for long periods are not well motivated. Moreover phantom models have no significant advantage over other DDE models with respect to the coincidence problem discussed here.

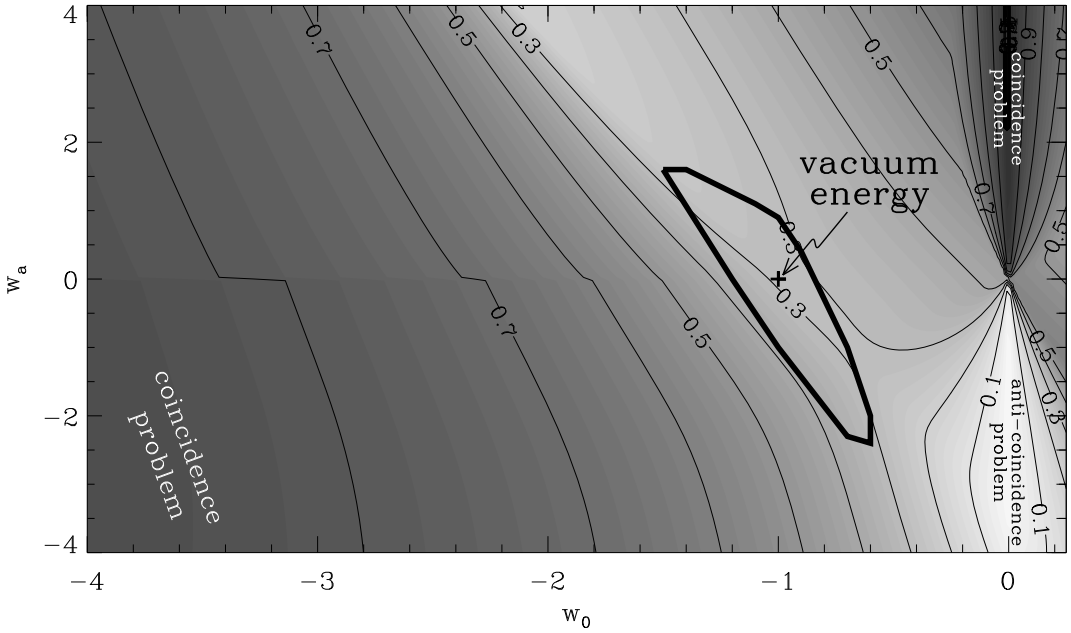

Figure 3.7 Here we plot contours of equal severity S in $w_0 - w_a$ parameter space. S is the fraction of observers who see $r < r_0$. If S is large, a large percentage of observers should see r lower than we do - those models suffer coincidence problems. The thick black contour represents the observational constraints on w_0 and w_a from Davis et al. (2007) (2σ confidence and marginalized over other uncertainties). In Lineweaver and Egan (2007) we showed that the severity of the coincidence problem is low for ΛCDM (indicated by the "+"). Values of w_0 and w_a that result in a mild coincidence problem (e.g. $S \gtrsim 0.7$) are already strongly excluded by observations. This leads to our main result: none of the models in the observationally allowed regime suffer a cosmic coincidence problem when our estimate of the temporal distribution of observers $P_{obs}(t)$ is used as a selection function.

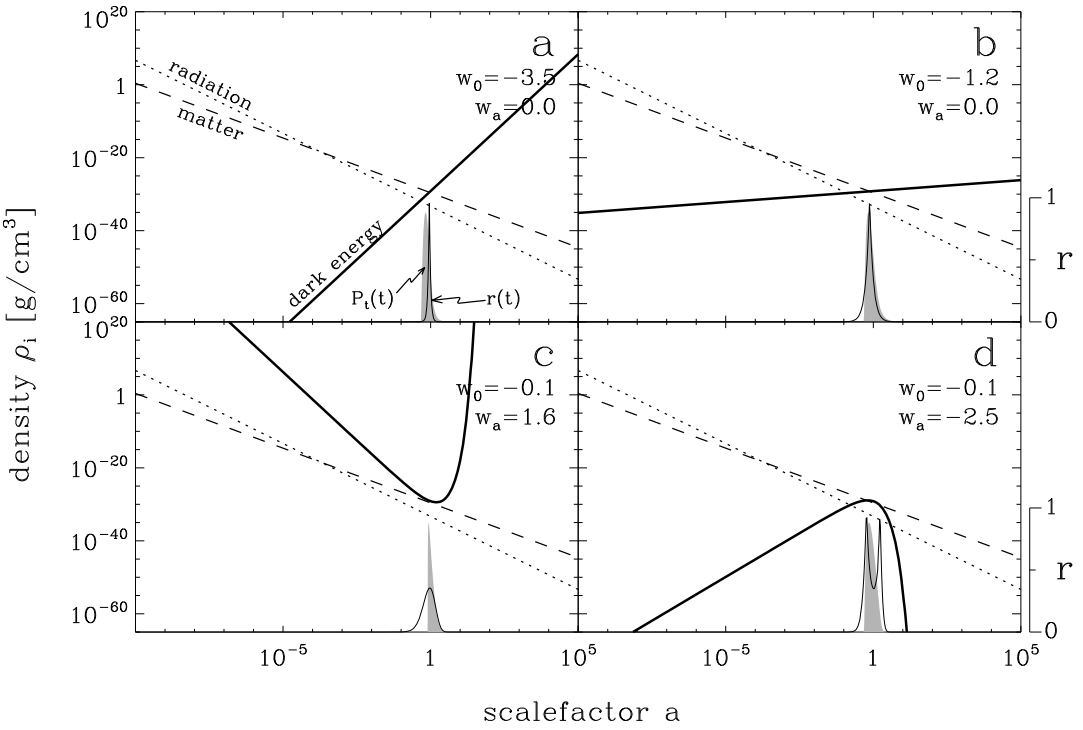

Figure 3.8 History of the energy densities in radiation (dotted line), matter (dashed line) and dark energy (thick black line) for four parameterized DE models from Fig. 3.7. The proximity parameter r (thin black line) and the temporal distribution of observers $P_t(t)$ (grey shade) are also given. **Panel a** shows a phantom model with a constant equation of state $w = -3.5$. In this model the phantom density increases quickly and the $r(t)$ peak is narrow. As a result, a large fraction of observers live while the matter and dark energy densities are vastly different ($r \approx 0$) and there is a mild coincidence problem ($S \approx 0.8$). This might be used to rule-out the model shown in Panel a, except that it is already strongly excluded by direct cosmological observations (refer to Fig. 3.7). **Panel b** shows a phantom model which lies within the observationally allowed 2σ region. There is no coincidence problem in this model ($S \approx 0.4$). **Panel c** shows a model in which there is a coincidence problem ($S \approx 0.95$). This models lies within the cluster of contours in the upper right-hand corner of Fig. 3.7. In this model the dark energy dominates the past *and* future energy budget. Again however, the coincidence problem can tell us nothing new, as this model is already strongly excluded by observations. **Panel d** shows a model in which there is an anti-coincidence problem. This models lies within the cluster of contours in the lower right-hand corner of Fig. 3.7. In this model the dark energy and matter densities are more similar (r is greater) in the recent past and near future (although $r \to 0$ further into the past or future). According to the observer distribution $P_t(t)$ most observers live near the current epoch, during $r > 0.35$, with just 7% living during $r < 0.35$ ($S = 0.07$) in this particular model. One might argue that this model can be ruled out because our value of r is anomalously small. However, this model too is already strongly excluded by observations.

ACKNOWLEDGMENTS

CE acknowledges a UNSW School of Physics postgraduate fellowship. CE thanks the ANU's RSAA for its kind hospitality, where this research was carried out.

Appendix A: Numerical Values for Parameters of Models Illustrated in Fig. 3.2

Model	Parameter	Value
power law tracker quintessence	α	2
	M	1.4×10^{-124}
exponential tracker quintessence	M	1.3×10^{-124}
tracking oscillating energy	M	1.8×10^{-126}
	λ	4
	A	0.99
	ν	2.7
interacting quintessence	A	1.4×10^{-119}
	B	9.7
	C	16
Chaplygin gas	α	1
	A	2.8×10^{-246}

Table 3.1 Free parameters of the DDE models illustrated in Fig. 3.2. These values were chosen such that observational constraints are crudely satisfied. These are by no means the only combinations fitting observations. These values are intended for the purposes of illustration in Fig. 3.2. Units are Planck units.

CHAPTER 4

COMPARING THE SUN TO OTHER STARS: SEARCHING FOR LIFE TRACERS AMONGST THE SOLAR PROPERTIES

Here comes the Sun,
here comes the Sun,
and I say it's alright.

- The Beatles, "Here Comes the Sun"

4.1. Introduction

In the past decade the first several hundred extra-solar planets have been detected using various techniques. These techniques are all biased towards massive planets in small orbits (so-called hot Jupiters). The next generation of projects (including NASA's Terrestrial Planet Finder and ESA's Darwin Project) is eagerly anticipated, with the discovery of Earth-like planets orbiting within habitable zones expected. In the mean time, the search for solar twins (stars with properties most like those of the Sun) in stellar surveys, continues. The reason behind our fascination with

Earth-like planets and Sun-like stars is that without a thorough understanding of the requirements of life, a reasonable strategy in the search for extra terrestrial life is to look in environments that we know are capable of hosting life, i.e. those planets and stars which are most like our own.

If the emergence of life and observers on a planet depends on special properties of the planet's host star, then we would expect our Sun to exhibit those properties and stand out when compared to a sample of randomly selected stars. In this way, the comparison of the Sun to other stars may be a way of identifying stellar properties important to the origin of life and the evolution of observers.

What we stand to gain by looking for anomalous properties in the Sun are statements about the dependence of life on various stellar properties (the reliability of which can be quantified). Such information could be used to improve searches for life in the universe by focussing them on the most important properties.

An early example of this type of work is Gonzalez (1999a,b) who proposed, based on his findings that the Sun was more massive than 91% of all stars, that life may exist preferentially around high-mass stars.

Taken together however, previous work of this type is inconsistent in its conclusions. While Gonzalez (1999a,b); Gonzalez et al. (2001) suggested the Sun to be anomalous, Gustafsson (1998); Allende Prieto (2006) found it to be typical. These discrepancies result from inconsistent use of language, stellar sample selection and inconsistency in the choice of stellar/solar properties compared.

In order to clarify these issues we have undertaken a joint 11-parameter χ^2 analysis that compares the Sun to representative samples of stars in 11 independent properties plausibly related to life and habitability. The analysis quantifies the degree of (a)typicality of the Sun and draws conclusions about the legitimacy of postulated links between particular properties and habitability.

4.2. Selection of Solar Properties and Stellar Samples

Since the purpose of our analysis is to identify significantly anomalous solar properties (or a lack thereof), it is important that our selection criteria is not dependent on any prior knowledge we may have about the (a)typicality of the Sun with respect to its properties. Intentionally selecting one (or a few) parameters in which the Sun is known to be anomalous would pre-load the result.

Suppose, for example, that the Sun has previously been compared to repres-

entative samples of stars in 20 uncorrelated parameters, none of which play any significant role in determining habitability. It should be expected that the Sun is a 2σ (95-percentile) outlier in one in these parameters (call it X) just by pure chance. If the present analysis were conducted using just X, naive that X had been selected, the results would erroneously suggest that X was related to habitability.

On the other hand, the indiscriminant inclusion of properties unlikely to have any connection to habitability could dilute a legitimate signal. Suppose that Y is a stellar property, and that only stars in the upper 2.5% with respect to Y are capable of hosting life (the upper 2.5% are amongst the 95-percentile outliers). The 2σ signal can be diluted away by including $\sim 1/0.05 = 20$ other parameters (and can be reduced to a 90% signal by including just 2 other parameters).

No single stellar survey contains unbiased measurements in as many parameters as we are interested in, and for this reason we have used different stellar samples for each parameter. The benefit of being able to choose the best available sample for each parameter comes at a cost, which is that we must eliminate any correlated parameters from our analysis.

With the above considerations in mind, we have included 11 maximally uncorrelated stellar properties all of which are plausibly related to habitability and for which a sufficiently large unbiased sample of stellar values exists. The included properties come from a full set of 23 candidates (refer to Robles et al. (2008b) for the full list and correlation analysis). Below we give a brief description of the 11 included properties, along with a brief description of their relevance to habitability and a description of the stellar samples we have used for each.

1. Mass: The mass of a star is arguably the most important property of a star. It determines luminosity, temperature and main sequence longevity, in turn influencing conditions and stability in the circumstellar habitable zone. Low mass stars are intrinsically dim, so large stellar samples are biased towards high-mass stars. We have used the nearest 125 stars from the RECONS compilation (Henry, 2006), which is complete to 7.1 *pc*.

2. Age: If the evolution of observers takes (on average) much longer than typical lifetime of a star (Carter, 1983) then observers may be expected to arise preferentially around older stars. We construct an age distribution for stars in the galaxy using galactic star formation history from Rocha-Pinto et al. (2000). Their star formation history is based on chromospheric ages of 552 dwarf stars at up to 200 *pc*, and has been corrected for scale-height, stellar evolution and volume incompleteness. We also consider the cosmic age distribution, using the cosmic star formation history from Hopkins

(2006).

3. Metallicity [Fe/H]: A star's iron content is a good proxy for its abundance in other elements heavier than helium. With regard to this analysis, metallically is correlated with abundance of the ingredients for terrestrial planets (O, Fe, Si and Mg) and life (C, O, N and S). We use the sample of 453 FGK stars of Grether and Lineweaver (2006, 2007) selected from the Hipparcos catalogue. This sample is complete to 25 *pc* for stars within the spectral range *F7-K3* and absolute magnitude of $M_V \geq 8.5$ (Reid, 2002) and contains metallicities derived from a range of spectroscopic and photometric surveys.

4. Carbon-to-oxygen ratio [C/O]: The relative abundance of carbon to oxygen impacts the abundance of oxygen (and the balance of REDOX chemistry) in the circumstellar habitable zone. If [C/O] is higher than 1, most oxygen forms carbon monoxide which is subsequently cleared by stellar winds leaving a chemically reducing habitable zone (Kuchner and Seager, 2005). For our stellar distribution in [C/O] we use 256 stars from Gustafsson et al. (1999); Reddy et al. (2003); Bensby and Feltzing (2006).

5. Magnesium-to-silicon ratio [Mg/Si]: After [Fe/H] and [C/O], the magnesium to silicon ratio is the next most important elemental abundance ratio, also impacting terrestrial planet chemistry. Our stellar distribution in [Mg/Si] consists of 231 stars from Reddy et al. (2003); Bensby et al. (2005).

6. Rotational velocity $v \sin i$: The rotational velocity of a star is related to the angular momentum of the protoplanetary disk. A low rotational velocity may be correlated with the presence of planets (Soderblom, 1983). We use the subset of 276 stars in the 0.9-1.1$M_\odot$ mass range from the sample of Valenti and Fischer (2005). By cutting near the solar value in mass we minimize the effects of a known correlation between stellar mass and $v \sin i$ which becomes significant at higher masses.

7. Eccentricity of the star's galactic orbit e: The galactic orbit of a star determines the stellar environments that the star passes through. Stars with highly eccentric orbits pass closer to the galactic center where the risk of a nearby supernova, and the flux of potentially harmful radiation is higher. We use the distribution of stellar eccentricities from 1987 stars witin 40 *pc* as computed by Nordström et al. (2004).

8. Maximum height away from the galactic plane $Z_{\max}$: As the Sun oscillates through the thin disk of the galaxy objects in the Oort cloud may be disrupted by tidal gravitational forces. It is plausible that the frequency of such disruptions (for which $Z_{\max}$ is a proxy) influences the frequency of

impacts on planets in the habitable zone. For $Z_{\max}$ we use the same stellar sample as we did for eccentricity.

9. Mean galactocentric radius R_{Gal}: The mean galactocentric radius is the most important of a star's galactic orbital properties. It determines (to a greater degree than eccentricity for typical eccentricities) the minimum approach to the galactic center, the risk of nearby supernova, and the flux of potentially harmful radiation from the galactic center. Our distribution of R_{Gal} is based on the model of Bahcall and Soneira (1980) assuming a scale length of 3.0 ± 0.4 *kpc* (Gould et al., 1996).

10. The stellar mass of the star's host galaxy M_{gal}: This influences the overall (galactic) metallically, including the metallically of the star's neighbourhood. We construct a distribution of M_{gal} based on the *K*-band luminosity function of Loveday (2000) and assume a constant stellar-mass-to-light ratio of 0.5 (Bell and de Jong, 2001). It is important to note that we are interested in the distribution of stars in M_{gal}, not the distribution of galaxies in M_{gal}.

11. The stellar mass of the star's host group of galaxies M_{group}: This is correlated with the density of the galactic environment. This influences the stability of the host galaxy. We use the *B*-band luminosity distribution of galactic groups from the 2dFGRS Percolation-Inferred Galaxy Groups catalogue (Eke et al., 2004) and assume a constant stellar-mass-to-light ratio of 1.5 (Bell and de Jong, 2001). As for host galaxy mass, we are interested in the distribution of stars in M_{group}, not the distribution of groups in M_{group}.

4.3. Analysis and Results

The solar values $x_{\odot,i}$ of the selected properties $i = 1, 11$ are taken (or derived from related properties) from the literature. The solar values are shown in Table 4.1.

We find the median $\mu_{1/2,i}$ and the 16^{th} and 84^{th} percentiles for each of the distributions. 68% of a distribution is between the 16^{th} and 84^{th} percentiles, and in the case of a Gaussian distribution this interval corresponds to the $\pm 1\sigma$ interval.

Our distributions are generally asymmetric. Since we are calculating the deviation of the Sun from the mean stellar sample we are most interested in the width of the distributions in the direction of the solar value. We define $\sigma_{68,i}$ as the difference between the median and the 16^{th} or 84^{th} percentile, depending on whether the solar value is below or above the median.

i	Parameter [*units*]	Solar Value $x_{\odot,i}$	Median Value $\mu_{1/2,i}$	$\sigma_{68,i}$
1	Mass [$M_\odot$]	1^a	0.33	0.37
2	Age [Gyr]	$4.9^{3.1}_{2.7}{}^b$	5.4	3.25
3	[Fe/H]	0^a	-0.08	0.20
4	[C/O]	0^a	0.07	0.09
5	[Mg/Si]	0^a	0.01	0.04
6	$v \sin i$ [$km\ s^{-1}$]	1.28^c	2.51	1.27
7	e	0.036 ± 0.002^d	0.10	0.05
8	$Z_{\max}$ [kpc]	0.104 ± 0.006^e	0.14	0.10
9	$R_{\rm Gal}$ [kpc]	7.62 ± 0.32^f	4.9	5.03
10	$M_{\rm Gal}$ [$M_\odot$]	$10^{10.55\pm0.16}{}^g$	$10^{10.2}$	0.47^α
11	$M_{\rm group}$ [$M_\odot$]	$10^{10.91\pm0.07}{}^h$	$10^{11.1}$	0.47^α

Table 4.1 The solar values of the 11 properties included in this analysis.
a. By definition.
b. Chromospheric age of the Sun from Wright et al. (2004).
c. Rotational velocity at the surface is $v = 1.63\ km\ s^{-1}$ (Valenti and Fischer, 2005). We calculate a $v \sin i$ which may be compared to our stellar $v \sin i$ distribution by apply a factor of $\frac{\pi}{4}$ (the average over of $\sin i$ over a 3-sphere; this simulates randomizing the inclination at which the Sun is viewed).
d. The eccentricity of the Sun's galactic orbit is calculated from solar motion reported in Dehnen and Binney (1998).
e. Found by integrating the solar orbit in the galactic potential (initial motion as reported in Dehnen and Binney (1998)).
f. Eisenhauer et al. (2005)
g. Derived in the same way as our distribution: by applying a 0.5 stellar-mass-to-light ratio to the K-band luminosity. The K-band luminosity is inferred from the V-band measured by Courteau and van den Bergh (1999) using the mean color of an Sbc spiral galaxy from the 2MASS Large Galaxy Atlas (Jarrett et al., 2003) and the color conversion prescription of Driver et al. (1994).
h. Derived in the same way as our distribution: by applying a 1.5 stellar-mass-to-light ratio to the B-band luminosity of 2PIGG and Local Group galaxies from Courteau and van den Bergh (1999).
α. These distributions span several orders of magnitude and are analyzed in $\log_{10}$-space. The $\sigma_{68,i}$ values for $M_{\rm Gal}$ and $M_{\rm group}$ represent widths measured in $\log_{10}$-space.

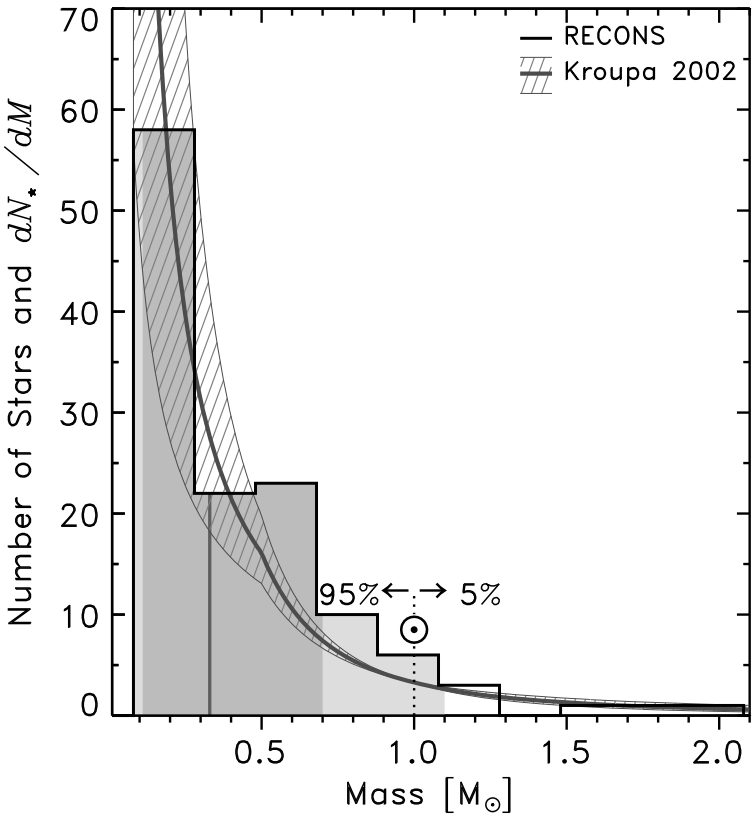

Figure 4.1 The histogram shows the masses of the volume complete sample of 125 stars from RECONS (Henry, 2006). The median of the distribution is indicated by the vertical grey line, and the 68% and 95% intervals are represented by the dark grey and light grey shades respectively. The Sun, indicated by the "⊙", is found to be more massive than 95 ± 2% of stars in the Universe when the RECONS sample is used to represent the cosmic distribution of stellar mass. We have also over-plotted the initial mass function (Kroupa, 2002), which we have normalized to 125-stars for the purposes of this plot. The initial mass function may be expected to trace the stellar mass function, since stars with masses lower than $\sim 1 M_\odot$ have main sequence lifetimes longer than the age of the Universe. We find good agreement between the histogram and the IMF: the Sun is more massive than 94 ± 2% of all stars when the IMF is used instead of the RECONS sample.

The medians $\mu_{1/2,i}$ and widths $\sigma_{68,i}$ of the stellar distributions are shown in the last two columns of Table 4.1. Figures 4.1, 4.2 and 4.3 show the stellar distributions in first three properties: mass, age and metallicity. These figures have been included as examples. The equivalent figures for parameters 4-11 are omitted from this summary, but can be found in the reviewed publication of this work (Robles et al., 2008b).

We compute the combined deviation of the solar properties from those of an average star using the χ^2 statistic.

$$\chi^2_\odot = \sum_{i=1}^{N=11} \frac{(x_{\odot,i} - \mu_{1/2,i})^2}{\sigma^2_{68,i}} \tag{4.1}$$

While uncertainties in the solar values are propagated directly, we employ a bootstrap (Efron, 1979) to account for the uncertainties in $\mu_{1/2,i}$ and $\sigma_{68,i}$ due to small number statistics. This involves randomly repeatedly resampling the distributions (from the original samples, but allowing the same star to be drawn multiple times), and calculating the corresponding $\mu_{1/2,i}$, $\sigma_{68,i}$ and $\chi^2_\odot$ each time.

We find the combined 11-parameter solar chi-square to be

$$\chi^2_\odot = 8.39 \pm 0.96. \tag{4.2}$$

The probability of selecting, at random, a star which is more normal than the Sun (a star with a lower χ^2) can be calculated using the standard χ^2 distribution for 11 degrees of freedom.

$$P(< \chi^2_\odot | N = 11) = 0.32 \pm 0.09 \tag{4.3}$$

The probability calculated above relies on the assumption that our 11 properties are normally distributed. Since several of our distributions are poorly approximated by Gaussians (for example age, see Figure 4.2), we have performed a Monte Carlo simulation (Metropolis and Ulam, 1949) to calculate a more accurate value of P. In the Monte Carlo simulation a large number of stars are randomly selected from our distributions and their χ^2 are calculated (according to equation 4.1). In this way we find that the probability of randomly selecting a star more normal than the Sun is

$$P_{MC}(< \chi^2_\odot | N = 11) = 0.29 \pm 0.11. \tag{4.4}$$

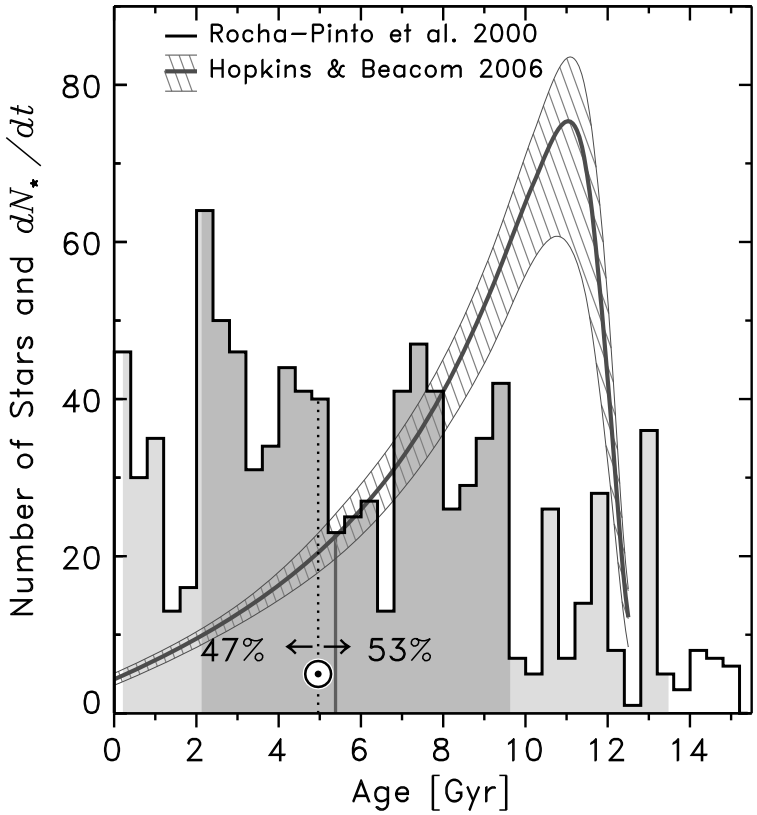

Figure 4.2 The distribution of ages of stars in our galaxy (the histogram) is inferred from the galactic star formation history of Rocha-Pinto et al. (2000). The Sun is found to be younger than $53 \pm 2\%$ of stars in the disk of the galaxy. The distribution of cosmic stellar ages from the cosmic star formation history of Hopkins (2006) (over-plotted) peaks at around 10 *Gyrs*, representing the burst of star formation associated with giant ellipticals 1-4 *Gyrs* after the big bang. The Sun is younger than $86 \pm 5\%$ of stars in the Universe.

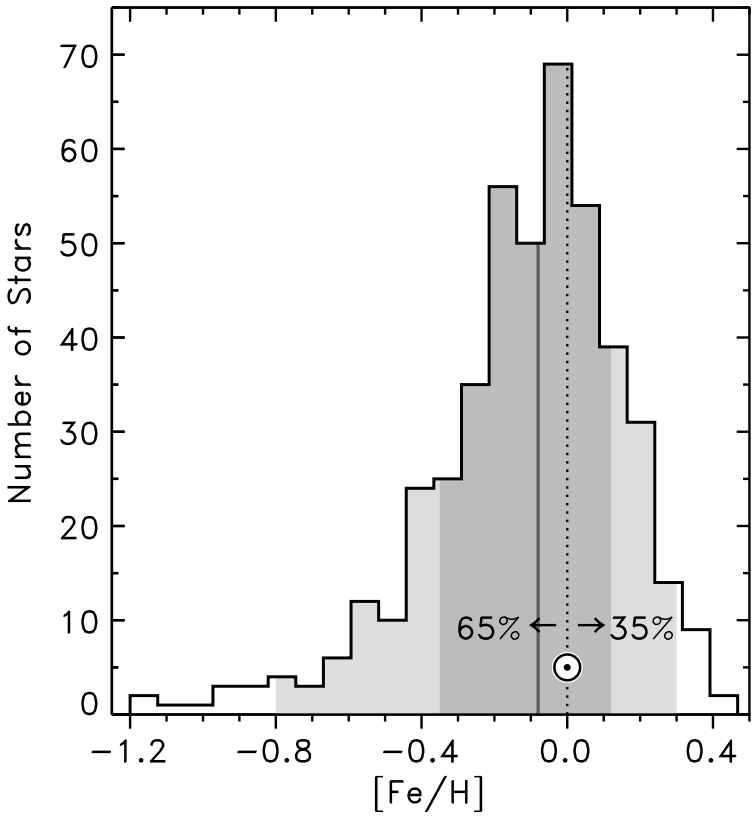

Figure 4.3 The distribution of stellar metallicities [Fe/H], represented by 453 FGK Hipparcos stars selected by Grether and Lineweaver (2007). The Sun's metallicity is higher than 65 ± 2% of other stars.

4.4. Discussion

Of the 11 stellar properties included in this study, the Sun is most anomalous in its mass (more massive than $95 \pm 2\%$ stars in our sample), in the eccentricity of its galactic orbit (which is lower than $93 \pm 1\%$ of stars in our sample) and in its rotational velocity (which is slower than $83 \pm 7\%$ of stars in our sample). Panel A of figure 4.4 illustrates how the solar values compare to the 68% and 95% intervals for each of the parameters. The levels of solar anomaly for each of the properties are shown in Panel D as a percentile, and in terms of the number of standard deviations from the median.

When mass, eccentricity and rotational velocity are combined with our other parameters, which are also plausibly related to habitability, the Sun looks entirely mediocre. The probability of selecting a star, at random, which is more typical than the Sun with respect to these parameters is only $23 \pm 11\%$.

This result undermines suggestions that an anthropic explanation is required for the Sun's unusually large mass. The alternative explanation, which is defended by our results is that in measuring the properties of the Sun we have come across a few mild outliers - as few and as mild as we should expect for a random star, given the number of properties measured. A convenient visualization of this is given in Panel C of figure 4.4. The 11 properties are arranged in decreasing order of $n\%$, where $n\%$ is the percentage of stars with sub-solar values in a given property. When arranged in this way, we expect the parameters to be near the line given by

$$n_{j,\text{expected}}\% = \left[1 - \frac{(j - 1/2)}{N}\right] \times 100\% \tag{4.5}$$

where $N = 11$ is the number of parameters. Any anomalies that cannot be attributed to noise would appear up as points significantly far from the line.

We have repeated the analysis without mass and eccentricity and find the Sun to be unexpectedly average: only $7 \pm 4\%$ of stars are more average than the Sun with respect to the remaining 9 parameters. This supports the proposition that the anomalies observed in mass and eccentricity are expected by pure chance. By including just mass and eccentricity, we find that the Sun is more anomalous than $94 \pm 4\%$ of stars. This would be some evidence (2σ) for an anthropic explanation for one or both of these properties, if they had not been selected to ensure this result.

Our parameter selection criteria selected a larger number of properties plausibly related to life. Without strong evidence suggesting that any are more important

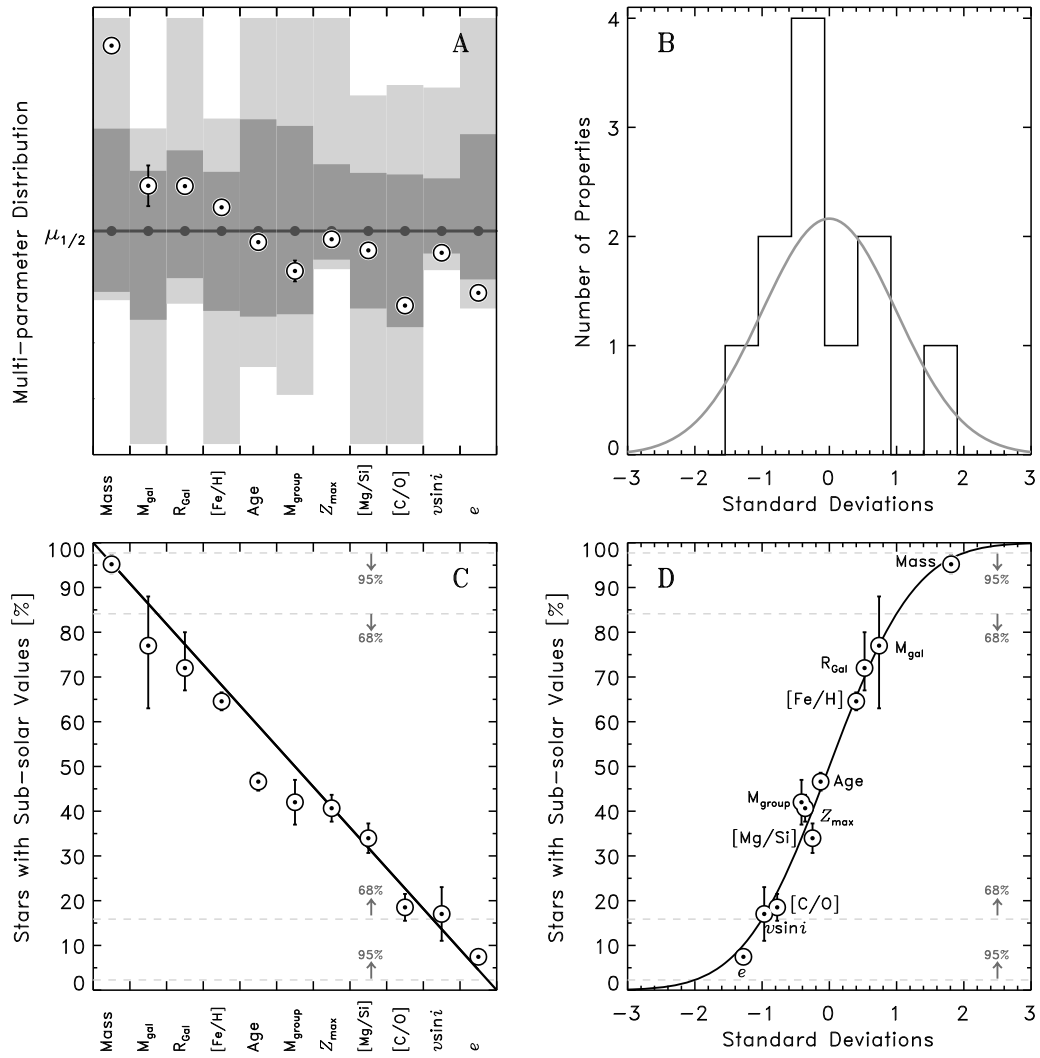

Figure 4.4 Various representations of our main results.

A. Comparing the solar values to the 68% (dark grey) and 95% (light grey) intervals for each parameter. The horizontal line represents the median of each of the distributions, and the vertical axis is normalized to the longer of the two 95% intervals for each of the distributions.

B. A histogram of the distribution of parameters in standard deviation compared to a gaussian.

C. The percentage of stars n% with sub-solar values for each of the parameters in decreasing order of n%. The line represents the expected arrangement of points "$\odot$" for randomized parameter values. Significant deviations from the line may indicate unexpected anomalies, none of which are seen here.

D. Each of the solar properties is plotted in n%-standard deviation space. If the distributions were Gaussian the points would fall along the solid line.

than any other, they have been treated equally. A potential extension of this work would be the inclusion of factors to weight the plausibility (based on planetary formation models and biology) that a property is related to life.

CHAPTER 5

A LARGER ESTIMATE OF THE ENTROPY OF THE UNIVERSE

We are all
made of stars.
We were created in the birth of stars.

- Encounter, "Starborn"

5.1. Introduction

The entropy budget of the universe is important because its increase is associated with all irreversible processes, on all scales, across all facets of nature: gravitational clustering, accretion disks, supernovae, stellar fusion, terrestrial weather, and chemical, geological and biological processes (Frautschi, 1982; Lineweaver and Egan, 2008).

Recently, Frampton et al. (2008) and Frampton and Kephart (2008) reported the entropy budget of the observable universe. Their budgets (listed aside others in Table 5.1) estimate the total entropy of the observable universe to be $S_{\rm obs} \sim 10^{102}k - 10^{103}k$, dominated by the entropy of supermassive black holes (SMBHs) at the centers of galaxies. That the increase of entropy has not yet been

capped by some limiting value, such as the holographic bound ('t Hooft, 1993; Susskind, 1995) at $S_{\max} \sim 10^{123}k$ (Frampton et al., 2008), is the reason dissipative processes are ongoing and that life can exist.

In this paper, we improve the entropy budget by using recent observational data and quantifying uncertainties. The paper is organized as follows. In what remains of the Introduction, we describe two different schemes for quantifying the increasing entropy of the universe, and we comment on caveats involving the identification of gravitational entropy. Our main work is presented in Sections 5.2 and 5.3, where we calculate new entropy budgets within each of the two accounting schemes. We finish in Section 5.4 with a discussion touching on the time evolution of the budgets we have calculated, and ideas for future work.

Throughout this paper we assume flatness ($\Omega_k = 0$) as predicted by inflation (Guth, 1981; Linde, 1982) and supported by observations (Spergel et al., 2007). Adopted values for other cosmological parameters are $h = 0.705 \pm 0.013$, $\omega_b = \Omega_b h^2 = 0.0224 \pm 0.0007$, $\omega_m = \Omega_m h^2 = 0.136 \pm 0.003$ (Seljak et al., 2006), and $T_{\rm CMB} = 2.725 \pm 0.002\ K$ (Mather et al. 1999; quoted uncertainties are 1σ).

5.1.1. Two Schemes for Quantifying the Increasing Entropy of the Universe

Modulo statistical fluctuations, the generalized second law of thermodynamics holds that the entropy of the universe (including Bekenstein-Hawking entropy in the case of any region hidden behind an event horizon), must not decrease with time (Bekenstein, 1974; Gibbons and Hawking, 1977). Within the FRW framework, the generalized second law can be applied in at least two obvious ways:

1. The total entropy in a sufficiently large comoving volume of the universe does not decrease with cosmic time,

$$dS_{\text{comoving volume}} \geq 0. \tag{5.1}$$

2. The total entropy of matter contained within the cosmic event horizon (CEH) plus the entropy of the CEH itself, does not decrease with cosmic time,

$$dS_{\text{CEH interior}} + dS_{\text{CEH}} \geq 0. \tag{5.2}$$

In the first of these schemes, the system is bounded by a closed comoving surface. The system is effectively isolated because large-scale homogeneity and

isotropy imply no net flows of entropy into or out of the comoving volume. The time-slicing in this scheme is along surfaces of constant cosmic time. Event horizons of black holes are used to quantify the entropy of black holes, however the CEH is neglected since the assumption of large-scale homogeneity makes it possible for us to keep track of the entropy of matter beyond it. A reasonable choice for the comoving volume in this scheme is the comoving sphere that presently corresponds to the observable universe, i.e., the gray area in Figure 5.1. Correspondingly, in Section 5.2 we calculate the present entropy budget of the observable universe and we do not include the CEH.

The second scheme is similar to the first in that we time-slice along surfaces of constant cosmic time. However, here the system (yellow shade in Figure 5.1) is bounded by the time-dependent CEH instead of a comoving boundary. Migration of matter across the CEH is not negligible, and the CEH entropy (Gibbons and Hawking, 1977) must be included in the budget to account for this (e.g. Davis et al. 2003). The present entropy of the CEH and its interior is calculated in Section 5.3.

5.1.2. Entropy and Gravity

It is widely appreciated that non-gravitating systems of particles evolve toward homogenous temperature and density distributions. The corresponding increase in the volume of momentum-space and position-space occupied by the constituent particles represents an increase in entropy. On the other hand, strongly gravitating systems become increasingly lumpy. With "lumpyness" naively akin to "orderliness", it is not as easy to see that the total entropy increases. In these systems the entropy is shared among numerous components, all of which must be considered.

For example, approximately collisionless long-range gravitational interactions between stars result in dynamical relaxation of galaxies (whereby bulk motions are dissipated and entropy is transferred to stars in the outer regions of the galaxy; Lynden-Bell 1967) and stellar evaporation from galaxies (whereby stars are ejected altogether, carrying with them energy, angular momentum and entropy, and allowing what remains behind to contract; e.g. Binney and Tremaine 2008). In more highly dissipative systems, i.e., accretion disks, non-gravitational interactions (viscosity and/or magnetorotational instability; Balbus and Hawley 2002) transfer angular momentum and dissipate energy and entropy.

In addition to these considerations, entropy also increases when gravitons are produced. A good example is the in-spiral of close binaries, such as the Hulse-Taylor binary pulsar system (Hulse and Taylor, 1975; Weisberg and Taylor, 2005).

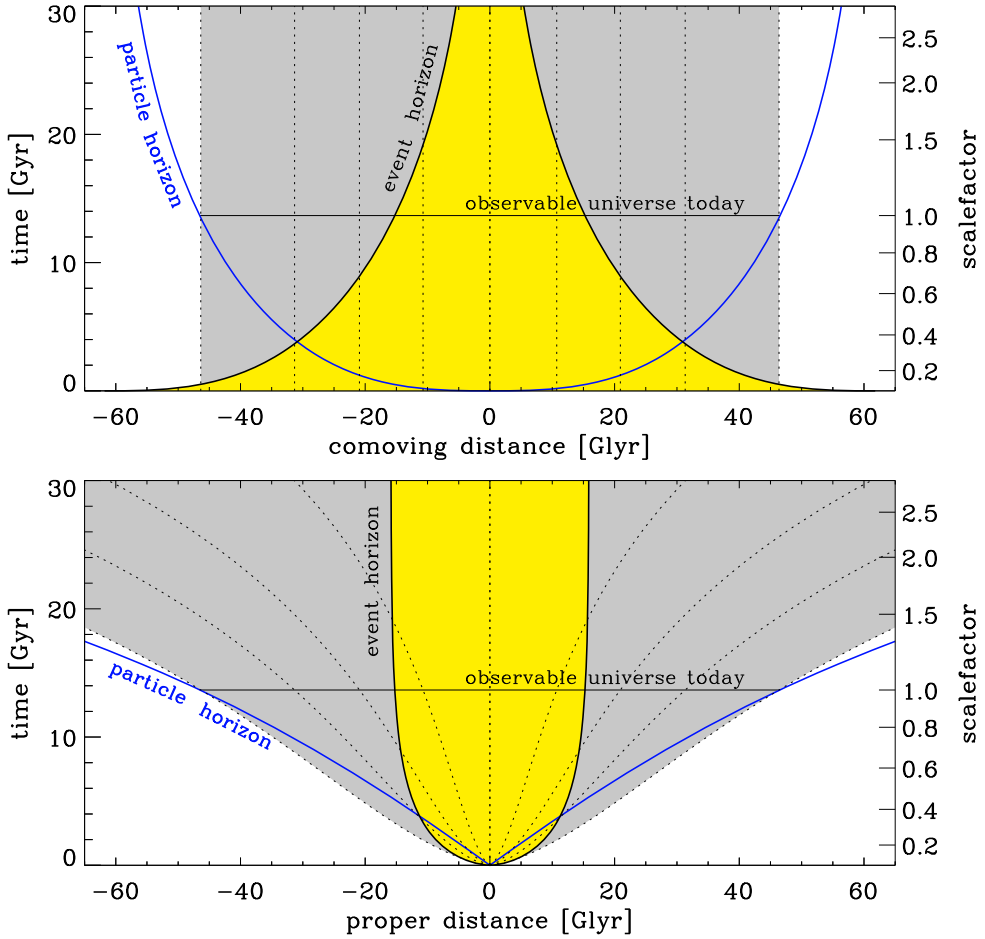

Figure 5.1 These two panels show the particle horizon (see Equation 5.42 and Figure 5.9) and the cosmic event horizon (see Equation 5.46) as a function of time. The difference between the two panels is the spatial coordinate system used: the x-axis in the bottom panel is proper distance D and in the top panel it is comoving distance $\chi \equiv \frac{D}{a}$, where a is the cosmic scalefactor. The origin is chosen so that our galaxy is the central vertical dotted line. The other dotted lines represent distant galaxies, which are approximately comoving and recede as the universe expands. The region inside the particle horizon is the observable universe. The comoving volume that corresponds to the observable universe today, about 13.7 *Gyr* after the big bang, is filled gray. In scheme 1, the entropy within this comoving volume increases (or remains constant) with time. Alternatively, in scheme 2 the entropy within the event horizon (the region filled yellow), plus the entropy of the horizon itself, increases (or remains constant) with time.

Gravitational waves emitted from the system extract orbital energy (and therefore entropy) allowing the system to contract.

The entropy of a general gravitational field is still not known. Penrose (1987, 1979, 2004) has proposed that it is related to the Weyl curvature tensor $W_{\mu\nu\kappa\lambda}$. In conformally flat spacetimes (such as an ideal FRW universe), the Weyl curvature vanishes and gravitational entropy is postulated to vanish (to limits imposed by quantum uncertainty). In clumpy spacetimes the Weyl curvature takes large values and the gravitational entropy is high. While Ricci curvature $R_{\mu\nu}$ vanishes in the absence of matter, Weyl curvature may still be non-zero (e.g. gravitational waves traveling though empty space) and the corresponding gravitational entropy may be non-zero.

If these ideas are correct then the low gravitational entropy of the early universe comes from small primordial gravitational perturbations. Gravitational entropy then increases with the growing amplitude of linear density fluctuations parameterized through the matter power spectrum $P(k)$. The present gravitational entropy, however, is expected to be dominated by the nonlinear overdensities (with large Weyl tensors) which have formed since matter-radiation equality.

In extreme cases, gravitational clumping leads to the formation of black holes. The entropy of black holes is well known (Bekenstein, 1973; Hawking, 1976; Strominger and Vafa, 1996). The entropy of a Schwarzschild black hole is given by

$$S_{\rm BH} = \frac{kc^3}{G\hbar}\frac{A}{4} = \frac{4\pi kG}{c\hbar}M^2 \tag{5.3}$$

where $A = \frac{16\pi G^2 M^2}{c^4}$ is the event-horizon area and M is the black hole mass.

Because gravitational entropy is difficult to quantify, we only include it in the two extremes: the thermal distribution of gravitons and black holes.

5.2. The Present Entropy of the Observable Universe

The present entropy budget of the observable universe was estimated most recently by Frampton et al. (2008) and Frampton and Kephart (2008). Those papers and earlier work (Kolb and Turner, 1981; Frautschi, 1982; Penrose, 2004; Bousso et al., 2007) identified the largest contributors to the entropy of the observable universe as black holes, followed distantly by the cosmic microwave background (CMB) and the neutrino background. The last column of Table 5.1 contains previous estimates of the entropy in black holes, the CMB and neutrinos, as well as several less significant components.

Sections 5.2.1 – 5.2.7 below describe the data and assumptions used to calculate our entropy densities (given in Column 2 of Table 5.1). Our entropy budget for the observable universe (Column 3 of Table 5.1) is then found by multiplying the entropy density by the volume of the observable universe $V_{\rm obs}$,

$$S_i = s_i V_{\rm obs} \tag{5.4}$$

where s_i is the entropy density of component i. The volume of the observable universe is (see Appendix)

$$\begin{aligned} V_{\rm obs} &= 43.2 \pm 1.2 \times 10^4 \text{ Glyr}^3 \\ &= 3.65 \pm 0.10 \times 10^{80}\ m^3. \end{aligned} \tag{5.5}$$

5.2.1. Baryons

For a non-relativistic, non-degenerate gas the specific entropy (entropy per baryon) is given by the Sakur-Tetrode equation (e.g. Basu and Lynden-Bell 1990)

$$(s/n_b) = \frac{k}{n_b} \sum_i n_i \ln \left[Z_i(T) (2\pi m_i kT)^{\frac{3}{2}} e^{\frac{5}{2}} n_i^{-1} h^{-3} \right], \tag{5.6}$$

where i indexes particle types in the gas, n_i is the ith particle type's number density, and $Z_i(T)$ is its internal partition function. Basu and Lynden-Bell (1990) found specific entropies between 11 k and 21 k per baryon for main-sequence stars of approximately solar mass. For components of the interstellar medium (ISM) and intergalactic medium (IGM) they found specific entropies between 20 k (H_2 in the ISM) and 143 k (ionized hydrogen in the IGM) per baryon.

The cosmic entropy density in stars s_* can be estimated by multiplying the specific entropy of stellar material by the cosmic number density of baryons in stars n_{b*}:

$$s_* = (s/n_b)_* n_{b*} = (s/n_b)_* \frac{\rho_*}{m_p} = (s/n_b)_* \left[\frac{3H^2}{8\pi G} \frac{\Omega_*}{m_p} \right]. \tag{5.7}$$

Using the stellar cosmic density parameter $\Omega_* = 0.0027 \pm 0.0005$ (Fukugita and Peebles, 2004), and the range of specific entropies for main-sequence stars around the solar mass (which dominate stellar mass), we find

$$s_* = 0.26 \pm 0.12\ k\ m^{-3}, \tag{5.8}$$

$$S_* = 9.5 \pm 4.5 \times 10^{80}\ k. \tag{5.9}$$

Component	Entropy Density s [$k\ m^{-3}$]	Entropy S [k]	Entropy S [k] (previous work)
SMBHs	$8.4^{+8.2}_{-4.7} \times 10^{23}$	$3.1^{+3.0}_{-1.7} \times 10^{104}$	10^{101}[1], 10^{102}[2], 10^{103}[3]
Stellar BHs ($2.5 - 15\ M_\odot$)	$1.6 \times 10^{17^{+0.6}_{-1.2}}$	$5.9 \times 10^{97^{+0.6}_{-1.2}}$	10^{97}[2], 10^{98}[4]
Photons	$1.478 \pm 0.003 \times 10^9$	$5.40 \pm 0.15 \times 10^{89}$	10^{88}[1, 2, 4], 10^{89}[5]
Relic Neutrinos	$1.411 \pm 0.014 \times 10^9$	$5.16 \pm 0.15 \times 10^{89}$	10^{88}[2],10^{89}[5]
WIMP Dark Matter	$5 \times 10^{7\pm1}$	$2 \times 10^{88\pm1}$	–
Relic Gravitons	$1.7 \times 10^{7^{+0.2}_{-2.5}}$	$6.2 \times 10^{87^{+0.2}_{-2.5}}$	10^{86}[2, 3]
ISM and IGM	20 ± 15	$7.1 \pm 5.6 \times 10^{81}$	–
Stars	0.26 ± 0.12	$9.5 \pm 4.5 \times 10^{80}$	10^{79}[2]
Total	$\mathbf{8.4^{+8.2}_{-4.7} \times 10^{23}}$	$\mathbf{3.1^{+3.0}_{-1.7} \times 10^{104}}$	**10^{101}[1], 10^{102}[2], 10^{103}[3]**
Tentative Components:			
Massive Halo BHs ($10^5\ M_\odot$)	10^{25}	10^{106}	10^{106}[6]
Stellar BHs ($42 - 140\ M_\odot$)	$8.5 \times 10^{18^{+0.8}_{-1.6}}$	$3.1 \times 10^{99^{+0.8}_{-1.6}}$	–

Table 5.1 Our budget is consistent with previous estimates from the literature with the exception that SMBHs, which dominate the budget, contain at least an order of magnitude more entropy as previously estimated, due to the contributions of black holes 100 times larger than those considered in previous budgets. Uncertainty in the volume of the observable universe (see Appendix) has been included in the quoted uncertainties. Massive halo black holes at $10^5\ M_\odot$ and stellar black holes in the range $42 - 140\ M_\odot$ are included tentatively since their existence is speculative. They are not counted in the budget totals. Previous work: [1] Penrose (2004), [2] Frampton et al. (2008), [3] Frampton and Kephart (2008), [4] Frautschi (1982), [5] Kolb and Turner (1981), [6] Frampton (2009b).

Similarly, the combined energy density for the ISM and IGM is $\Omega_{\rm gas} = 0.040 \pm 0.003$ (Fukugita and Peebles, 2004), and by using the range of specific entropies for ISM and IGM components, we find

$$s_{\rm gas} = 20 \pm 15\ k\ m^{-3}, \tag{5.10}$$

$$S_{\rm gas} = 7.1 \pm 5.6 \times 10^{81}\ k. \tag{5.11}$$

The uncertainties in Equations (5.9) and (5.11) are dominated by uncertainties in the mass weighting of the specific entropies, but also include uncertainties in Ω_*, $\Omega_{\rm gas}$ and the volume of the observable universe.

5.2.2. Photons

The CMB photons are the most significant non-black hole contributors to the entropy of the observable universe. The distribution of CMB photons is thermal (Mather et al., 1994) with a present temperature of $T_\gamma = 2.725 \pm 0.002\ K$ (Mather et al., 1999).

The entropy of the CMB is calculated using the equation for a black body (e.g. Kolb and Turner (1990)),

$$s_\gamma = \frac{2\pi^2}{45}\frac{k^4}{c^3\hbar^3} g_\gamma T_\gamma^3 \tag{5.12}$$

$$= 1.478 \pm 0.003 \times 10^9\ k\ m^{-3},$$

$$S_\gamma = 2.03 \pm 0.15 \times 10^{89}\ k, \tag{5.13}$$

where $g_\gamma = 2$ is the number of photon spin states. The uncertainty in Equation (5.13) is dominated by uncertainty in the size of the observable universe.

The non-CMB photon contribution to the entropy budget (including starlight and heat emitted by the ISM) is somewhat less, at around $10^{86}k$ (Frautschi, 1982; Bousso et al., 2007; Frampton et al., 2008).

5.2.3. Relic Neutrinos

The neutrino entropy cannot be calculated directly since the temperature of cosmic neutrinos has not been measured. Standard treaties of the radiation era (e.g. Kolb and Turner 1990; Peacock 1999) describe how the present temperature (and entropy) of massless relic neutrinos can be calculated from the well known CMB photon temperature. Since this background physics is required for Sections 5.2.4 and 5.2.5, we summarize it briefly here.

A simplifying feature of the radiation era (at least at known energies $\lesssim 10^{12} eV$) is that the radiation fluid evolves adiabatically: the entropy density decreases as the cube of the increasing scalefactor $s_{\rm rad} \propto a^{-3}$. The evolution is adiabatic because reaction rates in the fluid are faster than the expansion rate H of the universe. It is convenient to write the entropy density as

$$s_{\rm rad} = \frac{2\pi^2}{45}\frac{k^4}{c^3\hbar^3} g_{*S} T_\gamma^3 \propto a^{-3} \tag{5.14}$$

where g_{*S} is the number of relativistic degrees of freedom in the fluid (with $m < kT/c^2$) given approximately by

$$g_{*S}(T) \approx \sum_{bosons,\ i} g_i \left(\frac{T_i}{T_\gamma}\right)^3 + \sum_{fermions,\ j} \frac{7}{8} g_j \left(\frac{T_j}{T_\gamma}\right)^3 . \tag{5.15}$$

For photons alone, $g_{*S} = g_\gamma = 2$, and thus Equation (5.14) becomes Equation (5.12). For photons coupled to an electron-positron component, such as existed before electron-positron annihilation, $g_{*S} = g_\gamma + \frac{7}{8} g_{e\pm} = 2 + \frac{7}{8} 4 = \frac{11}{2}$.

As the universe expands, massive particles annihilate, heating the remaining fluid. The effect on the photon temperature is quantified by inverting Equation (5.14),

$$T_\gamma \propto a^{-1} g_{*S}^{-1/3}. \tag{5.16}$$

The photon temperature decreases less quickly than a^{-1} because g_{*S} decreases with time. Before electron-positron $e^\pm$ annihilation the temperature of the photons was the same as that of the almost completely decoupled neutrinos. After $e^\pm$ annihilation, heats only the photons, the two temperatures differ by a factor C,

$$T_\nu = C\ T_\gamma. \tag{5.17}$$

A reasonable approximation $C \approx (4/11)^{1/3}$ is derived by assuming that only photons were heated during $e^\pm$ annihilation, where 4/11 is the ratio of g_{*S} for photons to g_{*S} for photons, electrons, and positrons.

Corrections are necessary at the 10^{-3} level because neutrinos had not completely decoupled at $e^\pm$ annihilation (Gnedin and Gnedin, 1998). The neutrino entropy density is computed assuming a thermal distribution with $T_\nu = (4/11)^{1/3} T_\gamma$, and we assign a 1% uncertainty.

$$\begin{aligned} s_\nu &= \frac{2\pi^2}{45}\frac{k^4}{c^3\hbar^3} g_\nu \left(\frac{7}{8}\right) T_\nu^3 \\ &= 1.411 \pm 0.014 \times 10^9\ k\ m^{-3}, \end{aligned} \tag{5.18}$$

where $g_\nu = 6$ (3 flavors, 2 spin states each). The total neutrino entropy in the observable universe is then

$$S_\nu = 5.16 \pm 0.14 \times 10^{89}\ k \tag{5.19}$$

with an uncertainty dominated by uncertainty in the volume of the observable universe.

Neutrino oscillation experiments have demonstrated that neutrinos are massive by measuring differences between the three neutrino mass eigenstates (Cleveland et al., 1998; Adamson et al., 2008; Abe et al., 2008). At least two of the mass eigenstates are heavier than $\sim 0.009\ eV$. Since this is heavier than their current relativistic energy ($\frac{k}{2}\ C\ T_\gamma = 0.0001\ eV$; computed under the assumption that they are massless) at least two of the three masses are presently non-relativistic.

Expansion causes non-relativistic species to cool as a^{-2} instead of a^{-1}, which would result in a lower temperature for the neutrino background than suggested by Equation (5.17). The entropy density (calculated in Equation 5.18) and entropy (calculated in Equation 5.19) are unaffected by the transition to non-relativistic cooling since the cosmic expansion of relativistic and non-relativistic gases are both adiabatic processes (the comoving entropy is conserved, so in either case $s \propto a^{-3}$).

We neglect a possible increase in neutrino entropy due to their infall into gravitational potentials during structure formation. If large, this will need to be considered in future work.

5.2.4. Relic Gravitons

A thermal background of gravitons is expected to exist, which decoupled from the photon bath around the Planck time, and has been cooling as $T_{\rm grav} \propto a^{-1}$ since then. The photons cooled less quickly because they were heated by the annihilation of heavy particle species (Equation 5.16). Thus we can relate the current graviton temperature to the current photon temperature

$$T_{\rm grav} = \left(\frac{g_{*S}(t_0)}{g_{*S}(t_{\rm planck})}\right)^{1/3} T_\gamma, \tag{5.20}$$

where $g_{*S}(t_{\rm planck})$ is the number of relativistic degrees of freedom at the Planck time and $g_{*S}(t_0) = 3.91$ today (this is appropriate even in the case of massive neutrinos because they decoupled from the photon bath while they were still relativistic). Given the temperature of background gravitons, their entropy can

be calculated as

$$s_{\rm grav} = \frac{2\pi^2}{45}\frac{k^4}{c^3\hbar^3} g_{\rm grav} T^3_{\rm grav} \quad (5.21)$$

where $g_{\rm grav} = 2$.

Figure 5.2 shows g_{*S} as a function of temperature. The function is well known for temperatures below about $10^{12} eV$, but is not known at higher temperatures. Previous estimates of the background graviton entropy have assumed $g_{*S}(t_{\rm planck}) \sim g_{*S}(10^{12} eV) = 106.75$ (Frampton et al., 2008; Frampton and Kephart, 2008), but this should be taken as a lower bound on $g_{*S}(t_{\rm planck})$ yielding an upper bound on $T_{\rm grav}$ and $s_{\rm grav}$.

To get a better idea of the range of possible graviton temperatures and entropies, we have adopted three values for $g_{*S}(t_{\rm planck})$. As a minimum likely value we use $g_{*S} = 200$ (Figure 5.2, thick blue line), which includes the minimal set of additional particles suggested by supersymmetry. As our middle value we use $g_{*S} = 350$, corresponding to the linear extrapolation of g_{*S} in $\log(T)$ to the Planck scale (Figure 5.2, gray line). And as a maximum likely value we use $g_{*S} = 10^5$, corresponding to an exponential extrapolation (Figure 5.2, thin blue line).

The corresponding graviton temperatures today are (Equation 5.20)

$$T_{\rm grav} = 0.61^{+0.12}_{-0.52}\ {\rm K}. \quad (5.22)$$

Inserting this into Equation (5.21) we find the entropy in the relic graviton background to be

$$s_{\rm grav} = 1.7 \times 10^{7^{+0.2}_{-2.5}}\ k\ m^{-3}, \quad (5.23)$$

$$S_{\rm grav} = 6.2 \times 10^{87^{+0.2}_{-2.5}}\ k. \quad (5.24)$$

It is interesting to note the possibility of applying Equation (5.20) in reverse, i.e., calculating the number of relativistic degrees of freedom at the Planck time using future measurements of the graviton background temperature.

5.2.5. Dark Matter

The most compelling interpretation of dark matter is as a weakly interacting superpartner (or weakly interacting massive particle, WIMP). According to this idea, dark matter particles decoupled from the radiation background at some energy above the particle mass.

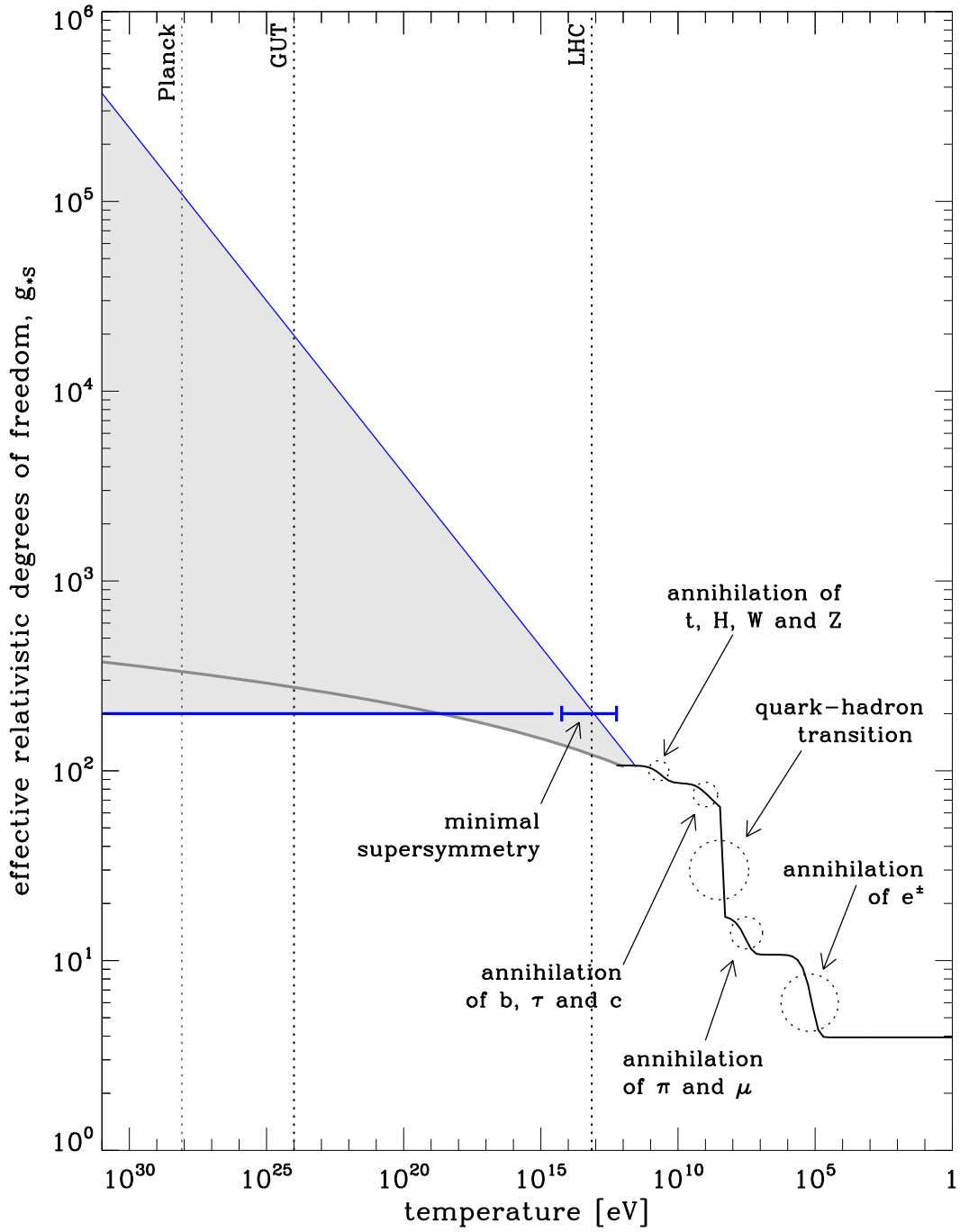

Figure 5.2 Number of relativistic degrees of freedom g_{*S} as a function of temperature, computed using the prescription given by Coleman and Roos (2003). All the particles of the standard model are relativistic at $T \gtrsim 10^{12}$ eV and $g_{*S}(10^{12}\ eV) = 106.75$. The value of g_{*S} is not known above $T \sim 10^{12}$. To estimate plausible ranges of values, we extrapolate g_{*S} linearly (gray line) and exponentially (thin blue line) in $\log(T)$. The minimum contribution to g_{*S} from supersymmetric partners is shown (blue bar) and taken to indicate a minimum likely value of g_{*S} at higher temperatures (thick blue line).

If this interpretation is correct, the fraction of relativistic background entropy in dark matter at the time dark matter decoupled $t_{\text{dm dec}}$ is determined by the fraction of relativistic degrees of freedom that were associated with dark matter at that time (see Equation 5.14).

$$s_{\text{dm}} = \frac{g_{*S\ \text{dm}}(t_{\text{dm dec}})}{g_{*S\ \text{non-dm}}(t_{\text{dm dec}})} s_{\text{non-dm rad}} \tag{5.25}$$

This can be evaluated at dark matter decoupling, or any time thereafter, since both s_{dm} and $s_{\text{non-dm rad}}$ are adiabatic ($\propto a^{-3}$).

We are unaware of any constraint on the number of superpartners that may collectively constitute dark matter. The requirements that they are only weakly interacting, and that they decouple at a temperature above their mass, are probably only satisfied by a few (even one) species. Based on these arguments, we assume $g_{*S\ dm}(t_{\text{dm dec}}) \lesssim 20$ and $g_{*S}(t_{\text{dm dec}}) \gtrsim 106.75$ which yields the upper limit

$$\frac{g_{*S\ \text{dm}}(t_{\text{dm dec}})}{g_{*S}(t_{\text{dm dec}})} \lesssim \frac{1}{5}. \tag{5.26}$$

On the other hand there may be many more degrees of freedom than suggested by minimal supersymmetry. By extrapolating g_{*S} exponentially beyond supersymmetric scales (to $10^{15}\ eV$), we find $g_{*S}(t_{\text{dm dec}}) \lesssim 800$. In the simplest case, dark matter is a single scalar particle so $g_{*S\ \text{dm}}(t_{\text{dm dec}}) \gtrsim 1$ and we take as a lower limit

$$\frac{g_{*S\ \text{dm}}(t_{\text{dm dec}})}{g_{*S\ \text{non-dm}}(t_{\text{dm dec}})} \gtrsim \frac{1}{800}. \tag{5.27}$$

Inserting this into Equation (5.25) at the present day gives

$$s_{\text{dm}} = 5 \times 10^{7\pm1}\ k\ m^{-3}, \tag{5.28}$$

where we have used the estimated limits given in Equations (5.26) and (5.27) and taken $s_{\text{non-dm rad}}$ to be the combined entropy of neutrinos and radiation today (Equations 5.12 and 5.18). The corresponding estimate for the total dark matter entropy in the observable universe is

$$S_{\text{dm}} = 2 \times 10^{88\pm1}\ k. \tag{5.29}$$

As with our calculated neutrino entropy, our estimates here carry the caveat that we have not considered changes in the dark matter entropy associated with gravitational structure formation.

5.2.6. Stellar Black Holes

In the top panel of Figure 5.3 we show the stellar initial mass function (IMF) parameterized by

$$\frac{dn_{\rm initial}}{d\log(M)} \propto \left(\frac{M}{M_\odot}\right)^{\alpha+1}, \tag{5.30}$$

with $\alpha = -1.35$ at $M < 0.5M_\odot$ and $\alpha = -2.35^{+0.65}_{-0.35}$ at $M \geq 0.5M_\odot$ (Elmegreen, 2007). We also show the present distribution of main-sequence stars, which is proportional to the initial distribution for $M \lesssim 1M_\odot$, but which is reduced by a factor of $(M/M_\odot)^{-2.5}$ for heavier stars (Fukugita and Peebles, 2004).

$$\frac{dn_{\rm present}}{d\log(M)} = \begin{cases} \frac{dn_{\rm initial}}{d\log(M)}, & \text{for } M < 1M_\odot \\ \frac{dn_{\rm initial}}{d\log(M)}\left(\frac{M}{M_\odot}\right)^{-2.5}, & \text{for } M \geq 1M_\odot \end{cases}. \tag{5.31}$$

The initial and present distributions are normalized using the present cosmic density of stars, $\Omega_* = 0.0027 \pm 0.0005$ (Fukugita and Peebles, 2004).

The yellow fill in the top panel represents stars of mass $1M_\odot \lesssim M \lesssim 8M_\odot$, which died leaving white dwarf remnants of mass $M \lesssim 1.4M_\odot$ (yellow fill, bottom panel). The blue fill represents stars of mass $8M_\odot \lesssim M \lesssim 25M_\odot$, which died and left neutron star remnants of mass $1.4M_\odot \lesssim M \lesssim 2.5M_\odot$. The light gray area represents stars of mass $25M_\odot \lesssim M \lesssim 42M_\odot$ which became black holes of mass $2.5M_\odot \lesssim M \lesssim 15M_\odot$ via supernovae (here we use the simplistic final-initial mass function of Fryer and Kalogera (2001)). Stars larger than $\sim 42M_\odot$ collapse directly to black holes, without supernovae, and therefore retain most of their mass (dark gray regions; Fryer and Kalogera 2001; Heger et al. 2005).

Integrating Equation (5.3) over stellar black holes in the range $M \leq 15M_\odot$ (the light gray fill in the bottom panel of Figure 5.3) we find

$$s_{\rm SBH\ (M<15M_\odot)} = 1.6 \times 10^{17^{+0.6}_{-1.2}}\ k\ m^{-3}, \tag{5.32}$$

$$S_{\rm SBH\ (M<15M_\odot)} = 5.9 \times 10^{97^{+0.6}_{-1.2}}\ k, \tag{5.33}$$

which is comparable to previous estimates of the stellar black hole entropy (see Table 5.1). Our uncertainty is dominated by uncertainty in the slope of the IMF, but also includes uncertainty in the normalization of the mass functions and uncertainty in the volume of the observable universe.

If the IMF extends beyond $M \gtrsim 42M_\odot$ as in Figure 5.3, then these higher mass black holes (the dark gray fill in the bottom panel of Figure 5.3) may contain more entropy than black holes of mass $M < 15\ M_\odot$ (Equation 5.32). For example,

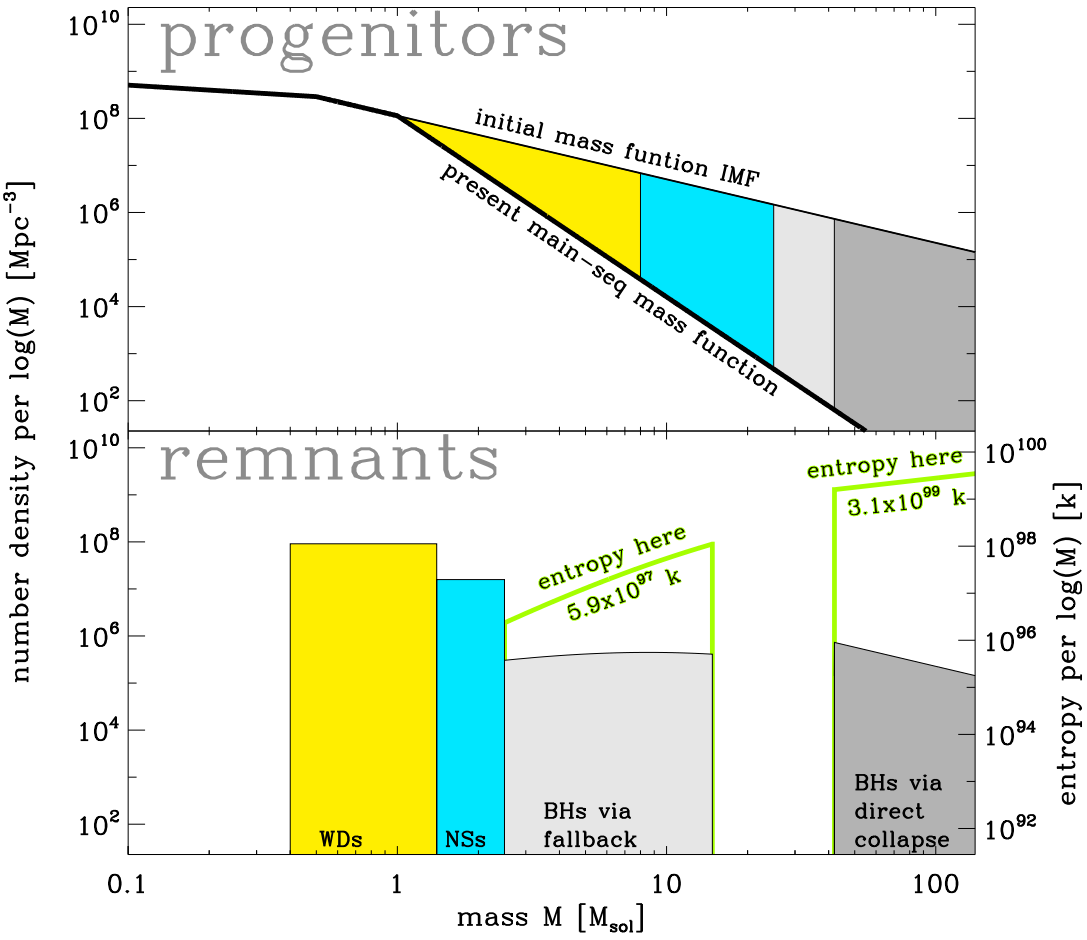

Figure 5.3 Progenitors in the IMF (top panel) evolve into the distribution of remnants in the bottom panel. The shape of the present main-sequence mass function differs from that of the IMF (top panel) by the stars that have died leaving white dwarfs (yellow), neutron stars (blue), and black holes (light and dark gray). The present distribution of remnants is shown in the bottom panel. Black holes in the range $2.5M_\odot \lesssim M \lesssim 15M_\odot$ (light gray) have been observationally confirmed. They form from progenitors in the range $25M_\odot \lesssim M \sim 42M_\odot$ via core collapse supernova and fallback, and we calculate their entropy to be $5.9 \times 10^{97^{+0.6}_{-1.2}}k$. Progenitors above about 42 $M_\odot$ may evolve directly to black holes without significant loss of mass (dark gray) and may carry much more entropy, but this population has not been observed. The green curve, whose axis is on the right, shows the mass distribution of stellar black hole entropies in the observable universe.

if the Salpeter IMF is reliable to $M = 140\ M_\odot$ (the Eddington limit and the edge of Figure 5.3), then black holes in the mass range 42 - 140 $M_\odot$ would contribute about $3.1 \times 10^{99^{+0.8}_{1.6}}\ k$ to the entropy of the observable universe. Significantly less is known about this potential population, and should be considered a tentative contribution in Table 5.1.

5.2.7. Supermassive Black Holes

Previous estimates of the SMBH entropy (Penrose, 2004; Frampton et al., 2008; Frampton and Kephart, 2008) have assumed a typical SMBH mass and a number density and yield $S_{\rm SMBH} = 10^{101} - 10^{103} k$. Below we use the SMBH mass function as measured recently by Graham et al. (2007). Assuming a three-parameter Schechter function

$$\frac{dn}{d\log(M)} = \phi_* \left(\frac{M}{M_*}\right)^{\alpha+1} \exp\left[1 - \left(\frac{M}{M_*}\right)\right] \tag{5.34}$$

(number density per logarithmic mass interval) they find $\phi_* = 0.0016 \pm 0.0004\ {\rm Mpc}^{-3}$, $M_* = 2.9 \pm 0.7 \times 10^8\ M_\odot$, and $\alpha = -0.30 \pm 0.04$. The data and best-fit model are shown in black in Figure 5.4.

We calculate the SMBH entropy density by integrating Equation (5.3) over the SMBH mass function,

$$s \;=\; \frac{4\pi k G}{c\hbar} \int M^2 \left(\frac{dn}{d\log(M)}\right) d\log(M). \tag{5.35}$$

The integrand is plotted using a green line in Figure 5.4 showing that the contributions to SMBH entropy are primarily due to black holes around $\sim 10^9 M_\odot$. The SMBH entropy is found to be

$$s_{\rm SMBH} \;=\; 8.4^{+8.2}_{-4.7} \times 10^{23}\ k\ m^{-3}, \tag{5.36}$$

$$S_{\rm SMBH} \;=\; 3.1^{+3.0}_{-1.7} \times 10^{104}\ k. \tag{5.37}$$

The uncertainty here includes uncertainties in the SMBH mass function and uncertainties in the volume of the observable universe. This is at least an order of magnitude larger than previous estimates (see Table 5.1). The reason for the difference is that the (Graham et al., 2007) SMBH mass function contains larger black holes than assumed in previous estimates.

Frampton (2009a,b) has suggested that intermediate mass black holes in galactic halos may contain more entropy than SMBHs in galactic cores. For example, according to the massive astrophysical compact halo object (MACHO) explanation

of dark matter, intermediate mass black holes in the mass range 10^2 - 10^5 $M_\odot$ may constitute dark matter. Assuming 10^5 $M_\odot$ black holes, these objects would contribute up to 10^{106} k to the entropy of the observable universe (Frampton, 2009b). Whether or not this is so depends on the number density and mass distribution of this population. Figure 5.5 combines Figures 5.3 and 5.4 and shows what intermediate black hole number densities would be required.

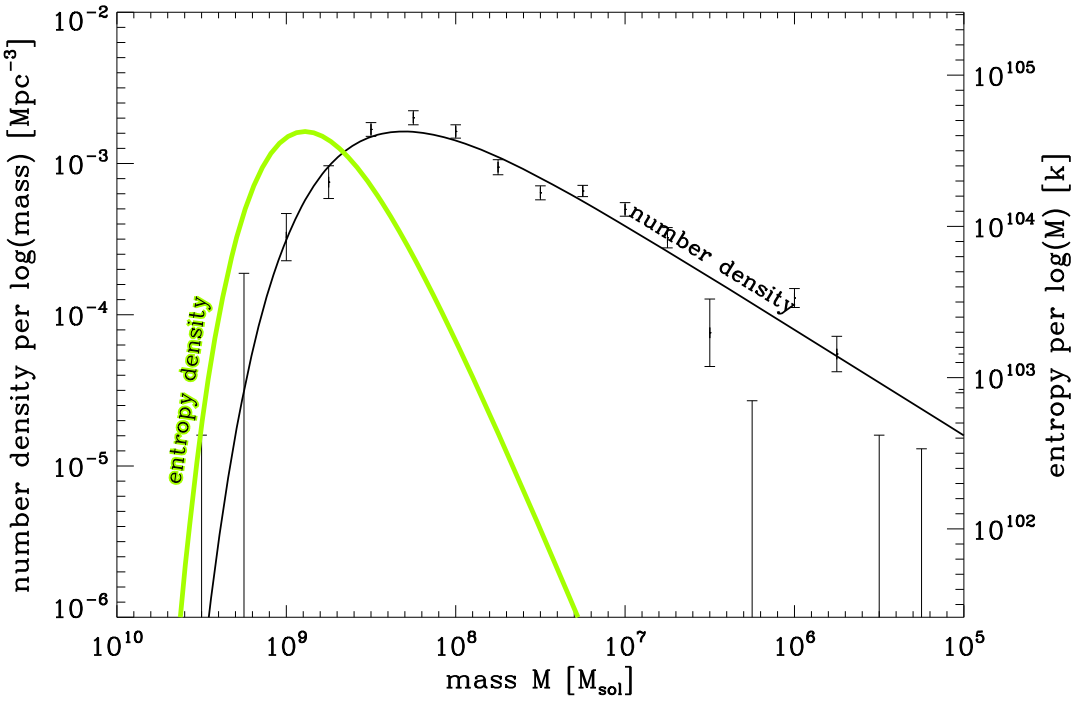

Figure 5.4 The black curve, whose axis is on the left, is the SMBH mass function from Graham et al. (2007), i.e., the number of supermassive black holes per Mpc^3 per logarithmic mass interval. The green curve, whose axis is on the right, shows the mass distribution of SMBH entropies in the observable universe.

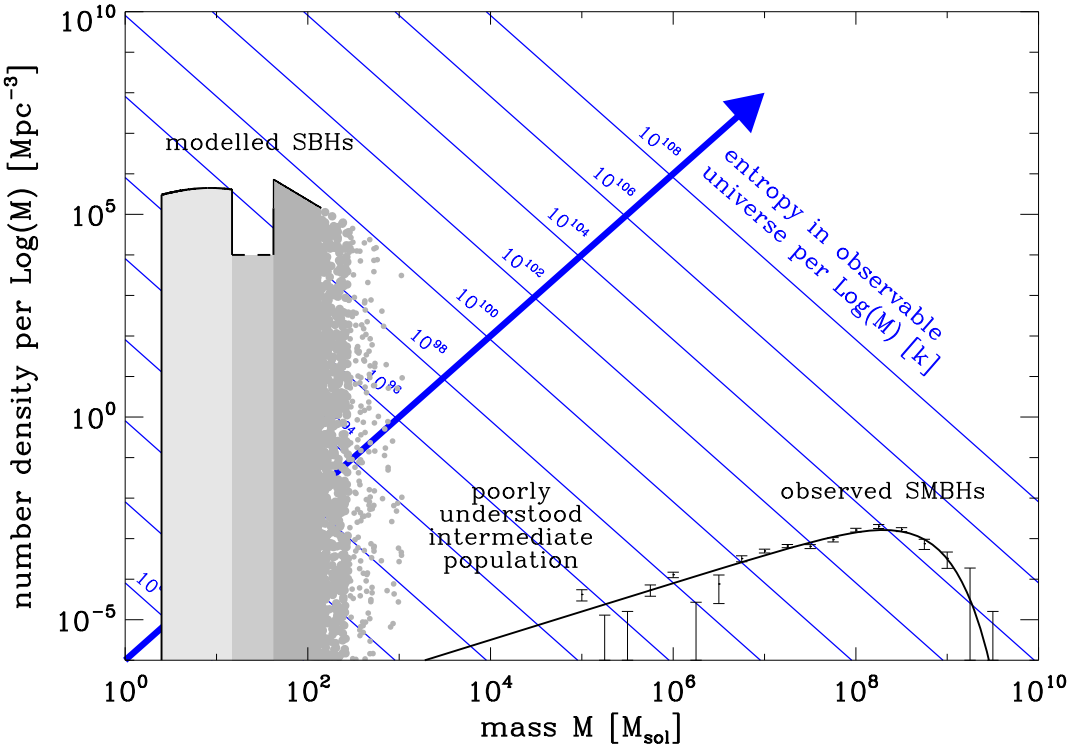

Figure 5.5 Whether or not the total black hole entropy is dominated by SMBHs depends on the yet-unquantified number of intermediate mass black holes.

5.3. The Entropy of the CEH and its Interior

In this section we calculate the entropy budget for scheme 2 (refer to discussion in Section 5.1.1). Scheme 2 differs from scheme 1 in two ways: first, along with the components previously considered (and listed in Table 5.1), here we consider the CEH as an additional entropy component; and second, the volume of interest is that within the event horizon not the particle horizon (or observable universe).

The proper distance to the CEH is generally time-dependent, increasing when the universe is dominated by an energy component with an equation of state $w > -1$ (radiation and matter) and remaining constant when the universe is dark energy dominated (assuming a cosmological constant, $w = -1$). Since our universe is presently entering dark energy domination, the growth of the event horizon has slowed, and it is almost as large now as it will ever become (bottom panel of Figure 5.1). In the Appendix, we calculate the present radius and volume of the CEH

$$R_{\mathrm{CEH}} = 15.7 \pm 0.4 \text{ Glyr}, \tag{5.38}$$

$$\begin{aligned} V_{\mathrm{CEH}} &= 1.62 \pm 0.12 \times 10^4 \text{ Glyr}^3 \\ &= 1.37 \pm 0.10 \times 10^{79}\ m^3. \end{aligned} \tag{5.39}$$

We also calculate the present entropy of the CEH (following Gibbons and Hawking 1977),

$$\begin{aligned} S_{\mathrm{CEH}} &= \frac{kc^3}{G\hbar}\frac{A}{4} \\ &= \frac{kc^3}{G\hbar}\pi R_{\mathrm{CEH}}^2 \\ &= 2.6 \pm 0.3 \times 10^{122}\ k. \end{aligned} \tag{5.40}$$

Entropies of the various components within the CEH are calculated using the entropy densities s_i from Section 5.2:

$$S_i = s_i V_{\mathrm{CEH}} \tag{5.41}$$

Table 5.2 shows that the cosmic event horizon contributes almost 20 orders of magnitude more entropy than the next largest contributor, supermassive black holes.

Component	Entropy S [k]
Cosmic Event Horizon	$2.6 \pm 0.3 \times 10^{122}$
SMBHs	$1.2^{+1.1}_{-0.7} \times 10^{103}$
Stellar BHs ($2.5 - 15\ M_\odot$)	$2.2 \times 10^{96^{+0.6}_{-1.2}}$
Photons	$2.03 \pm 0.15 \times 10^{88}$
Relic Neutrinos	$1.93 \pm 0.15 \times 10^{88}$
WIMP Dark Matter	$6 \times 10^{86 \pm 1}$
Relic Gravitons	$2.3 \times 10^{86^{+0.2}_{-3.1}}$
ISM and IGM	$2.7 \pm 2.1 \times 10^{80}$
Stars	$3.5 \pm 1.7 \times 10^{78}$
Total	$\mathbf{2.6 \pm 0.3 \times 10^{122}}$
Tentative Components:	
Massive Halo BHs ($10^5\ M_\odot$)	10^{104}
Stellar BHs ($42 - 140\ M_\odot$)	$1.2 \times 10^{98^{+0.8}_{-1.6}}$

Table 5.2 This budget is dominated by the cosmic event horizon entropy. While the CEH entropy should be considered as an additional component in scheme 2, it also corresponds to the holographic bound ('t Hooft, 1993) on the possible entropy of the other components and may represent a significant overestimate. Massive halo black holes at $10^5\ M_\odot$ and stellar black holes in the range $42 - 140\ M_\odot$ are included tentatively since their existence is speculative.

5.4. Discussion

The second law of thermodynamics holds that the entropy of an isolated system increases or remains constant, but does not decrease. This has been applied to the large-scale universe in at least two ways (Equation 5.1 and 5.2). The first scheme requires the entropy in a comoving volume of the universe to not decrease. The second scheme requires the entropy of matter contained within the event horizon, plus the entropy of the event horizon, to not decrease.

We have calculated improved estimates of the current entropy budget under scheme 1 (normalized to the current observable universe) and scheme 2. These are given in Tables 5.1 and 5.2, respectively.

The entropy of dark matter has not been calculated previously. We find that dark matter contributes $10^{88\pm1}\ k$ to the entropy of the observable universe. We note that the neutrino and dark matter estimates do not include an increase due to their infall into gravitational potentials during structure formation. It is not clear to us a priori whether this non-inclusion is significant, but it may be since both components are presently non-relativistic. This should be investigated in future work.

Previous estimates of the relic graviton entropy have assumed that only the known particles participate in the relativistic fluid of the early universe at $t \gtrsim t_{\rm planck}$. In terms of the number of relativistic degrees of freedom, this means $g_{*S} \rightarrow 106.75$ at high temperatures. However, additional particles are expected to exist, and thus g_{*S} is expected to become larger as $t \rightarrow t_{\rm planck}$. In the present work, we have calculated the relic graviton entropy corresponding to three high-energy extrapolations of g_{*S} (constant, linear growth and exponential growth) and reported the corresponding graviton temperatures and entropies.

In this paper, we have computed the entropy budget of the observable universe today $S_{\rm obs}(t = t_0)$. Figure 5.6 illustrates the evolution of the entropy budget under scheme 1, i.e., the entropy in a comoving volume (normalized to the current observable universe). For simplicity, we have included only the most important components.

At the far-left of the figure, we show a brief period of inflation. During this period all of the energy is in the inflaton (Guth, 1981; Linde, 1982), which has very few degrees of freedom and low entropy (blue fill; Linde 2009; Steinhardt 2008). Inflation ends with a period of reheating somewhere between the Planck scale ($10^{-45}s$) and the GUT scale ($10^{-35}s$), during which the inflaton's energy is transferred into a relativistic fluid (yellow fill). During reheating, the entropy increases by many orders of magnitude. After reheating, the constitution of the

relativistic fluid continues to change, but the changes occur reversibly and do not increase the entropy.

After a few hundred million years ($\sim 10^{16}s$), the first stars form from collapsing clouds of neutral hydrogen and helium. Shortly thereafter the first black holes form. The entropy in stellar black holes (light gray) and SMBHs (dark gray) increases rapidly during galactic evolution. The budget given in Table 5.1 is a snapshot of the entropies at the present time ($4.3\times10^{17}s$). Over the next $10^{26}s$, the growth of structures larger than about 10^{14} $M_\odot$ will be halted by the acceleration of the universe. Galaxies within superclusters will merge and objects in the outer limits of these objects will be ejected. The final masses of SMBHs will be $\sim 10^{10}M_\odot$ (Adams and Laughlin, 1997) with the entropy dominated by those with $M \sim 10^{12}M_\odot$.

Stellar black holes will evaporate away into Hawking radiation in about $10^{80}s$ and SMBHs will follow in $10^{110}s$. The decrease in black hole entropy is accompanied by a compensating increase in radiation entropy. The thick black line in Figure 5.6 represents the radiation entropy growing as black holes evaporate. The asymptotic future of the entropy budget, under scheme 1, will be radiation dominated.

Figure 5.7 illustrates the evolution of the entropy budget under scheme 2, i.e., the entropy within the CEH, plus the entropy of the CEH.

Whereas in scheme 1 we integrate over a constant comoving volume, here the relevant volume is the event horizon. The event horizon is discussed in some detail in the Appendix. During radiation domination, the comoving radius of the CEH is approximately constant (the proper distance grows as $R_{\rm CEH} \propto a$) and in the dark energy dominated future, it is a constant proper distance ($R_{\rm CEH}$ = constant). The few logarithmic decades around the present time cannot be described well by either of these.

Since the event horizon has been approximately comoving in the past, the left half of Figure 5.7 is almost the same as in Figure 5.6 except that we have included the event horizon entropy (green fill). The event horizon entropy dominates this budget from about $10^{-16}s$.

After dark energy domination sets in, the CEH becomes a constant proper distance. The expansion of the universe causes comoving objects to recede beyond the CEH. On average, the number of galaxies, black holes, photons etc. within our CEH decreases as a^{-3}. The stellar and SMBH entropy contained within the CEH decreases accordingly (decreasing gray filled regions).

The decreasing black hole entropy (as well as other components not shown)

is compensated by the asymptotically growing CEH entropy (demonstrated explicitly for a range of scenarios in Davis et al. 2003), and thus the second law of thermodynamics is satisfied. See Egan and Lineweaver (2010b, in preparation) for further discussion of the time-dependence of the entropy of the universe.

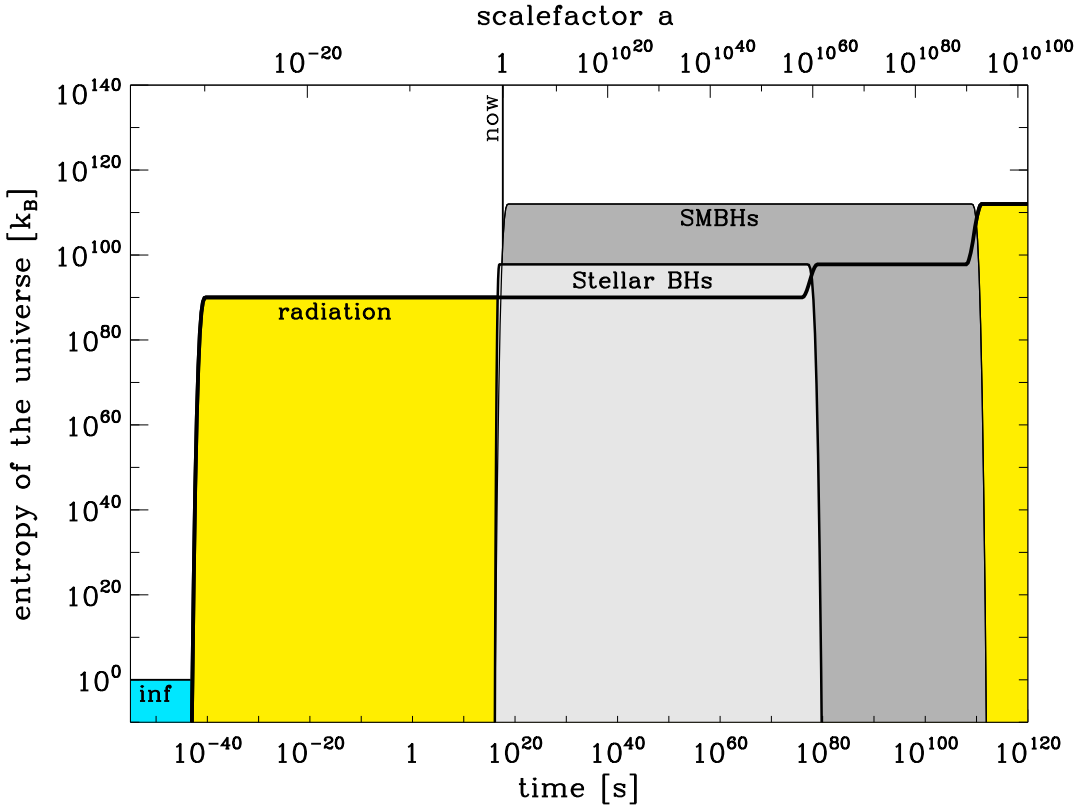

Figure 5.6 The entropy in a comoving volume (normalized to the present observable universe). This figure illustrates the time-dependence of the scheme 1 entropy budget. N.B. $10^{10^{100}} = 1$ googolplex.

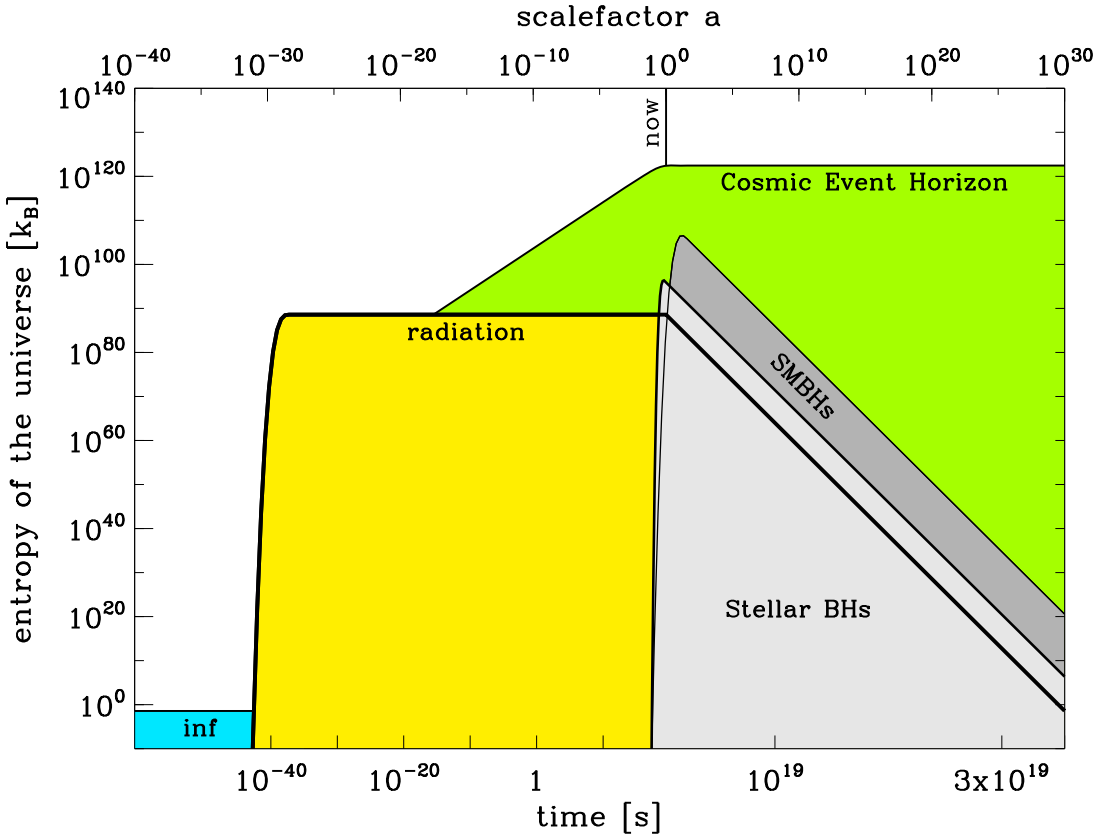

Figure 5.7 Entropy of matter within the CEH, and the entropy of the cosmic event horizon. This figure illustrates the time dependence of the scheme 2 entropy budget. Note: the horizontal axis is shorter than in Figure 5.6.

Acknowledgments

We are grateful for many useful discussions with Tamara Davis, Ken Freeman, Pat Scott, Geoff Bicknell, Mike Turner, Andrei Linde, and Paul Steinhardt. C.A.E. thanks Anna Fransson for financial support and the Research School of Astronomy and Astrophysics, Australian National University, for its hospitality during the preparation of this paper.

Appendix: The observable universe and the cosmic event horizon

Here we calculate the radius and volume of the observable universe (for use in Section 5.2); and we calculate the radius, volume, and entropy of the CEH (for use in Section 5.3). We use numerical methods to track the propagation of errors from the cosmological parameters.

The radius of the observable universe (or particle horizon) is

$$R_{\rm obs} = a(t) \int_{t'=0}^{t} \frac{c}{a(t')} dt'. \tag{5.42}$$

Here $a(t)$ is the time-dependent scalefactor of the universe given by the Friedmann equation for a flat cosmology

$$\frac{da}{dt} = \sqrt{\frac{\Omega_r}{a^2} + \frac{\Omega_m}{a} + \frac{\Omega_\Lambda}{a^{-2}}}\,. \tag{5.43}$$

Hubble's constant and the matter density parameter are taken from Seljak et al. (2006): $h = H/100\ km\ s^{-1}\ Mpc^{-1} = 0.705 \pm 0.013$, $\omega_m = \Omega_m h^2 = 0.136 \pm 0.003$. The radiation density is calculated from the observed CMB temperature, $T_{\rm CMB} = 2.725 \pm 0.002\ K$ (Mather et al., 1999), using $\Omega_r = \frac{8\pi G}{3H^2} \frac{\pi^2 k^4 T^4}{15 c^5 \hbar^3}$. The vacuum energy density parameter is determined by flatness, $\Omega_\Lambda = 1 - \Omega_r - \Omega_m$.

A distribution of $R_{\rm obs}$ values is built up by repeatedly evaluating Equation (5.42) at the present time (defined by $a(t_0) = 1$) using cosmological parameters randomly selected from the allowed region of $h - \omega_m - T_{\rm CMB}$ parameter space (assuming uncorrelated Gaussian errors in these parameters). We find

$$R_{\rm obs} = 46.9 \pm 0.4\ {\rm Glyr} \tag{5.44}$$

with an approximately Gaussian distribution. The quoted confidence interval here, and elsewhere in this Appendix, is 1σ. The volume of the observable

universe V_{obs} is calculated using the normal formula for the volume of a sphere.

$$\begin{aligned} V_{\text{obs}} &= 43.2 \pm 1.2 \times 10^4 \text{ Glyr}^3 \\ &= 3.65 \pm 0.10 \times 10^{80} \ m^3 \end{aligned} \tag{5.45}$$

See Figure 5.8. Uncertainty in R_{obs} and V_{obs} is predominantly due to uncertainty in ω_m however h also makes a non-negligible contribution.

The radius of the CEH at time t is given by integrating along a photon's world line from the time t to the infinite future.

$$R_{\text{CEH}} = a(t_{now}) \int_{t=t_{now}}^{\infty} \frac{c}{a(t)} dt \tag{5.46}$$

This integral is finite because the future of the universe is dark energy dominated. Using the same methods as for the observable universe, we find the present radius and volume of the CEH to be

$$R_{\text{CEH}} = 15.7 \pm 0.4 \text{ Glyr}, \tag{5.47}$$

and

$$\begin{aligned} V_{\text{CEH}} &= 1.62 \pm 0.12 \times 10^4 \text{ Glyr}^3, \\ &= 1.37 \pm 0.10 \times 10^{79} \ m^3. \end{aligned} \tag{5.48}$$

The entropy of the CEH is calculated using the Bekenstein-Hawking horizon entropy equation as suggested by Gibbons and Hawking (1977).

$$\begin{aligned} S_{\text{CEH}} &= \frac{kc^3}{G\hbar} \frac{A}{4} = \frac{kc^3}{G\hbar} \pi R_{\text{CEH}}^2 \\ &= 2.6 \pm 0.3 \times 10^{122} \ k \end{aligned} \tag{5.49}$$

Uncertainty in the CEH radius, volume, and entropy are dominated by uncertainties in Hubble's constant (Figure 5.9).

The CEH monotonically increases, asymptoting to a constant radius and entropy slightly larger than its current value (see Figure 5.10). We calculate the asymptotic radius, volume, and entropy to be

$$\begin{aligned} R_{\text{CEH}}(t \to \infty) &= 16.4 \pm 0.4 \text{ Glyr} \\ &= 1.55 \pm 0.04 \times 10^{26} \ m \end{aligned} \tag{5.50}$$

$$\begin{aligned} V_{\text{CEH}}(t \to \infty) &= 1.84 \pm 0.15 \times 10^4 \text{ Glyr}^3 \\ &= 1.56 \pm 0.13 \times 10^{79} \ m^3 \end{aligned} \tag{5.51}$$

$$S_{\text{CEH}}(t \to \infty) = 2.88 \pm 0.16 \times 10^{122} \ k. \tag{5.52}$$

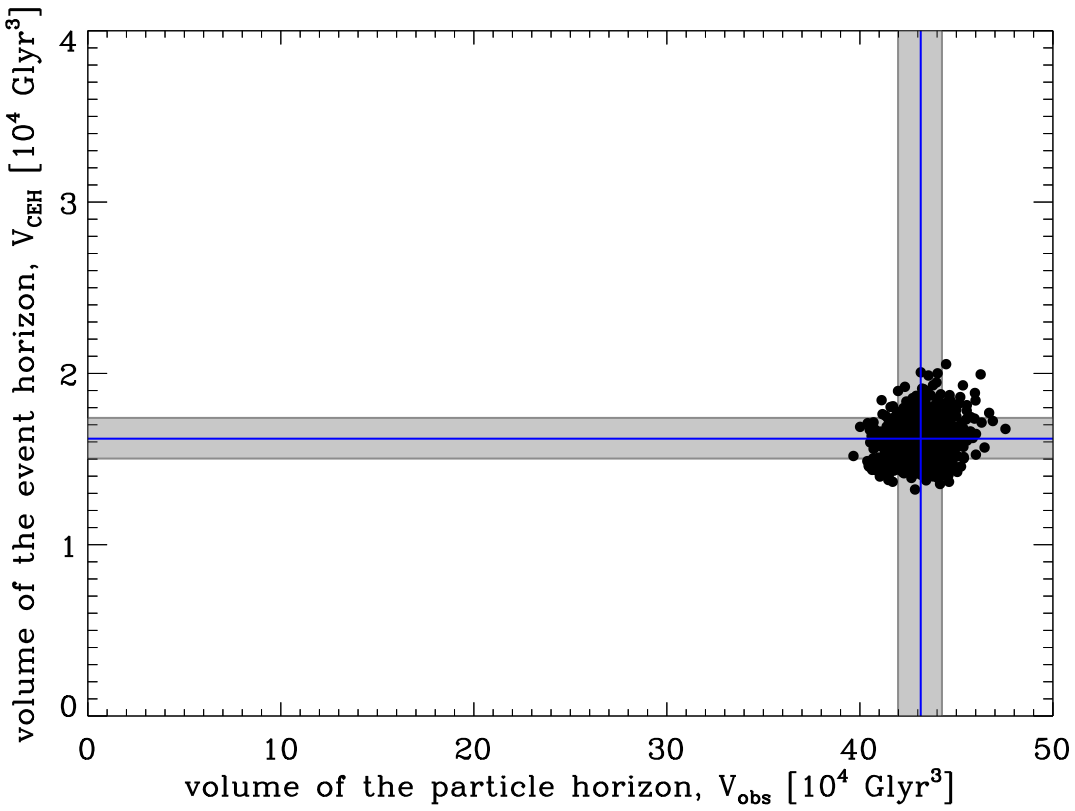

Figure 5.8 Eight hundred realizations of $V_{\rm obs}$ and $V_{\rm CEH}$ indicate the volume of the observable universe is $43.2 \pm 1.2 \times 10^4$ Glyr^3 (horizontal axis) and the volume of the cosmic event horizon is $V_{\rm CEH} = 1.62 \pm 0.12 \times 10^4$ Glyr^3 (vertical axis). We note that there is only a weak correlation between uncertainties in the two volumes.

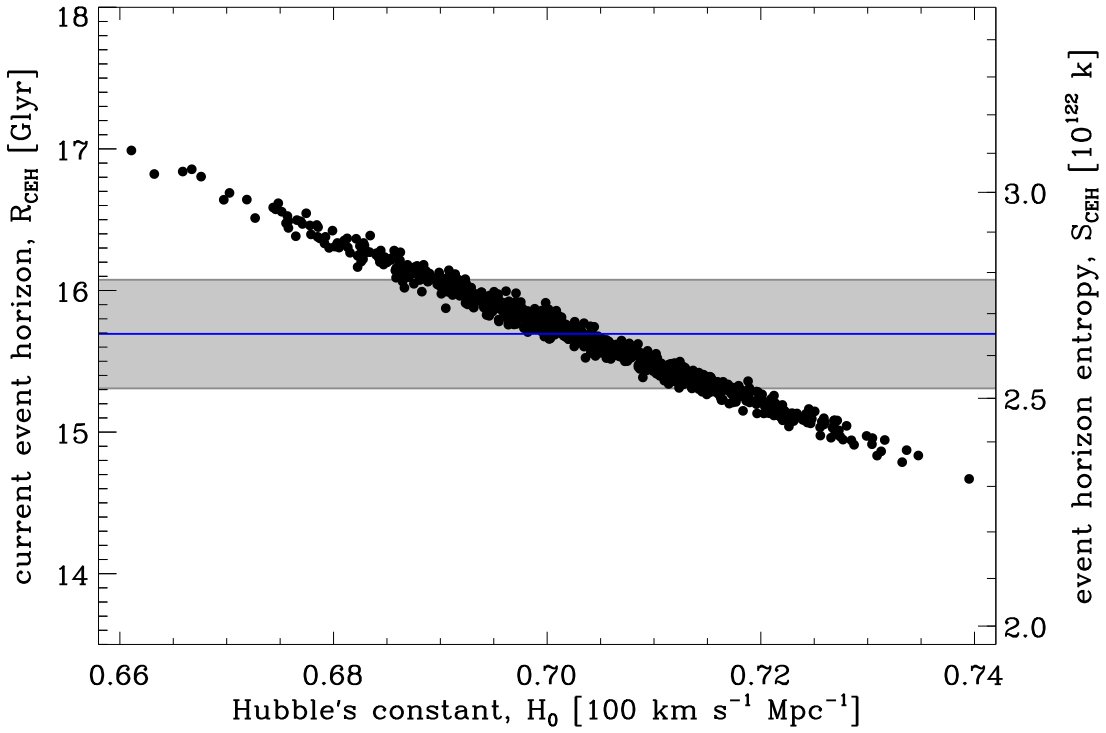

Figure 5.9 We find $S_{\mathrm{CEH}} = 2.6 \pm 0.3 \times 10^{122}\ k$, in agreement with previous estimates $S_{\mathrm{CEH}} \sim 10^{122}\ k$ (Bousso et al., 2007). Uncertainties in S_{CEH} come from uncertainties in R_{CEH}, which are almost exclusively due to uncertainties in h.

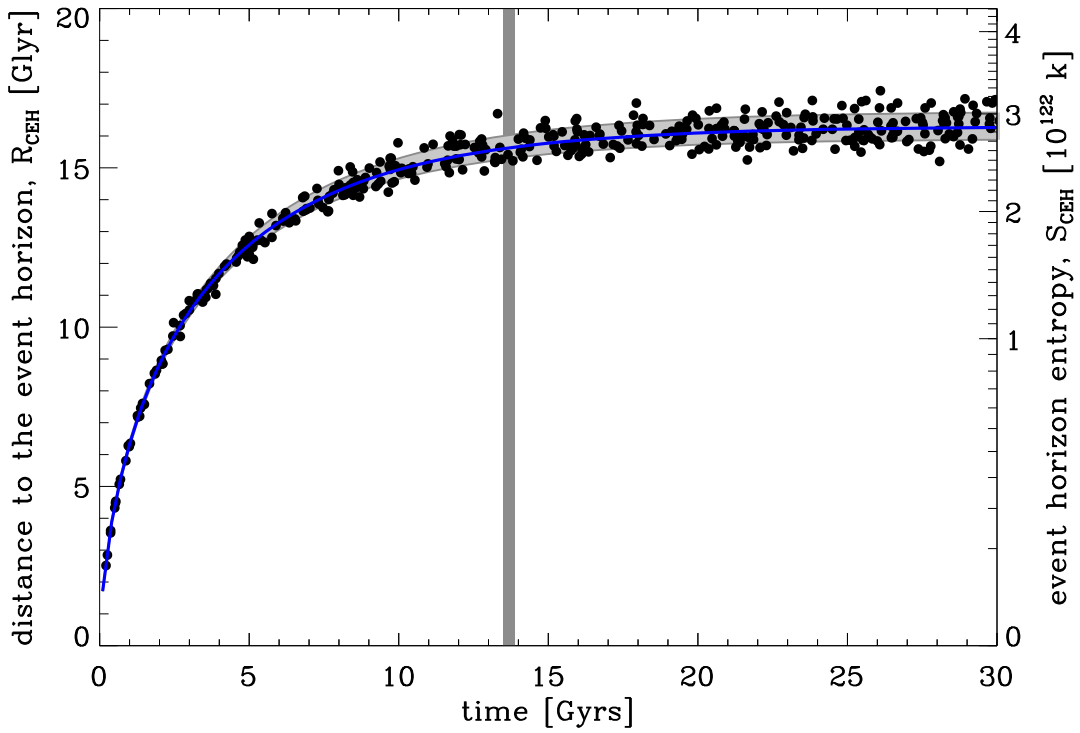

Figure 5.10 Proper distance to the event horizon is shown as a function of time. The vertical gray line represents the present age of the universe (and its width, the uncertainty in the present age). During dark energy domination, the proper radius, proper volume, and entropy of the CEH will monotonically increase, asymptoting to a constant.

CHAPTER 6

HOW HIGH COULD THE ENTROPY BE AND WILL THE UNIVERSE END IN A HEAT DEATH?

If we should stay silent,
if fear should win our hearts,
our light will have long diminished,
before it reaches the farthest star.

- VNV Nation, "The Farthest Star"

6.1. Introduction

The increase of entropy (and use of free energy) drives all dissipative physical processes in the universe including gravitational clustering, accretion disks and supernovae, stellar fusion, terrestrial weather, chemical reactions, geological processes and terrestrial-planet-bound biology (Frautschi, 1982; Lineweaver and Egan, 2008).

The long-term sustainability of dissipative processes (including life) depends on the availability of free energy in the future. If, for any reason, the entropy

of the universe S_{uni} achieves a value that cannot be further increased, then the universe enters a heat death (see figure 6.1). This idea motivates the exploration of potential entropy growth and entropy limits.

Frampton et al. (2008); Frampton and Kephart (2008) recently estimated that the present entropy of the observable Universe is $10^{102}\ k - 10^{103}\ k$ and that the maximum entropy the universe could have was $S_{max} \sim 10^{123}\ k$. Their maximum entropy was calculated by applying the holographic bound ('t Hooft, 1993; Susskind, 1995) to the present volume of the observable Unvierse. That the increase of entropy has not yet been capped by some limiting value is the reason that dissipative processes are ongoing and that life can exist.

However there remains some ambiguity about how to best define the maximum entropy S_{max} and whether or not the entropy of the Universe S_{uni} will reach S_{max}. Figure (6.2) shows several illustrations depicting the relationship between S_{uni} and S_{max} that have appeared in the literature, books and popular science over the past three decades.

Adams and Laughlin (1997) provide an excellent overview of the processes which, according to our current understanding, will dominate the future evolution of the universe, but in their brief discussion of the thermodynamic fate of a ΛCDM universe (now the standard model of our Universe) they ultimately leave the question of whether our Universe will reach equilibrium, and end in a heat death, open.

More recently (e.g. Bousso et al. 2007; Mersini-Houghton and Adams 2008), the maximum entropy of a de Sitter future has been discussed in the context of anthropic explanations for the low density of the dark energy (the so-called cosmological constant problem), but several issues remain to be clarified.

Below are a number of considerations we have identified to help understand disagreement in the literature. We resolve some, and some deserve further discussion.

1. **Theoretically motivated S_{max}:** If S_{max} is defined using a theoretically motivated entropy bound such as the Bekenstein bound (Bekenstein, 1981) or the holographic bound ('t Hooft, 1993; Susskind, 1995) (both of which apply to weakly gravitating systems) or using the more recent covariant entropy bound Bousso (1999, 2002) (which may apply to strongly gravitating systems), then the result depends on which of these is used.

2. **Should we condition on the available energy?** In a spherical system of radius R which contains mass $M << \frac{Rc^2}{2G}$, the entropy is maximized by converting that energy into massless radiation rather than a black hole

(see Page (1981)). The resulting entropy is $S = \frac{M}{T} << R^{3/2}$ (in Planck units and dropping constants of order 1) and is much less than the holographic bound $S << R^2$ (same conventions). This example illustrates that even while theoretically motivated bounds may hold, they are not always the best choice for S_{max}. If our system is constrained by the amount of energy that is available, then a lower S_{max} may apply.

3. **Should we condition on the equation of state?** The energy in a comoving volume ρ_χ is not conserved in an expanding universe (see e.g. (Carroll, 2004)). Generally $\rho_\chi = \rho a^3 \propto a^{-3w}$ where w is the equation of state, with $w = 1/3$ for radiation, $w = 0$ for matter and $w = -1$ for dark energy. The amount of energy available at a future time does depend on what form (what w) the energy is stored in. The question of the future of entropy production of the universe therefore depends on whether or not we suppose that energy can be transferred between different equations of state. Harrison (1995) pointed out that energy could be mined from the universe by tethering distant galaxies. A network of tethered galaxies has a negative pressure and an equation of state $w < 0$ and is among the scenarios we may be interested in considering in an analysis of possible future entropy production.

4. **Normalization volume:** Whether the entropy of the universe is increasing or not can depend on the definition of "the Universe". For example, while the entropy in a comoving volume is constant during adiabatic expansion, the entropy in the observable universe may grow due to the growth of the particle horizon (which bounds the observable universe).

5. **How efficiently can energy be collected?** If dissipative processes require the collection of matter, then the transport costs (energy and entropy) need to be included in the calculations.

6. **Other possible constraints:** When asking what the entropy of the universe could be, one is suggesting a universe which is different to the real universe, but has not specified how it is different. Some of the above points, such as "Should we condition on the available energy?" and "Should we condition on the equation of state?" are examples of aspects which are not clearly defined, but there may also be other, more subtle, issues. For example, Frautschi (1982) evaluates S_{max} during the radiation era by supposing the creation of a large black hole from radiation, but given that mechanisms for this did not exist, the available free energy so calculated have little to do with reality, and may not be of interest.

In the present work we assume an FRW expanding universe with the concordance

ΛCDM parameter values, $h_0 = 0.71$, $\Omega_m = 0.27$ and $\Omega_{DE} = 0.73$ (Seljak et al., 2006).

When we say "the entropy of the universe, S_{uni}" we mean the entropy in the sphere of comoving radius 46 *Glyr* that is now the observable universe. Since the particle horizon grows in comoving coordinates, our 46 *Glyr* comoving sphere was larger than the observable universe in the past and will not include the whole observable universe in the future.

Our aim is to investigate the issues we have listed in this introduction, and others that may arise.

In Section 6.2 we evaluate various entropy bounds S_{max} that have been proposed in the literature. By applying these bounds on our chosen volume, using a consistent cosmology, we gain some insight into their differences and similarities. In Section 6.3 we explore a natural definition of S_{max} as the entropy at which the universe has zero free energy F given the available energy U and exhaust temperatures T_{exh}. The conclusions of these preliminary investigations are also given in Section 6.3.

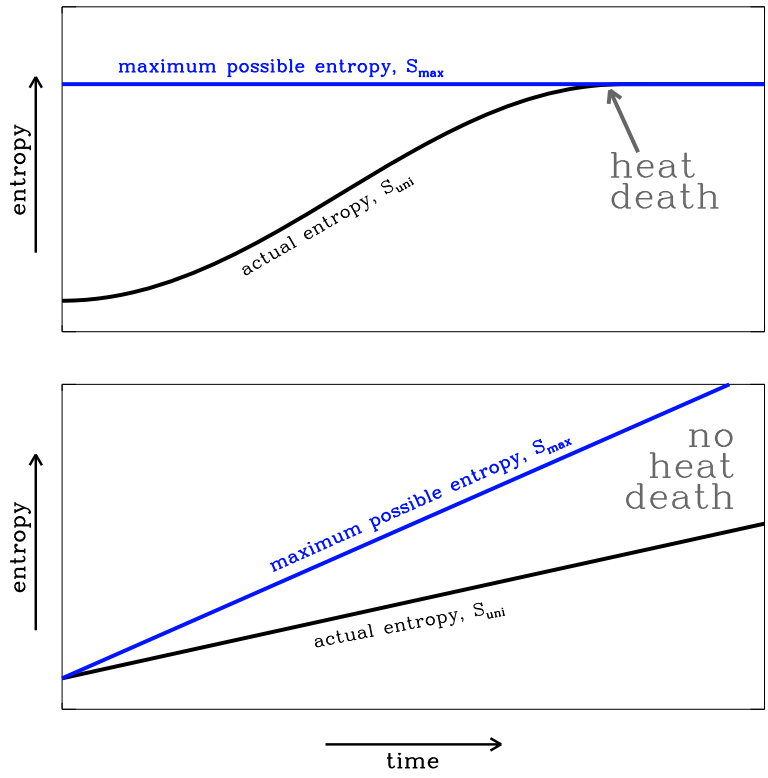

Figure 6.1 Whether the Universe eventually achieves maximum entropy depends on the time dependence of the maximum entropy S_{max} and the actual entropy of the Universe, S_{uni}. There is some ambiguity about how to best define S_{max}.

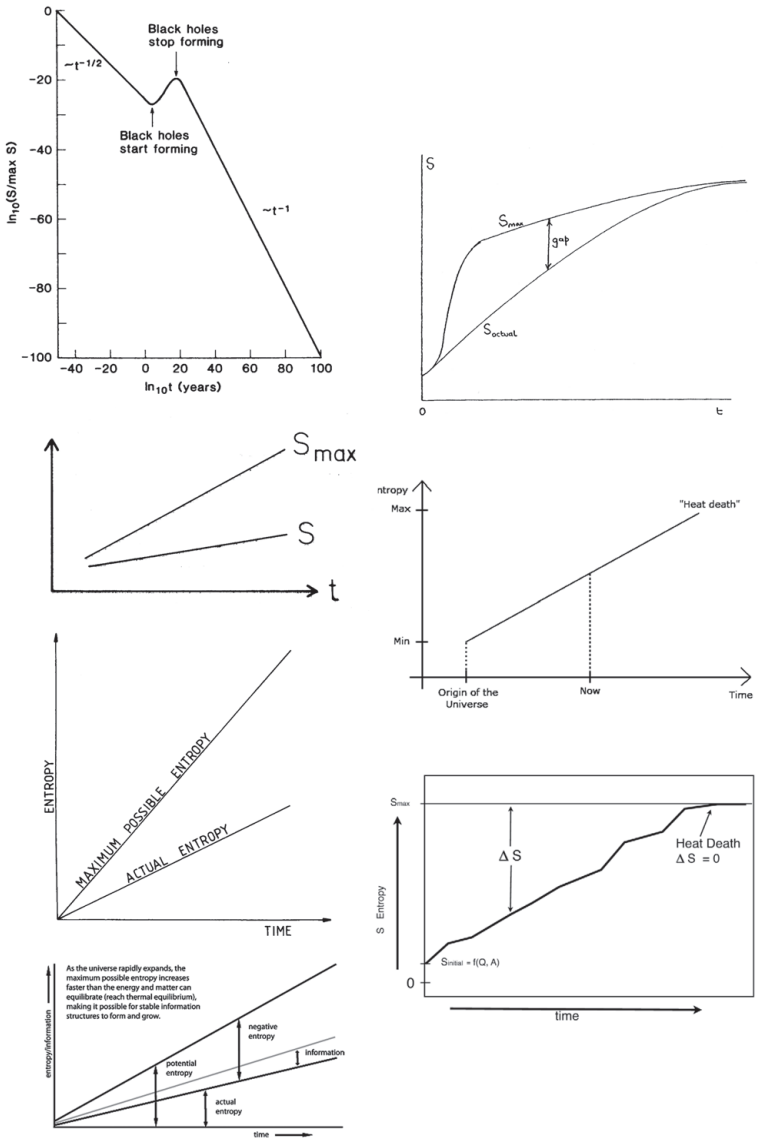

Figure 6.2 The figures in the left column are, starting at the top, from Frautschi (1982), Frautschi (1988), Barrow (1994) and Layzer (2009) and show S_{max} growing indefinitely (and faster than S_{uni}). In these figures the universe does not end in a heat death and free energy is always available to drive dissipative processes (including life). The figures in the right column are, starting at the top, from Davies (1994), Thomas (2009) (depicting the description given by Penrose (2004)) and Lineweaver and Egan (2008). They show S_{max} as a constant, or asymptoting to a constant, which is eventually reached by the actual entropy of the universe S_{max}. The future depicted in these figures is very different to those in the left column: here the universe runs out of free energy and all dissipative processes cease. The goal of this work is to understand the differences between these two points of view and help lead to a resolution of the fate of life in the Universe.

6.2. Different Versions of S_{max}

6.2.1. The Holographic Bound

The most discussed entropy bound is the holographic bound ('t Hooft, 1993; Susskind, 1995): the entropy within a sphere of radius R will not exceed that of a black hole of radius R,

$$S_{sphere\ R} \leq S_{Hol-Bound} = \frac{kc^3}{G\hbar}\pi R^2. \tag{6.1}$$

For a comoving volume of physical radius $R = \chi a$ the holographic bound grows as the square of the cosmic scalefactor,

$$S_{Hol-Bound} = \frac{kc^3}{G\hbar}\pi\chi^2 a^2, \tag{6.2}$$

and becomes exponentially large in the future.

In figure 6.3 the holographic bound is applied to a sphere of comoving radius 46 $Glyr$ (the purple line). The actual entropy in the comoving sphere violates the holographic bound during part the radiation era, as shown in the figure. This occurs because the entropy density s of the Universe is approximately homogenous on large scales. The entropy in a volume V is $S \propto V \propto length^3$ whereas the holographic bound grows as the surface area of the volume $S_{Hol-Bound} \propto length^2$ and for a large enough volume $S > S_{Hol-Bound}$. This violation has been used by Bousso (2002) to motivate a covariant form of the holographic bound. At least in its original form, the holographic bound does not deliver a suitable maximum entropy S_{max} for the universe.

6.2.2. The Bekenstein Bound

Historically preceding the holographic bound, the Bekenstein bound (Bekenstein, 1981) is the result of a gedankenexperiment in which a package of energy E, radius R and entropy S is deposited into a black hole. The bound,

$$S_{Bek-Bound} = 2\pi\frac{k}{\hbar c}RE, \tag{6.3}$$

is required by the second law: the entropy S lost into the black hole must not be larger than the increase in the horizon entropy of the black hole. Several papers have studied the related effect whereby entropy-containing-matter recedes across

the cosmic event horizon to extract similar bounds on the entropy density of matter (Davies, 1987; Bousso, 2001).

The plausibility of the Bekenstein bound was confirmed for numerous weakly gravitating systems (Bekenstein, 2005), but the bound is now known to fail for some gravitationally unstable systems (e.g. Bousso 2002).

In the context of the flat-FRW universe,

$$\begin{aligned} S_{Bek-Bound} &= 2\pi\frac{k}{\hbar c}(\chi a)\left(\rho\frac{4\pi\chi^3 a^3}{3}\right) \\ &= \frac{8\pi^2}{3}\frac{k}{\hbar c}\chi^4\rho a^4. \end{aligned} \tag{6.4}$$

The Bekenstein bound is constant during the radiation era (when $\rho \propto a^{-4}$) and increases during the matter and de Sitter eras ($\rho \propto a^{-3}$ and $\rho = const$ respectively). Compared to the Holographic bound, the Bekenstein bound is weaker when applied to regions larger than the Hubble sphere, and stronger when applied to regions smaller than the Hubble sphere. Notice that the Bekenstein bound is not violated in figure 6.3 (the green line).

6.2.3. The Covariant Entropy Bound

A covariant formulation of the Holographic bound was advanced by Bousso (1999): the entropy S on convergent light-sheets L from a closed surface B will not exceed $\frac{1}{4}$ the area of B,

$$S[L(B)] \leq \frac{kc^3}{G\hbar}\frac{A(B)}{4}. \tag{6.5}$$

In flat spacetime convergent light-sheets from a closed surface B cover the entire interior of B and the covariant entropy bound (CEB) is the same as the original holographic bound: the entropy interior to B cannot exceed $\frac{1}{4}$ the area of B. In general spacetimes the convergent light-sheets may not cover the interior of B. Specifically, the light sheets may be terminated by a singularity (such as the big bang) or they may stop converging and start to diverge (in which case they are truncated). In both of these cases the light sheets only cover part of the interior of B and the CEB is weaker than the corresponding holographic bound.

We calculate the covariant entropy bound in an expanding, flat, FRW universe by choosing the surface B and light-sheet L such that the entropy density bound on the light-sheets is strongest (following the prescription given in Bousso (1999)). We find that the strongest bound on the comoving entropy density

comes from the past-outgoing lightsheet of a closed spherical surface B with a radius infinitessimaly larger than c/H. In this case the comoving entropy density is limited to

$$s_{\chi\ ceb} \leq \frac{kc^2}{G\hbar}\frac{1}{4\eta + 4\eta^2 H + \frac{4\eta^3 H^2}{3}} \tag{6.6}$$

where $\eta \equiv \int_0^t \frac{dt}{a(t)}$ is the conformal time. The dark blue line in figure 6.4 shows this bound applied to a sphere of comoving radius 46 $Glyr$, i.e.

$$S_{ceb} = s_{\chi\ ceb}\frac{4\pi(46\ Glyr)^3}{3}. \tag{6.7}$$

The bound is saturated by the entropy of radiation fields at the Planck time, increases during radiation and matter domination, and asymptotes to a constant during the de Sitter future,

$$\begin{aligned} s_{\chi\infty} &\leq \frac{kc^2}{G\hbar}\frac{3}{4\eta_\infty^3 H_\infty^2} \\ &\leq 4.7 \times 10^{18}\ J\ K^{-1}\ m^{-3}. \end{aligned} \tag{6.8}$$

What Bousso has done is to introduce causal limitations to the regions on which the holographic bound can be applied, and intriguingly this seems to prevent the bound from being violated (at least in the cases studied in Bousso (1999, 2001) and in the concordance FRW universe here).

6.2.4. Frautschi's Maximum Entropy

Frautschi (1982) identifies the maximum entropy inside a causal region (particle horizon) as the entropy produced by the collection of all matter into a single black hole.

Following Frautschi (1982), the mass available in any causal region for the formation of the black hole is

$$M_{max\ BH} = \rho\frac{4\pi}{3}\chi_{PH}^3 a^3 \tag{6.9}$$

where χ_{PH} is the comoving radius of the particle horizon. The corresponding entropy is

$$\begin{aligned} S_{max\ BH} &= \frac{4\pi kG}{c\hbar}\left[\rho\frac{4\pi}{3}\chi_{PH}^3 a^3\right]^2 \\ &= \frac{64\pi^3 kG}{9c\hbar}\rho^2\chi_{PH}^6 a^6 \end{aligned} \tag{6.10}$$

We are interested in the total entropy in a comoving volume of radius 46 *Glyrs*. In the early universe this comoving volume contains many adjacent particle horizons, each with potentially $S = S_{max\ BH}$. The corresponding maximum entropy for a comoving volume is thus

$$\begin{aligned} S_{Frautschi} &= \frac{64\pi^3 kG}{9c\hbar}\rho^2\chi_{PH}^6 a^6 \frac{\chi^3}{\chi_{PH}^3} \\ &= \frac{64\pi^3 kG}{9c\hbar}\chi^3\rho^2\chi_{PH}^3 a^6 \end{aligned} \tag{6.11}$$

The brown line in figure 6.4 applies this bound to a sphere of comoving radius 46 *Glyr*. During radiation domination $\rho \propto a^{-4}$ and $\chi_{PH} \propto a$ so the limit on s_χ grows as a. During matter domination $\rho \propto a^{-3}$ and $\chi_{PH} \propto a^{1/2}$ so the limit on s_χ grows as $a^{3/2}$. During vacuum domination (but assuming black holes cannot be made from dark energy), $\rho \propto a^{-3}$ and $\chi_{PH} \propto constant$ so the limit on s_χ is $\propto constant$.

The possibility of limited gravitational clustering was acknowledged by Frautschi (1982), but in the closed cosmology of the day his work on S_{max} led him and others to favor increasingly instability. The same idea, as presented here with updated cosmology, now predicts stability and a constant $s_{max\ BH}$.

Note that the qualitative future of $s_{max\ BH}$ depends strongly on whether or not black holes can be made from dark energy. If we include the dark energy, then $\rho \propto constant$ and $\chi_{PH} \propto constant$ so the limit on s_χ grows as a^6 (not shown in figure 6.4).

Since black holes may radiate via the Hawking process they do not generally represent the maximum entropy state Page and McKee (1981); Frautschi (1982), i.e. it may be the case that Frautschi's bound is not only attainable (it is that by construction), but in sufficiently empty universes it will be surpassed by the evaporation of black holes. This is explored in the next section.

We note that Frautschi's idea may be unreliable in recent times. After matter domination, the black holes suggested in equation 6.9 have radii larger than the Hubble sphere and are not Schwarzschild black holes. Further work on the interaction between large black holes and the FRW universe is needed to understand the entropy in such situations.

6.2.5. Page's Evaporated Matter

Stellar black holes (with masses $\sim 4M_\odot$) and SMBHs at the center of galaxies (with masses $\sim 10^7 M_\odot$) emit Hawking radiation with characteristic temperatures

of 10^{-8} K and 10^{-14} K respectively. Both these temperatures are far below that of the present CMB (2.725 K) and consequently both classes of BHs currently absorb more radiation than they emit. As the universe is starting to grow at an exponential rate, the CMB will be quickly redshifted below the temperatures of these black holes. 10^{-8} K should come when the universe is 330 $Gyrs$ old and 10^{-14} K when it is 550 $Gyrs$.

By the time black holes stop growing by accretion, the background temperature of the universe will be lower than the temperature of any black holes. They will begin to evaporate. The formation of cluster-sized SMBHs up to $10^{12} M_{\odot}$ is expected (see e.g. (Frampton and Kephart, 2008)). Subsequent evolution will depend on the Hawking process. Black holes this large will have temperatures of 10^{-19} K, which will be hotter than the background after the universe is just 730 $Gyrs$ old.

It may be possible in principle to transmute matter in the universe into radiation via black hole evaporation. In principle this could be done locally everywhere, in an arbitrarily short time, by using sufficiently small black holes. After evaporation, further entropy could be produced by re-thermalizing the Hawking radiation (e.g. by scattering off trace particles). The immediate transmutation and re-thermalization of all radiation, baryons and dark matter would result in a new blackbody background with temperature

$$T_{\gamma} = \left[\frac{15\hbar^3 c^5}{\pi^2 k^4} (\rho_r + \rho_m) \right]^{\frac{1}{4}}, \tag{6.12}$$

and entropy

$$\begin{aligned} \frac{S_{\gamma}}{V} &= \frac{4\pi^2 k^4}{45\hbar^3 c^3} T_{\gamma}^3 \\ &= \frac{4}{3} \left[\frac{\pi^2 k^4 c^3}{15\hbar^3} \right]^{\frac{1}{4}} (\rho_r + \rho_m)^{\frac{3}{4}} \end{aligned} \tag{6.13}$$

This was identified by Page and McKee (1981) as an upper limit to the entropy of the universe. Since $(\rho_r + \rho_m)$ decreases less quickly than a^{-4} more entropy is produced per comoving volume if the transmutation and re-thermalization is done later rather than sooner. Page and McKee (1981) suggested that the entropy in a comoving region of the universe could be made arbitrarily large in this way.

The orange line in figure 6.4 shows the entropy produced by the immediate transmutation and re-thermalization of all radiation, baryons and dark matter in the universe. The current maximum entropy of the universe calculated in this way is

$$S_{\gamma} = 9.2 \times 10^{92} k. \tag{6.14}$$

This is much lower than the actual current entropy ($3.1^{+3.0}_{-1.7} \times 10^{104} k$; Egan and Lineweaver 2010a). This is because BHs and SMBHs are much colder than the CMB; in environments as hot as the present universe BHs and SMBHs do not spontaneously evaporate.

6.2.6. Page's Evaporated Matter - de Sitter Limited

A minor adjustment of Page's idea is required in the presence of a de Sitter cosmic horizon. At $t \sim 1000 Gyrs$ the temperature in equation 6.12 falls below the de Sitter temperature T_{deS}. However, the de Sitter radiation would prevent any (re-)emission of radiation at temperatures lower than T_{deS}.

Thus the final minimum temperature of the evaporated black hole radiation is

$$T_\gamma = Max\left[\left[\frac{15\hbar^3 c^3}{\pi^2 k^4}(\rho_r + \rho_m)\right]^{\frac{1}{4}}, T_{deS}\right], \tag{6.15}$$

and the entropy density is

$$\frac{S_\gamma}{V} = Min\left[\frac{4}{3}\left[\frac{\pi^2 k^4}{15\hbar^3 c^3}\right]^{\frac{1}{4}}(\rho_r + \rho_m)^{\frac{3}{4}}, \frac{4}{3}\frac{\rho_r + \rho_m}{T_{deS}}c^2\right]. \tag{6.16}$$

Figure 6.4 shows this entropy bound applied to a sphere of comoving radius 46 *Glyr* (the dotted orange line). Since the density $(\rho_r + \rho_m)$ tends to decay as a^{-3} in late times, the maximum entropy in a comoving volume tends to a constant.

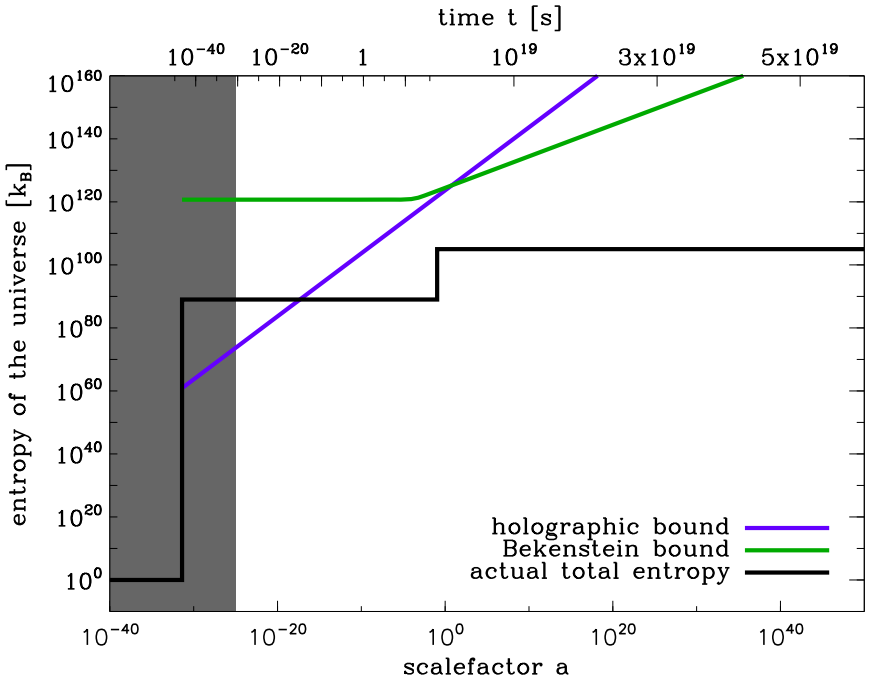

Figure 6.3 Two versions of S_{max}: the holographic bound and the Bekenstein bound. The actual entropy history of the universe from Egan and Lineweaver (2010a) is plotted in black. The holographic bound is violated by the actual entropy history of the universe during the radiation epoch. We shade regions above the GUT temperature, where the evolution of the universe (and its entropy) becomes more speculative.

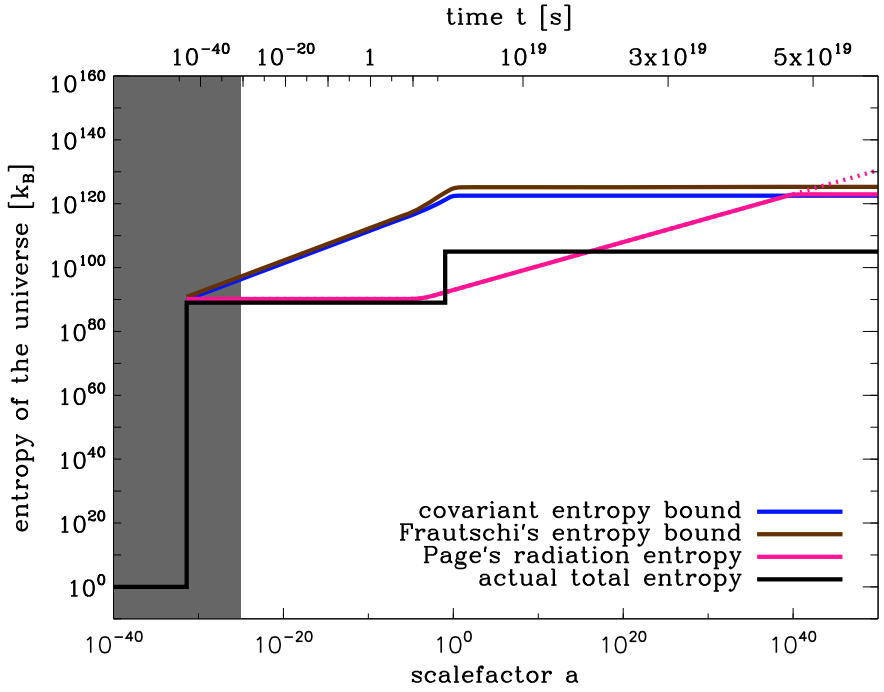

Figure 6.4 More versions of S_{max}: the covariant entropy bound, Frautschi's maximum entropy and Page's evaporated matter entropy in orange with (solid) and without (dotted) consideration for the de Sitter temperature. The actual entropy of the universe is plotted in black. Page's evaporated matter entropy is presently exceeded by the actual entropy history of the universe.

6.3. Discussion

The definition of "the universe" as a comoving volume is a practical answer to *issue 4*. We have not checked whether using this definition reveals any more or less than if we had defined the universe to be the region within the particle horizon (i.e. the time-dependent observable universe), or the event horizon.

Our interest in the entropy history is primarily driven by the question of the long-term sustainability of dissipative processes including life. These processes depend on the availability of free energy (not energy). Dissipative processes deplete free energy by degrading an amount of high-grade (low entropy) energy into an equivalent amount of low-grade (high entropy) energy. As an example of this, dissipative weather action diffuses high-grade energy received from the Sun ($\sim 6000K$ photons) into low-grade energy which is re-transmitted to space (20 times as many photons at $\sim 300K$) (Lineweaver and Egan, 2008).

6.3.1. Free Energy and an S_{max} Defined by Zero Free Energy

Consider a system with total energy U and entropy S_{sys}, which is connected via a heat engine to an infinite exhaust bath at temperature T_{exh}. The system, which is used to fuel the engine has free energy

$$F_{sys} = U_{sys} - T_{exh}S_{sys}, \tag{6.17}$$

which is generally less than its total energy. That is to say, the engine may extract all but $T_{exh}S_{sys}$ of the energy. The unextractable energy is necessarily expelled as exhaust and guarantees that the entropy of products is at least as large as the entropy of the consumed fuel.

$$S_{exh} = Q/T_{exh} \geq (T_{exh}S_{sys})/T_{exh} = S_{sys} \tag{6.18}$$

For real systems the exhaust bath may not be infinite and the temperature T_{exh} may not be constant. In this case 6.17 should be replaced by an integral equation.

The most natural definition of S_{max} is one at which the system has zero free energy.

$$\begin{aligned} F &\sim U - TS \\ S_{max} &\equiv S(F = 0) \\ &\sim \frac{U}{T} \end{aligned} \tag{6.19}$$

The universe is not in a heat death today because $S < S_{max}$ (and so $F \neq 0$). Nevertheless, the amount of energy U in a comoving volume, and the minimum

available exhaust temperature T, are both finite and so there is some finite entropy S_{max} which, if $S = S_{max}$ today, there would presently be no free energy.

$S = S_{max}$ means that no free energy *is* available, but it does not mean that no free energy can *become* available. Both quantities on the right-hand-side of equation 6.19 potentially change with time. Figure 6.5 shows the evolution of U (thick black; taken to be energy in radiation and matter in a comoving volume) and three potential exhaust temperatures,

$$T_{exh} = \begin{cases} T_{CMB}, \\ T_{max\ BH}, \\ T_{deS}. \end{cases} \tag{6.20}$$

The first potential exhaust that we have considered is the cosmic microwave background (CMB; shown in green), the second are large black holes (the largest causal black hole is shown in thick pink; refer to Section 6.2.4), and the third potential exhaust is the the de Sitter background (thick purple).

Today the lowest available exhaust temperature is that of a large black hole (not that of the CMB). If we suppose that large causal black holes could have existed during the radiation era, then those black holes would have been the lowest available exhausts then, and dissipative processes might have been driven by the CMB-black hole temperature gradient. In the near future the CMB temperature will drop below the de Sitter temperature, and that will become the lowest available exhaust.

The maximum entropy S_{max} is calculated using equation 6.19 and is shown in thick blue in the bottom panel of Figure 6.5. Since U and T become constant in the future, and the entropy within the considered comoving volume S_{uni} can only increase, the amount of free energy in the comoving volume decreases in the future (see equation 6.17).

The S_{max} that we have discussed in this section is defined in terms of the available energy and exhaust temperatures (equation 6.19). It is quantitatively similar to the maximum entropy of Frautschi (1982, 1988) by construction (see Section 6.2.4). It is also quantitatively similar to the covariant entropy bound of Bousso (1999) (applied to the same volume; see Section 6.2.3), although the reason for this is not clear to us.

In this section we used the conserved matter in a comoving volume and the constant de Sitter temperature to show that maximum entropy in the comoving volume becomes approximately constant in the future. The bleak implication for dissipative processes is that there is a finite amount of free energy in any comoving volume. On the other hand, the fraction of U that is not free (due to

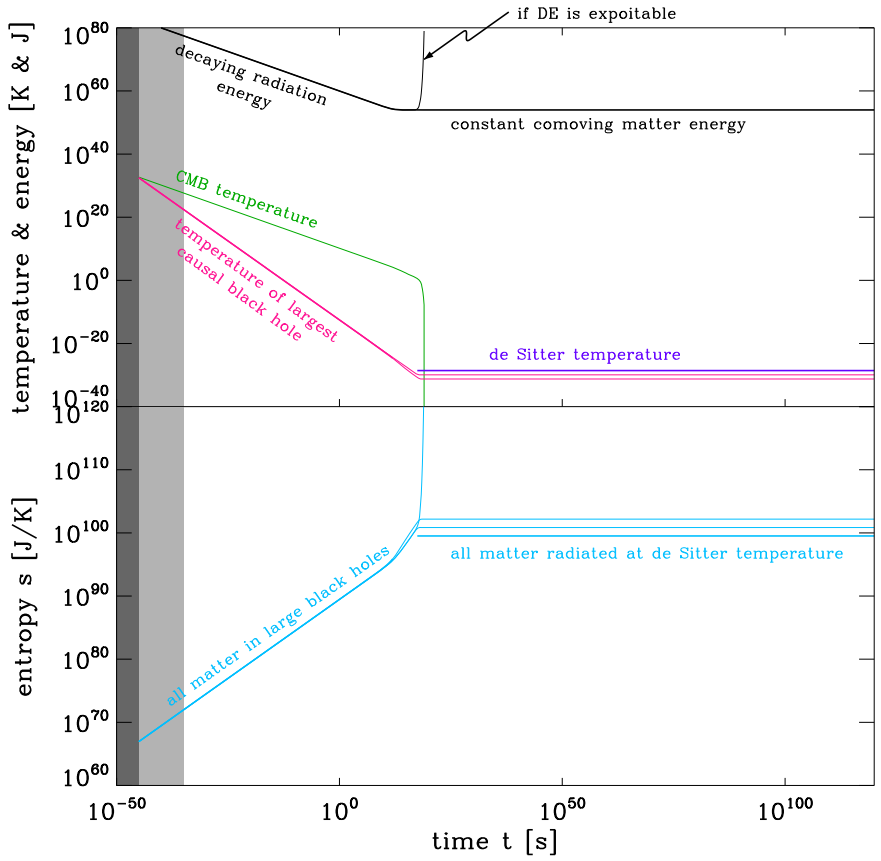

Figure 6.5 The most useful definition of S_{max} is the entropy at which there is no more free energy, $S_{max} \sim U/T_{exh}$. In this figure we show the time evolution of U and T_{exh}. The volume we are considering is the comoving volume that currently corresponds to the observable universe. The energy U is taken to be the total radiation and matter in this volume (thick black). If we include dark energy as a potential fuel U then the energy in the comoving volume rapidly increases around the present time (thin black). Three candidates for T_{exh} are explored: the CMB background temperature (in green), largest causal black holes (in thick pink) and the de Sitter background (thick purple). We use thin pink lines for dubious black holes (these have Schwarzschild radii larger than the hubble sphere). The maximum entropy S_{max} (shown in thick blue) is calculated using $T_{max\ BH}$ at early times (which is lower than T_{CMB}) and T_{deS} at late times.

the cumulative increase in entropy to the present day) is only

$$\frac{ST_{exh}}{U} \lesssim 10^{-10}. \tag{6.21}$$

As mentioned in the introduction (issue 3) future entropy production may depend on whether or not the equation of state of matter can be changed. Using figure 6.5 it is easy now to see the effect this might have. If energy was converted from matter into a form with a lower equation of state $w < w_{matter} = 0$ then the energy U (the black line in Figure 6.5) would increase into the future instead of becoming constant. The exhaust temperature (de Sitter temperature) would not change significantly, since it depends primarily on the dark energy density. As a consequence the maximum entropy, and the free energy would increase. On the other hand, if matter were converted into a form with $w > 0$ (such as radiation, $w_{rad} = 1/3$) would cause U to decrease into the future. Again, T_{deS} remains unchanged and S_{max} and and F would decrease with time.

CHAPTER 7

CONCLUSIONS

As the music finishes again,
have you thought about,
how we almost never lift our eyes,
from the ground,
to the black space above the clouds.

- Kent, "View From a Castle in the Sky"

The Cosmic Coincidence Problem

Matter and dark energy are observed to presently contribute to the total cosmic energy density in the ratio

$$r_0 \equiv \min\left[\frac{\rho_{m0}}{\rho_{de0}}, \frac{\rho_{m0}}{\rho_{de0}}\right] \approx 0.4. \tag{7.1}$$

Since the matter and dark energy densities dilute at different rates during the expansion of the Universe, we are faced with the cosmic coincidence problem: Why are the current matter and dark energy densities the same order of magnitude today? In other words, why is r (as defined above), so large?

We have used the temporal distribution of terrestrial planets in the Universe to estimate the temporal range during which terrestrial-planet-bound observers are

likely to arise. Using this observer distribution we have quantified the severity of the cosmic coincidence problem by computing the probability $P(r > 0.4)$ of observing values of r larger than 0.4.

Assuming the standard ΛCDM density histories for ρ_m and ρ_{de} we find

$$P(r > 0.4) = 68^{+14}_{-10}\%. \tag{7.2}$$

Given the temporal distribution of terrestrial planets, terrestrial-planet-bound observers have a large probability of observing the matter and dark energy densities to be at least as close as we measure them to be.

The same method is applied under the assumption of dynamic dark energy, with an equation of state parameterized by w_0 and w_a. We find that some regions of w_0-w_a parameter space can be discriminated against on grounds of the coincidence problem. I.e. for some regions of w_0-w_a parameter space, the probability of observing values of $r > 0.4$ is very low (Figure 3.7). However those regions are already strongly excluded by observations.

Our main result is an understanding of the coincidence problem as a temporal selection effect if observers emerge preferentially on terrestrial planets which is found to hold under any model of dark energy fitting current observational constraints. The cosmic coincidence problem is therefore removed as a factor motivating dark energy models.

Searching for Life Tracers Amongst the Solar Properties

We have compared the Sun to representative stellar samples in 11 properties. The properties were selected based a plausible relation to life, availability of a representative stellar sample for comparison, and such that they were maximally uncorrelated. No properties were added to, or removed from the analysis based on previous information about whether or not the Sun was anomalous in those properties.

Those selected properties were

1. mass,
2. age,
3. metallicity,

4. carbon-to-oxygen ratio,
5. magnesium-to-silicon ratio,
6. rotational velocity,
7. galactic orbital eccentricity,
8. maximum height above galactic plane,
9. mean galactocentric radius,
10. host galaxy mass and
11. host group mass.

Our main results are:

- Mass and galactic orbital eccentricity are the most anomalous properties of those included in our study. The Sun is more massive than $95 \pm 2\%$ of nearby stars and has a Galactic orbit which is more circular than 93 ± 1 of FGK stars within 40 *pc*.
- When the 11 parameters are considered together, the probability of selecting a star, at random, which is more anomalous than the Sun, is just $29 \pm 11\%$.

The observed "anomalies" in mass and galactic orbital eccentricity are consistent with statistical noise (refer to Figure 4.4). This contrasts with previous work suggesting anthropic explanations for the Sun's high mass.

To our knowledge, this is the most comprehensive comparison of the Sun to other stars.

The Entropy of the Present and Future Universe

We present budgets of the entropy of the observable Universe (Table 5.1) and of the cosmic event horizon and its interior (Table 5.2). To our knowledge these are the most comprehensive and quantitative budgets of the present entropy of the Universe. The components included are

1. the cosmic event horizon (only applicable to the latter budget),
2. supermassive black holes,

3. tentative stellar black holes in the range 42-140 $M_\odot$,
4. confirmed stellar black holes in the range 2.5-15 $M_\odot$,
5. photons,
6. relic neutrinos,
7. dark matter,
8. relic gravitons,
9. interstellar and intergalactic media and
10. stars.

The present entropy of the observable universe is found to be

$$S_{obs} = 3.1^{+3.0}_{-1.7} \times 10^{104}\ k, \tag{7.3}$$

and is dominated by supermassive black holes. This is to be compared with previous estimates in the range $10^{101}\ k$ to $10^{103}\ k$. Our larger value arises from the inclusion of a new measurement of the supermassive black hole mass function.

The present entropy of the cosmic event horizon is calculated to be

$$S_{CEH} = 2.6 \pm 0.3 \times 10^{122}\ k, \tag{7.4}$$

dwarfing that of its interior,

$$S_{CEH\ int} 1.2^{+1.1}_{-0.7} \times 10^{103}\ k. \tag{7.5}$$

Figure 5.5 illustrates the possible role played by intermediate mass black holes. The time evolution of these two budgets is discussed (see Section 5.4 and Figures 5.6 and 5.7).

Entropy bounds from the literature are applied to a comoving volume normalized to the present observable Universe (Fgures 6.3 and 6.4). While the Bekenstein bound and the holographic bound become arbitrarily large, Bousso's covariant entropy bound on this volume increases monotonically and asymptotes to a constant around $10^{123}\ k$. As does a simplistic bound based on the assumption that the comoving matter density is constant and that the future background temperature is the de Sitter temperature. According to both of these bounds the free energy in the comoving volume is also finite and a heat death is therefore expected (either in a finite time or asymptotically).

APPENDICES

APPENDIX A

ENTROPY AND THE FREE ENERGY PREREQUISITES FOR LIFE IN THE UNIVERSE

Charles H. Lineweaver
Chas A. Egan

A.1. The Irreversible History of Entropy

A.1.1. Pedagogical Pitfalls

Although an undergraduate education in the physical sciences contains no explicit warnings against thinking about biology, most physics graduates come out believing that the most fundamental aspects of the universe are dead things in equilibrium obeying conservative forces. Frictionless pendulums may be simple, but when studied for too long, students begin to believe that they really exist. They don't. Friction is not just an optional accessory inserted into simple equations to make life difficult. Friction, dissipation and the unequal sign in the second law of thermodynamics is what makes life possible. The first law of thermodynamics (energy conservation) precedes the second (entropy increase) in textbooks, but there is no evidence that this precedence reflects any natural order of things in the universe.

Physicists are taught that whatever biology is about, it can be reduced to chem-

istry; and that whatever the chemists are up to, it can be reduced to physics. However, physics as we know it can also be viewed as a subset of biology since all physicists are the products of biological evolution.

Much has been made of our current inability to unify general relativity and quantum mechanics to arrive at a theory of everything. Although the murky relationship between gravity and entropy may provide key insights into the theory of everything, it has received much less attention. Although gravitational collapse plays the most important role in converting the initial low entropy of the universe into the dissipative structures we see all around us (including ourselves), gravity is almost universally ignored in thermodynamics textbooks.

> "We do not yet know if the second law applies to gravitational interactions. Is the second law valid only from a given (or "slowly" varying) gravitational state? Can we include gravitation?" (Prigogine 1980, p. 196)

In this paper, we attempt to make sense out of the relationship between life, gravity and the second law of thermodynamics. In Section A.1 we briefly review the history of attempts by physicists to understand life. In Section A.2 we describe how free energy and low entropy radiation from the Sun maintains the low entropy structures of Earth. We review the entropy of photons in an expanding universe in Section A.3 and consider the relationship between gravity and entropy in Section A.4. We conclude by discussing the heat death of the universe (Section A.5). Our goal is to understand more clearly how gravitational collapse is the source of free energy for life in the universe. Appendices contain mathematical details.

A.1.2. Physicists and Life

When iconoclastic physicists move out of equilibrium and think generally about the question "What is life?", the concepts of entropy and free energy play central roles. In the first half of the 19th century, Carnot(1824), Clausius(1867) and others came to understand that although energy is conserved and can not be destroyed, useful work – or extractable free energy – could be destroyed. Irreversible processes are destroying free energy all the time. Ludwig Boltzmann (1886) was concerned about entropy and the distinction between energy and free energy:

> "The general struggle for existence of animate beings is therefore not a struggle for raw materials — these, for organisms, are air, water

> and soil all abundantly available – nor for energy which exists in plenty in any body in the form of heat (albeit unfortunately not transformable), but a struggle for entropy, which becomes available through the transition of energy from the hot sun to the cold earth."

In Section A.2 we describe and quantify this "transition of energy from the hot sun to the cold earth". Although Boltzmann explicitly talks about "animate beings", the same thing could be said about any far from equilibrium dissipative structure: convection cells, hurricanes, eddies, vortices and accretion disks around black holes (Glansdorff & Pirgogine 1971, Nicolis & Prigogine 1977, Prigogine 1980). Life is a subset of this general class of dissipative structure (Schneider & Kay 1994, 1995, Lineweaver 2006, Schneider & Sagan 2006).

In "What is Life?" (Schroedinger 1944) made it clear that Boltzmann's animate beings were not struggling for entropy. If they were struggling at all, it was to get rid of entropy, or to absorb negentropy:

> "What an organism feeds upon is negative entropy. Or, to put it less paradoxically, the essential thing in metabolism is that the organism succeeds in freeing itself from all the entropy it cannot help producing while alive."

In the notes for a later edition (1956) Schroedinger apologizes to his physicist colleagues and admits that instead of negative entropy, he should have been talking about free energy. There is general agreement that life on Earth (and elsewhere) depends on the non-equilibrium of the universe and requires free energy to live.

> "[T]he one unequivocal thing we know about life is that it always dissipates energy and creates entropy in order to maintain its structure." (Andersen and Stein 1987).

In our search for extraterrestrial life, we can use the most fundamental aspects of terrestrial life to guide us. At the top of the list is life's requirement for free energy. Despite uncertainties in the temperature limits of life ($< 130^{\circ}$ C?), despite uncertainties in which solvent life can use (water?), despite uncertainties in its chemistry (carbon-based?) - extraterrestrial life, like terrestrial life, will need a source of free energy. Free energy is a more basic requirement that all life anywhere must have. Thus, instead of "follow the water", our most fundamental life-detection strategy should be "follow the free energy". To find chemistry-based life we should look for the redox gradients between electron donors and

acceptors. These considerations motivate us to quantify and understand the origin of free energy (Fig. A.1).

In the beginning, 13.7 billion years ago, the universe was very hot. There was no life and there were no structures in the universe. The universe was a thermal heat bath of photons and a soup of nuclei (and later atoms) in chemical equilibrium. Life is not possible in such an environment. In thermal equilibrium and chemical equilibrium, no free energy is available. As the universe expanded, the heat bath cooled and life emerged. Life did not emerge simply because the universe cooled down to have the right temperature for H_2O to be a liquid. Life needed a source of free energy unavailable from an environment in chemical and thermal equilibrium. In this paper we try to clarify the idea that the origin of all sources of free energy can be traced back to the initial low gravitational entropy of the unclumped matter in the universe (e.g. Penrose 2004). The gravitational collapse of this matter produced galaxies, stars and planets and is the source of all dissipative structures and activities, including life in the universe. See Dyson (1979), Zotin (1984) and Chaisson (2001) for discussion of how life (unlike abiotic dissipative structures) seems to evolve toward more complexity.

A.1.3. The Pyramid of Free Energy Production

Usually bacteria are considered to be at the bottom of the food chain or at the base of the primary production pyramid, but an interesting perspective comes when we add layers to the base of the pyramid. At the top of Fig. A.1 are heterotrophs, who eat (= extract free energy from) organic compounds (including other heterotrophs) produced by the primary producers one level down. Heterotrophs include wolfs, humans, fish and mushrooms. Supporting all heterotrophic life are the primary producers (phototrophs and chemotrophs). Although phototrophs and chemotrophs are usually considered to be primary producers, they get their free energy from solar photons and inorganic compounds, respectively. Phototrophs include plants and cyanobacteria and all photosynthesizers. Chemotrophs include iron and manganese oxidizing bacteria living off the non-equilibrium chemistry of igneous lava rock.

The vertical line in Fig. A.1 indicates that stars are the free energy sources for phototrophs while the chemical and thermal disequilibrium of the Earth is the source of the free energy in the inorganic compounds used in the metabolisms of chemotrophs. The source of both the free energy provided by stars and by planets comes from gravitational collapse in the level below in the sense that the source of starlight is the fusion reactions taking place in the hot, dense center of the Sun that is the result of gravitational collapse. The chemical and thermal

disequilibrium of the Earth also has its source in the free energy of gravitational collapse.

Moving one level lower in the pyramid, gravitational collapse is made possible by an initially very diffuse, almost unclumped distribution of baryons. Unclumped baryons in the early universe provided the initial low entropy of the universe. At the lowest level in the pyramid, the source of these almost unclumped baryons is baryon non-conservation (Sakharov 1967). The low initial gravitational entropy of the universe and baryon non-conservation are discussed further in Section A.4.

The sources of free energy in the universe are summarized in Fig. A.2. In a gravitational system (left panel), such as a protoplanetary accretion disk, consider a small mass m in orbit at distance r from a large mass M at $r = 0$. The effective potential, including angular momentum L is $\phi(L, r) = \frac{L^2}{2mr^2} - \frac{GmM}{r}$ (e.g. Goldstein 1980). Angular momentum L must be reduced for gravitational collapse to happen. Consider two small masses, originally in identical effective potentials (two light grey balls). They come close to each other and exchange some angular momentum. The one that lost L, sinks into the well closer to M, the one that gained L distances itself from M. Since the L of each mass has changed, their effective potentials have diverged. One m collapses, the other is expelled. Without the dissipation of energy, expulsion of matter and transfer of angular momentum that occurs in the turbulence and viscosity of an accretion disk (e.g. Balbus 2003), matter would not gravitationally collapse. The efficiency of star formation in a molecular cloud is a few percent. A substantial fraction of the infalling matter is scattered, or receives a large dose of angular momentum as it is processed through the accretion disk and then expelled (Balbus 2003). Therefore accretion disks are also expulsion disks (see Fig. A.3 for the role of dynamical friction in the gravitational collapse of less-viscous non-accretionary systems). Gravitational collapse creates entropy by radiating away the MG/r potential energy and expelling high velocity, high angular momentum material.

Fusion in the core of the Sun was made possible by the gravitational collapse of $\sim 10^{31}$ kg of hydrogen resulting in high densities and temperatures. Gravitational collapse also provides the conditions in the cores of stars to make matter roll down the nuclear binding energy curve to the energy minimum (middle panel, Fig. A.2).

The right panel of Fig. A.2 shows that the amount of energy extractable from chemical bonds depends on the energy difference ΔE between the electron in the potential well of the donor and that of the acceptor (Nealson & Conrad 1999). Life takes in energy-rich atoms with electrons in high orbitals (electron donors) and excretes the same atoms with the electrons in the deeper atomic

or molecular orbitals of electron acceptors. Solar photons provide the energetic kick ΔE to lift the electrons back up during photosynthesis in phototrophs, who provide the energy-rich materials for heterotrophs (e.g. Szent-Gyorgi 1961).

A.1.4. Big Bang Nucleosynthesis and the Subsequent Low Entropy of Nuclei

As the universe expands, the scale factor R increases, the temperature decreases ($T \propto R^{-1}$) and the density decreases $\rho \propto R^{-3}$. Thus, $\frac{T}{T_i} = \left(\frac{\rho}{\rho_i}\right)^{1/3}$. This is the path the universe takes in Fig. A.4 starting at some initial temperature and density: T_i, ρ_i. The early universe expanded and cooled too quickly for big bang nucleosynthesis to fuse hydrogen into iron and reach equilibrium at the lowest nuclear binding energy per nucleon (middle panel, Fig. A.2). Thus, big bang nucleosynthesis left nuclei in a low entropy, high energy state. Similarly, reheating after inflation (Kolb & Turner 1990) left unclumped baryons in a state of low gravitational entropy since the baryons are not at the bottom of the gravitational potential wells.

Entropy is produced when free energy is extracted from the sources of potential energy shown in Fig. A.2. For example, dissipation of gravitational energy (left panel) happens when the turbulent viscosity and friction of an accretion disk transfers angular momentum away from the central mass and makes some material fall onto the central mass while other material is expelled. Without such collisions, turbulence and friction, angular momentum would not be transferred and material would not gravitationally collapse or be expelled. Figure A.8 illustrates gravitational systems with minimal dissipation.

Dissipation happens and entropy is produced whenever a photon gets absorbed by a material at a temperature colder than the emission temperature. The photon energy gets reemitted and distributed among many photons. This happens as a gamma ray produced by fusion at the center of the Sun makes its way to the photosphere where its energy is distributed among millions of photons (Frautschi 1988). It also happens when the energy of solar photons (T = 5760 K) are harvested for photosynthesis by plants at temperatures below T = 5760 K, and when the Earth reemits solar energy at infrared wavelengths.

Energy cannot be created or destroyed. Therefore, strictly speaking, we cannot "use energy" or "waste energy". Energy can however be degraded. Low-entropy, high-grade energy dissipates into high-entropy, low-grade energy. Life does not "use" energy since the same amount of energy that enters the biosphere, leaves the biosphere. Life needs a source of free energy, and is unable to use

high entropy energy. Life takes in energy at low entropy and excretes it at high entropy. Any engine does the same thing. When coal burns, energy is conserved. Electrons are high in the electric potentials of the fuel and lower in the potentials of the ashes and exhaust gases. The difference (ΔE in the right panel of Fig. A.2) has been transfered into heat and work.

Two types of free energy are described in the literature: Gibbs free energy and Helmholtz free energy (e.g. Sears & Salinger 1975). For simplicity and convenience (cf. Appendix A.5) we focus on the Helmholtz free energy F of a system:

$$F = U - TS, \tag{A.1}$$

where U is the internal energy of the system, T is its temperature and S is its entropy. The free energy F, is the amount of energy that can be extracted from the system to do any kind of useful work such as climbing a tree or assembling fat molecules. Equation A.1 shows that all of the internal energy U is not available to be extracted as free energy F. There is an entropic tax: TS. TS is the penalty one must pay for extracting the energy from the system and using it to do any useful work. U is how much money is in the bank and TS are the bank fees you have to pay to get it out. The higher the temperature T and the higher the entropy S of the system, the higher the penalty and the lower will be the extractable, usable, life-supporting, life-giving free energy F. Good engines produce minimal entropy and have $TS << U$ and thus $F \approx U$ (Bejan 2006, Eq. 3.7).

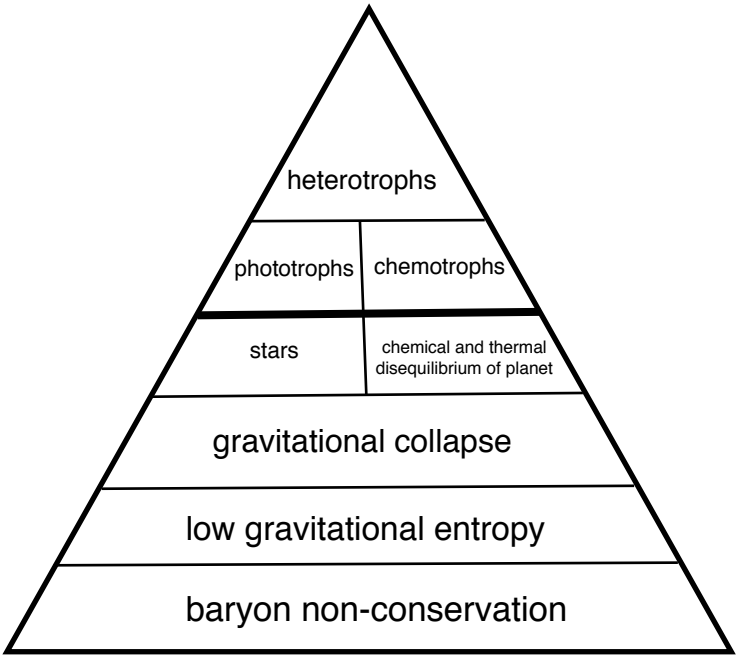

Figure A.1 Pyramid of Free Energy Production. The free energy available at one level comes from the level below it. The lower levels are prerequisites for the life above it. The top two levels are traditionally classified as life forms in the primary production pyramid. The pyramid shape represents the decreasing amount of free energy available at higher trophic levels.

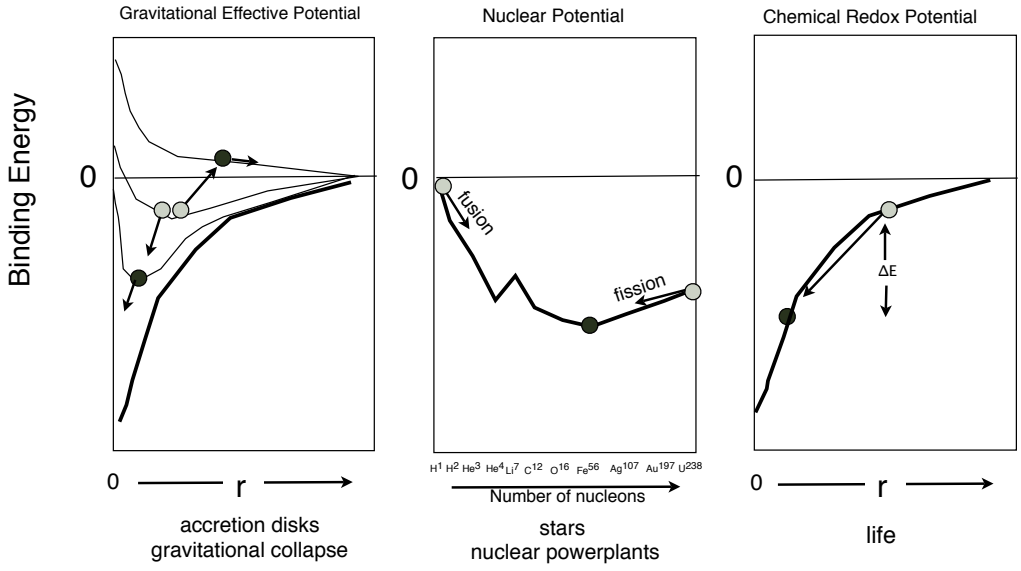

Figure A.2 Sources of Free Energy in the Universe: Gravitational (left), Nuclear (middle) and Chemical (right). Left panel: dissipation in an accretion disk leads to angular momentum exchange between two small masses (two light grey balls). The mass that loses angular momentum falls in. The one that gains momentum is expelled. Middle panel: the binding energy per nucleon due to the strong nuclear force provides the gradient that makes fusion and fission drive nuclei towards iron. Right panel: the energy that heterotrophic life extracts from organic compounds or that chemotrophic life extracts from inorganic compounds can be understood as electrons sinking deeper into an electrostatic potential well $\phi(r) \propto 1/r$. In every redox pair, the electron starts out high in the electron donor (light grey ball) and ends up (black ball) lower in the potential of the electron acceptor (cf. Nealson and Conrad 1999, their Fig. 3).

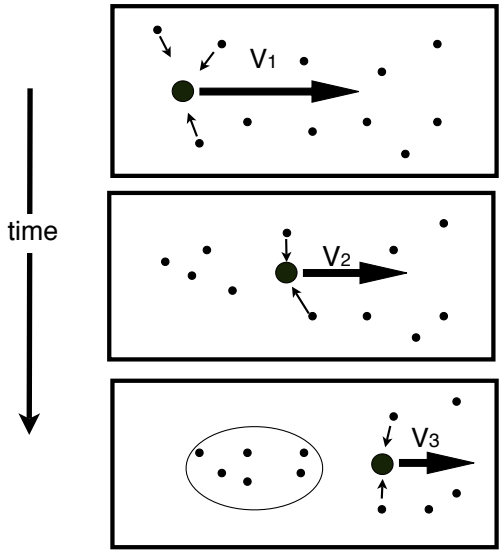

Figure A.3 Dynamical Friction. Consider a massive particle with velocity V_1 moving through a cloud of less massive particles. The less massive particles are attracted to the massive particle and end up clumped in the wake of the massive particle. From there, the less massive particles will have a net gravitational force slowing down the massive particle. This causes the most massive objects to fall into the center of the potential and is why clusters of galaxies have massive cD galaxies at their cores. (Binney and Tremaine 1987).

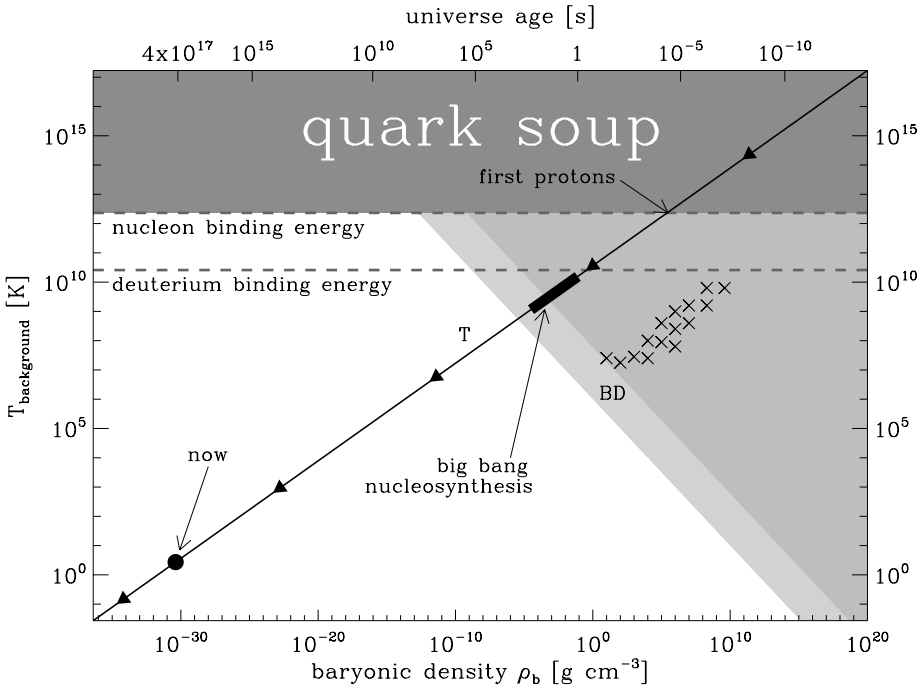

Figure A.4 Regions of the density-temperature plane where nuclear fusion reactions occur. Our universe cooled along the line from top right to lower left. Between one second and three minutes after the big bang, big bang nucleosynthesis (BBN) produced deuterium ^{3}He, ^{4}He, and several other light isotopes whose abundances we can measure in stellar atmospheres today (Weinberg 1977). If the baryonic density of the universe were much larger and the expansion rate of the universe were slower (e.g. Peacock 2000), BBN would have produced many other elements and could have burned all the hydrogen into iron and precluded the production of starlight from stellar fusion. After BBN, most of the baryons in the universe were in hydrogen and helium. Thus the universe was in a state of low nuclear entropy. This allowed stars to subsequently access the free energy from nuclear fusion in their hot, dense cores. The cores of main sequence stars are labeled "X". The cores of brown dwarfs, where deuterium (but not hydrogen) is fusing into helium, is labeled "BD". The conditions inside a Tokamak reactor are labeled "T". The diagonal shades indicate contours of constant reaction rate $\propto \rho^2 T^4$: the light region indicates reaction rates similar to those in BDs; the darker region indicates reaction rates $\gtrsim$ those in main sequence stars.

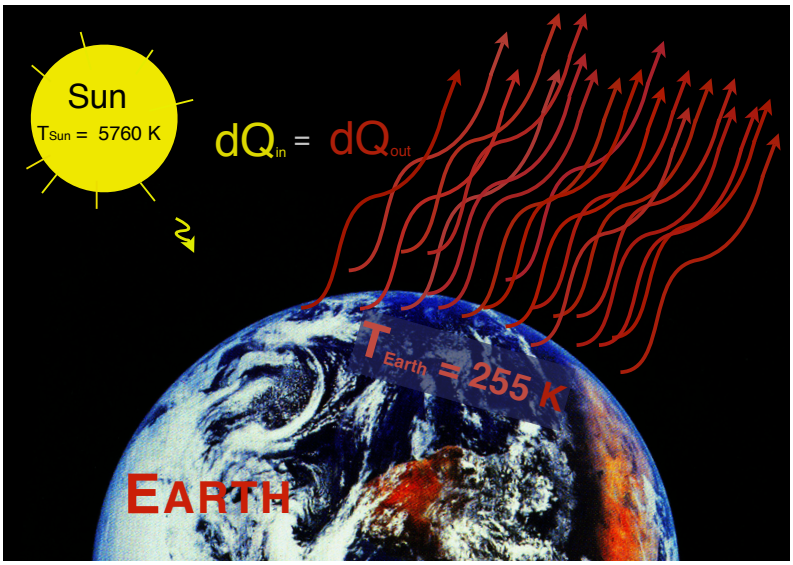

Figure A.5 The Sun provides the Earth with a continuing source of free energy. Energy that comes to Earth from the Sun "dQ_{in}" is balanced by the energy radiated by the Earth into outer space "dQ_{out}". The temperature of the incoming photons is the temperature of the photosphere of the Sun: T_{Sun} = 5760 K. The temperature of the outgoing photons is the effective temperature of the Earth: T_{Earth} = 255 K. When the Earth absorbs one solar photon (yellow squiggle), the Earth emits 20 photons (red squiggles, Eq. A.7) with wavelengths 20 times longer. The entropy of photons is proportional to the number of photons (Eq. A.27). Hence when the Earth absorbs a high energy solar photon at low entropy and distributes that energy among 20 photons and radiates them back to space, the Earth is exporting entropy; the waste entropy from the maintenance of the low entropy structures on Earth.

A.2. The Sun is the Source of Earth's Free Energy

Consider the amount of free energy that is delivered to the Earth in solar photons. We make the reasonable assumption that the Earth is in a steady state (e.g. Kleidon 2008). It is not in equilibrium because there is an energy flow in to the system (sunlight) and out of the system (Earth radiates to space, Fig. A.5).

Steady state means that the average effective temperature of the Earth is constant. It also means that the amount of energy delivered to the Earth in solar photons dQ_{in}, is the same as the amount of energy radiated away by the Earth as infrared photons, dQ_{out}. Thus, $dQ_{in} = dQ_{out}$. If this were not so, the internal energy U of the Earth would be increasing – the Earth would be getting hotter or the speed of winds and the number of hurricanes would increase, or there would be a net increase in biomass. However, the number of organisms that are born is about the same as the number that die. The strength of the winds that dissipate the pole to equator temperature gradients are about the same and the number of hurricanes which equilibrate thermal, pressure and humidity gradients, is about the same. (We are ignoring variations in the temperature of the Earth due to variations of the greenhouse gas content of the Earth or the Milankovich cyles or the secular increase in solar luminosity.) Thus, in steady state, the Earth is at a constant temperature T, constant energy U, constant entropy S and constant free energy F.

Let $\frac{dS_D}{dt}$ be all the entropy produced by all the dissipative structures on Earth (including winds, hurricanes, ocean currents, life forms, and the thermal dissipation when heat is transfered through the soil from hot sunny spots to cool shady spots). Then we have for the entropy of the Earth:

$$\frac{dS}{dt} = \frac{dS_\gamma}{dt} + \frac{dS_D}{dt} = 0, \tag{A.2}$$

or the net decrease in entropy from photons coming in and out ($\frac{dS_\gamma}{dt}$) is compensated for by the increase in entropy from all the dissipative, low entropy structures on Earth. Thus,

$$\frac{dS_\gamma}{dt} = -\frac{dS_D}{dt}. \tag{A.3}$$

Since the energy in the photons arriving and leaving is equal, $dQ_{in} = dQ_{out}$, we have $|dS_{in,\gamma}| < |dS_{out,\gamma}|$ since:

$$dS_{in,\gamma} = \frac{dQ_{in}}{T_{Sun}} \tag{A.4}$$

$$dS_{out,\gamma} = -\frac{dQ_{in}}{T_{Earth}}. \tag{A.5}$$

Thus,

$$\left|\frac{dS_{out,\gamma}}{dS_{in,\gamma}}\right| = \frac{T_{Sun}}{T_{Earth}} = \frac{5760}{255} \sim 20 \tag{A.6}$$

Thus, the Earth exports twenty times as much entropy as it receives. Equation (A.27) then tells us that the ratio of the number of emitted photons to the number of absorbed photons is:

$$\frac{N_{out,\gamma}}{N_{in,\gamma}} \sim 20. \tag{A.7}$$

This is shown in Fig. A.5 with its 1 incoming solar photon and 20 outgoing infrared photons. The entropy flux to and from the Earth from the absorbtion of solar photons and the emission of infrared photons is:

$$\begin{aligned}
\frac{dS_\gamma}{dt} &= \frac{dS_{in,\gamma}}{dt} + \frac{dS_{out,\gamma}}{dt} \\
&= \frac{dQ}{dt}\left(\frac{1}{T_{Sun}} - \frac{1}{T_{Earth}}\right) \\
&= -\frac{dQ}{dt}\frac{1}{T_{Earth}}\left(1 - \frac{T_{Earth}}{T_{Sun}}\right) \\
&= -\frac{dQ}{dt}\frac{1}{T_{Earth}}(0.95).
\end{aligned} \tag{A.8}$$

Since the amount of free energy is not building up in the Earth, we have $\frac{dF}{dt} = 0$. Let $\frac{dF_\gamma}{dt}$ be the amount of free energy delivered to the Earth by solar photons and $\frac{dF_D}{dt}$ be the amount of free energy dissipated by all the dissipative structures on Earth, then (cf. Eqs. A.2 and A.3) we have,

$$\frac{dF}{dt} = \frac{dF_\gamma}{dt} + \frac{dF_D}{dt} = 0 \tag{A.9}$$

or

$$\frac{dF_\gamma}{dt} = -\frac{dF_D}{dt} \tag{A.10}$$

where the minus sign indicates that $\frac{dF_D}{dt}$ is the loss or dissipation of free energy. Eqs. (A.9) and (A.10) are the key to understanding how the Earth can keep absorbing free energy from the Sun without the amount of free energy in the Earth going up. The free energy in the food we eat goes to cell repair and movement, and is dissipated when we die or move. Similarly, all of the free energy delivered by the Sun is dissipated in winds, hurricanes, ocean currents, life forms, or thermal conduction through soil between sunny spots and shady spots.

The Earth is exporting much entropy but the entropy of the Earth is not decreasing. That is because the dissipative structures on the Earth are producing the entropy that is exported. They need the input of free energy to stay at low entropy – just as a refridgerator needs free energy to stay at a constant low temperature (= low entropy steady state). Without a supply of free energy a fridge will heat up, a hot water tank will cool down, and life will die. Things approach equilibrium. It takes free energy to keep a fridge cool, the tank hot and the chemical order in life forms. Free energy (or work) is needed to remove the heat and entropy that naturally leaks into the fridge. The lower the temperature of the fridge and the more imperfect the insulation, the more free energy is needed to maintain the low entropy steady state.

The export of entropy does not lower the entropy of the Earth. Rather it keeps the entropy of the Earth at a constant low level. In the absence of a flow of negentropy, the low entropy structures, such as hurricanes, dust devils, the hydrological cycle, thermal gradients and life forms would run down and dissipate away. The export of entropy compensates for this natural dissipation and is the reason why low entropy structures endure.

A.2.1. How much entropy is produced and how much free energy can be extracted from a solar photon?

We can compute the amount of free energy available on the Earth to drive the winds, hurricanes and all of life (Kleidon 2008). Starting from Eq. A.1, taking differentials and then dividing by dt yields the rate of increase of free energy of the Earth:

$$\frac{dF}{dt} = \frac{dU}{dt} - T\frac{dS}{dt} - S\frac{dT}{dt}. \tag{A.11}$$

Since we are assuming steady state, F, U, T and S are all constants and all of the

terms in Eq. A.11 are zero. However, using Eqs. (A.2) and (A.9) we can write:

$$\frac{dF_\gamma}{dt} + \frac{dF_D}{dt} = -T_{Earth}\left(\frac{dS_\gamma}{dt} + \frac{dS_D}{dt}\right). \tag{A.12}$$

Separating terms to count only the contribution from photons we get:

$$\frac{dF_\gamma}{dt} = -T_{Earth}\frac{dS_\gamma}{dt}. \tag{A.13}$$

With Eq. A.8 this yields,

$$\frac{dF_\gamma}{dt} = \frac{dQ}{dt}0.95 \tag{A.14}$$

Thus, 95% of the incoming solar energy can be used to do work, i.e. photovoltaics at the temperature of the Earth have a maximum efficiency of 95%. To get a numerical value for the free energy in Eq. (A.14): the solar flux impinging on the disk of the Earth (πR^2_{Earth}) at 1 AU from the Sun is 1366 Wm^{-2}. Since $dQ_{in} = dQ_{out}$, the average flux I_o from the Earth's surface ($4\pi R^2_{Earth}$) balances the solar flux:

$$\pi R^2_{Earth} 1366\ Wm^{-2} = 4\pi R^2_{Earth} I_o \tag{A.15}$$

where, $I_o = 342\ Wm^{-2}$.

Therefore, to get a numerical value for $\frac{dQ}{dt}$ (= the flux density of solar radiation through a unit area of 1 m^2) we have:

$$\begin{aligned} \frac{dQ}{dt} &= \sigma\, T^4_{Earth} = I_o(1 - A_{Earth}) && \text{(A.16)} \\ &= 342\ (0.7)\ Wm^{-2} \\ &= 238\ Wm^{-2} && \text{(A.17)} \end{aligned}$$

where $A_{Earth} \approx 0.3$ is the albedo of the Earth, and the Stefan-Boltzmann constant is $\sigma = 5.67 \times 10^{-8}\ Wm^{-2}K^{-4}$. Thus the flux of free energy through unit area (Eq. A.14) is

$$\frac{dF_\gamma}{dt} = 238\ Wm^{-2}(0.95) = 228\ Wm^{-2} \tag{A.18}$$

This flux of free energy maintains all thermal gradients on the surface of the Earth, all winds and hurricanes and all life, and is equal to the flux of free energy that is dissipated by all dissipative structures (Eq. A.10).

The total free energy available from sunlight is the flux per unit area times the area of the Earth: 228 $Wm^{-2} \times 4\pi R^2_{Earth} \sim 1.2 \times 10^{17}$ W, which is about ten thousand times larger than the 1.3×10^{13} W of global power consumption from burning fossil fuels. Terrestrial life (including humans) is a subdominant dissipator of the free energy delivered to Earth (Kleidon 2008).

There are no hurricanes or ocean currents on the Moon, so how does the free energy delivered by solar photons get dissipated there? Performing the same computation for the Moon as we did for the Earth we have:

$$I_o(1 - A_{Moon}) = \sigma \, T^4_{Moon} \tag{A.19}$$

where the Moon's albedo is lower than the Earth's, ($A_{Moon} \approx 0.07$). The Moon's effective temperature $T_{Moon} = 274$ K is higher than the Earth's because of the Moon's lower albedo. Instead of having hurricanes, winds, ocean currents and life forms, the free energy of the Moon is dissipated by heat flow due to the large temperature gradients (low entropy structures) between regolith in the sunshine at 350 K and the shadows at 150 K. The input of low entropy solar radiation maintains the gradients. The maximum temperature variation on the Moon is $\Delta T \sim 300$ K between ~ 390 K at the equator in the early afternoon and ~ 70 K in the shade at the poles. On Earth, this variation is only $\Delta T \sim 120$ K between ~ 320 K and ~ 200 K. If the Moon were the same temperature as the Sun, $T_{Sun} \approx 5760$ K then the "shadows" would be the same temperature as the Sun and there would be no export of entropy. If the Moon were a smooth ball instead of having a bumpy surface then the large scale hemispheric temperature gradient would be the only low entropy structure and a larger temperature gradient would be created to dissipate the same constant amount of free energy from the low entropy photons. A further refinement to the computation above would consider the low entropy associated with sunlight coming from a particular direction rather than isotropically.

A.3. The Entropy of the Cosmic Microwave Background Remains Constant as the Universe Expands

It is difficult to talk about the total entropy in the universe without knowing how big the universe is, so we talk about the entropy in a representative sample of the expanding universe. Typically we put an imaginary sphere around a few thousand galaxies and consider the entropy in this expanding sphere – the entropy per comoving volume. We parameterize the expansion of the universe with a scale factor R. This means that when the universe increases in size by a given factor, R increases by the same factor (Fig. A.6).

The expansion of the universe is adiabatic since the photons in any arbitrary volume of the universe have the same temperature as the surrounding volume. There is no net flow of heat. The entropy of a photon gas does not increase under adiabatic expansion. Specifically, the entropy S of a gas of photons in a volume V at temperature T is $S \propto VT^3$ (e.g. Eq. A.23 or Bejan 2006, eq. 9.20).

The photon wavelengths λ, increase (are redshifted) with the scale factor: $\lambda \propto R$. There is no absorbtion or reemission associated with the redshifting of cosmic microwave background photons. These photons were last scattered at the surface of last scattering $\sim 480,000$ years after the big bang. Since the volume V increases as $V \propto R^3$, and since the temperature of the microwave background goes down as the universe expands: $T \propto \frac{1}{R}$, we have the result that the entropy of a given comoving volume of space is constant (Kolb & Turner 1990, Frautshi 1982, 1988):

$$S \propto VT^3 \propto R^3\left(\frac{1}{R^3}\right) = constant. \tag{A.20}$$

The adiabatic expansion (or contraction) of a gas in equilibrium is reversible. Thus the expansion of the universe by itself is not responsible for any entropy increase in the photons (Fig. A.6 top panel). Another way to understand that the entropy of the photons in the universe remains constant as the universe expands, is to realize that entropy is proportional to the number of photons $S_\gamma \propto N_\gamma$ (Eq. A.27). The number of photons N_γ in the volume remains constant and therefore so does the entropy. Thus, we obtain the result indicated in the top panel of Fig. A.6: $S_{\gamma,i} = S_{\gamma,f}$.

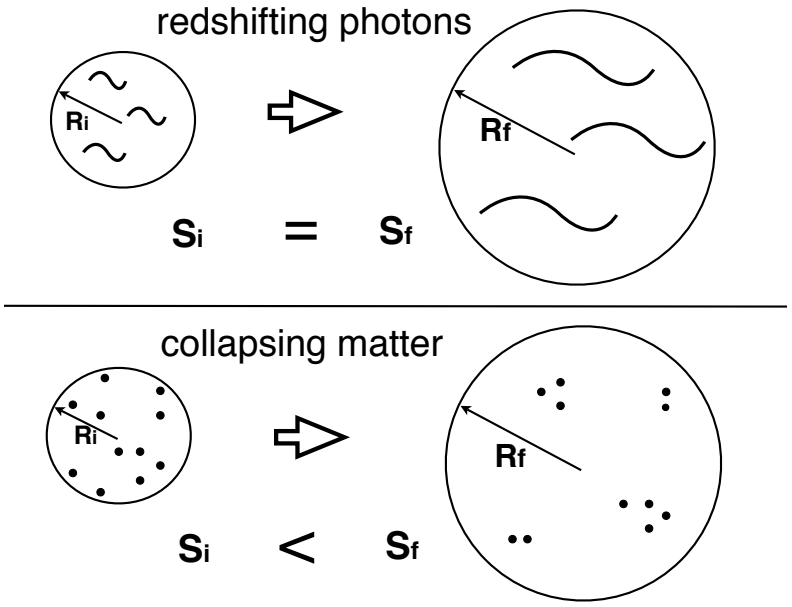

Figure A.6 The entropy of the universe changes as the universe expands. Notice that the photons (squiggles) stay spread out while the baryons (dots) clump due to gravity. Top: as the universe expands, the entropy of cooling redshifted photons remains constant (Eq. A.20) while the entropy produced when material clumps into galaxies, stars and planets, increases the total entropy of the universe. At a given initial time, the circles on the left represent an arbitrary volume of the universe with an initial scale factor R_i. The small circle on top contains 3 cosmic microwave background photons (squiggles). At a later time (right), the volume has expanded but contains the same number of photons and thus $S_{\gamma,i} = S_{\gamma,f}$ (see Eq. A.27). The entropy of the universe, however, includes contributions from photons and the net effect of gravitational collapse. In the lower panel, the 11 baryons (dots) start out fairly unclumped then clump. The net entropic effect of clumped matter and the heat given off to allow the clumping and the matter expelled to allow the clumping is: $S_{m,i} < S_{m,f}$. Thus, the total entropy of the universe increases: $S_i < S_f$. The photon to baryon ratio of our universe is about one billion, not the 3/11 shown here.

A.4. Gravity and Entropy

In the big bang model, the early universe was in thermal and chemical equilibrium. In the previous section we showed how the expansion of the universe is not responsible for changing the entropy of the photons in the universe. If the universe were in equilibrium, it should have stayed in equilibrium (top panel of Fig. A.6). Our existence shows that the universe could not have started from equilibrium. The missing ingredient that solves this dilemma is gravity. Matter, evenly distributed throughout the universe, has much potential energy and low entropy. In the standard inflationary scenario describing the earliest moments after the big bang, matter originates (during a short period at the end of inflation called reheating) from the decay of the evenly distributed potential energy of a scalar field. âĂŸFalse vacuumâĂŹ decays into our true vacuum. Vacuum energy cannot clump. However, once the potential energy of the scalar field is dumped almost uniformly into the universe in the form of relativistic particles, these can cool and clump if they have mass (Fig. A.6, lower panel). Unclumped matter has a lower entropy than clumped matter:

$$S_{unclumped} << S_{clumped}. \tag{A.21}$$

By $S_{clumped}$ we mean the entropy of the phase space volume of the collapsed material as well as the phase space volume of the material expelled during the clumping, plus the entropy of the heat given off during the collapse and dumped into the environment which allowed the unclumped baryons to clump. That is a lot to include but ignoring the full picture has led to much confusion about the relationship between gravity and entropy.

The gravitational potential energy is enormous. In this inflationary picture the potential energy of the false vacuum is the ultimate source of all energy and the matter/antimatter pairs which annihilate and create a bath of photons. Because of an intrinsic asymmetry (baryon non-conservation), the annihilation is incomplete and leaves one baryon for every billion photons. The subsequent cooling (due to the expansion) and clumping of the residual baryons (due to gravity) is the source of all the free energy, dissipative structures and life in the universe (bottom level in Fig. A.1).

The relationship between entropy and gravity is similar to the relationship between energy and heat 200 years ago when the concept of energy conservation in thermodynamics was being developed. It took many decades for the different forms of energy to be recognized. Kinetic energy was different from potential energy, "caloric" became heat energy and Einstein showed us there was energy in mass and in the momentum of massless particles: $E^2 = p^2c^2 + m^2c^4$. It

seems to be taking even longer to recognize and define the different forms of entropy, including gravitational entropy and informational entropy (Brissard 2005, Shannon 1950).

There is some confusion about life being in violation of the second law. If $dS > 0$ how can life be so ordered? The answer is that the order and low entropy of life is maintained by the production and export of entropy. Similarly, there is confusion about clumped material or gravitational structures being in violation of the second law. The resolution is the same: the entropy of the environment needs to be included in the calculation.

Life is trying to maintain its order, while the second law is trying to decrease order. Superficially it seems that life and the second law are at cross purposes. In fact, life and the second law are allies, since the maintainence of a highly ordered structure increases the disorder of the universe more than would be the case without the structure. Similarly, maintaining the low entropy of the structures produced during gravitational collapse (e.g. bipolar outflows of active galactic nuclei and accretion disks) exports entropy such that the net result is an increase of the entropy of the universe, not a decrease.

A.4.1. Diffusion and Gravitational Collapse

A misleading idea is that entropy makes things spread out while gravitational collapse makes things clump together, and therefore gravity seems to work against or even violate the second law.

> "A recurring theme throughout the life of the universe is the continual struggle between the force of gravity and the tendency for physical systems to evolve toward more disorganized conditions. The amount of disorder in a physical system is measured by its entropy content. In the broadest sense, gravity tends to pull things together and thereby organizes physical structures. Entropy production works in the opposite direction and acts to make physical systems more disorganized and spread out. The interplay between these two competing tendencies provides much of the drama in astrophysics." Adams and Laughlin (1999).

The part of this quote that is easily misleading is "In the broadest sense, gravity tends to pull things together and thereby organizes physical structures. Entropy production works in the opposite direction ..."

See Fig 27.10 of Penrose (2004) for some clarity on this issue. Gravity organizes physical structures but at the expense of disorganizing and expelling other material. This supposed struggle between entropy and gravity is misleading because lots of material is expelled (then ignored in the computation). The heat is ignored too. Consideration of only the centralized accreted remains, does not encompass the full entropic effects of gravitational collapse (Binney and Tremaine 1987).

> "If one part of the system becomes well ordered and loses entropy, the system as a whole must pay for it by increasing its entropy somewhere else for compensation" (Adams & Laughlin 1999).

Gravity can only pull things together if angular momentum and energy are exported. If we ignore the entropy associated with the angular momentum and energy export, it is easy to imagine that gravity pulling things together is acting in the opposite direction of the second law, just as it is easy to believe that life is acting in the opposite direction of the second law. If one focuses on the collapsed object while ignoring the increased entropy of the surrounding distribution of stars (which puffs up when part of it collapses), one could believe that:

> "The gravitational contribution to entropy is negative and the correlations of clustering decrease this entropy. If we retain the notion that systems evolve in the direction of an entropy extreme (a maximum negative value in the gravitational case), then we should expect infinite systems of galaxies to form tighter and tighter clumps over larger and larger scales.... Spherical systems of stars evolve toward maximum negative gravitational entropy." (Saslaw 1985 p. 65)

When we ignore the entropy produced during the gravitational collapse of the "spherical systems of stars", and concentrate only on the collapsed system itself, then Saslaw may be correct, but this seems to contradict the idea that the entropy of a black hole is large and positive $S_{BH} > 0$. The transition from a negative value to a positive value when an object collapses into its event horizon is problematic (Frampton 2008, Hsu & Reeb 2008).

Neither gravitational collapse nor life violate the second law when we include the increased entropy of the environment. Thus, the maintenance of a fridge or an accretion disk or life, increases the total entropy of the universe.

Thermal (random kinetic energy) can be written as $E_{kin} = \frac{p^2}{2m}$, while gravitational binding energy is $E_{grav} = \frac{GMm}{r}$. When things are hot, $E_{kin} >> E_{grav}$ and diffusion

dominates. The maximum entropy state is reached when the atoms, or molecules or stars or galaxies fill up the space randomly. They occupy a larger volume of phase space. This is labeled "Diffusion" in the top panel of Fig. A.7. When things are cold, $E_{kin} << E_{grav}$, gravitational collapse occurs and leads to a black hole. Fig. A.7 describes what happens in a universe that is not expanding. However, consider what happens to E_{kin} and E_{grav} when the universe expands (the scale factor R increases as is shown in Fig. A.6). Since $p = \frac{p_o}{R}$ and any distance scales as $r = r_o R$ we have $E_{kin} = \frac{E_{kin,o}}{R^2}$ and $E_{grav} = \frac{E_{grav,o}}{R}$. Thus, as the universe expands, E_{kin} decreases faster than E_{grav} and we will always eventually have $E_{kin} << E_{grav}$, which leads to gravitational collapse, black holes and then their evaporation into a diffuse gas of photons – the maximum entropy state of the universe, within which no life can exist. Thus, to depict our universe, the bottom panel of Fig. A.7 should be moved to the right and tacked onto the top panel.

A.4.2. Black Holes and Heat Death

Bekenstein (1973) and Hawking (1974) showed that a black hole of mass M has a temperature, $T_{BH} = \frac{\hbar c^3}{8\pi G k}\frac{1}{M}$ and evaporates predominantly as photons when its temperature is hotter than the background temperature. Thus, although the entropy of a black hole, $S = \frac{4\pi k G}{\hbar c}M^2 = \frac{k c^3}{\hbar G}\frac{A}{4}$, is sometimes referred to as a maximum entropy state, the sharp gravitational gradient at the event horizon leads to evaporation, photon emission and a higher entropy state of randomly distributed photons. If the background temperature is larger than T_{BH} then the black hole will increase in mass and cool down. However in an expanding universe, $T_{CMB} \propto \frac{1}{R}$ and as the universe expands, R increases, T_{CMB} decreases and eventually we have $T_{BH} > T_{CMB}$, which leads to the evaporation of the black hole and the diffusion of the photons produced.

The second law establishes the arrow of time. Since we are far from equilibrium dissipative structures, we must move through time in the direction in which entropy increases and in which free energy is available. Since all observers are dissipative, our existence depends on $dS > 0$. The situation $dS = 0$ is unobservable. This may be an anthropic explanation for the initial low entropy of the universe. No other explanations are known to us. Just as a universe, with a value of a cosmological constant that is too big, is unobservable because stars never form (e.g. Weinberg 1987), so too, a universe that starts at maximum entropy is unobservable. Since life (and any other dissipative structures) needs gradients to form and survive, the initial condition of any universe that contains life will be one of low entropy, not high entropy. You can not start an observable universe from a heat death.

In the multiverse scenario, we imagine universes with varying degrees of baryon non-conservation. If baryon number were conserved, the early universe would have had the same amount of matter as anti-matter. The universe would be filled with a diffuse gas of photons at maximum entropy. There would be no matter homogeneously distributed that would provide the low initial gravitational entropy. Low energy photons, spread out evenly over the volume of the universe, is a maximum entropy state. Baryons spread out evenly, is a minimal gravitational entropy state.

In addition to baryon non-conservation, a requirement for life is that the baryons not be already clumped into black holes. They can be very smoothly distributed, or clumped a bit, but not too much. In other words, non-clumped (but clumpable) matter is required to start the universe at low entropy.

Penrose (1979, 1987, 1989, 2004) has been concerned with the relationship between entropy and gravity for more than three decades (see also Barrow & Tipler 1986). He has stressed the amazingly unlikely initial low gravitational entropy of the universe that ensured that dissipative structures formed as gravity clumped matter and produced gradients to drive dissipative structures.

This low initial entropy of the universe is quantified by the low amplitude of the power spectrum of density perturbations measurable in the cosmic microwave background and in the large scale structure of galaxies. According to the inflationary scenario, these low amplitude density fluctuations have their origin in irreducible vacuum fluctuations that became real during inflation, in a manner analogous to the way electrons and positrons are created out of the vacuum by ultra-strong electric fields between capacitor plates. The initial low amplitude of fluctuations is measured as the amplitude Q of CMB fluctuations or the amplitude A of the power spectrum $P(k)$ of large scale structure. The lower the initial values of Q or A, the lower the degree of clumpiness and the lower the initial gravitational entropy of the universe. Penrose (1979) describes these low entropy initial conditions in terms of small values for the Weyl curvature tensor. We are uncertain how to explain the low values of Q or A or the Weyl curvature. In a multiverse scenario, perhaps there is some mother distribution of values from which each universe gets its own initial entropy and ours is low because it has to be for us to evolve and observe it (Tegmark & Rees 1998).

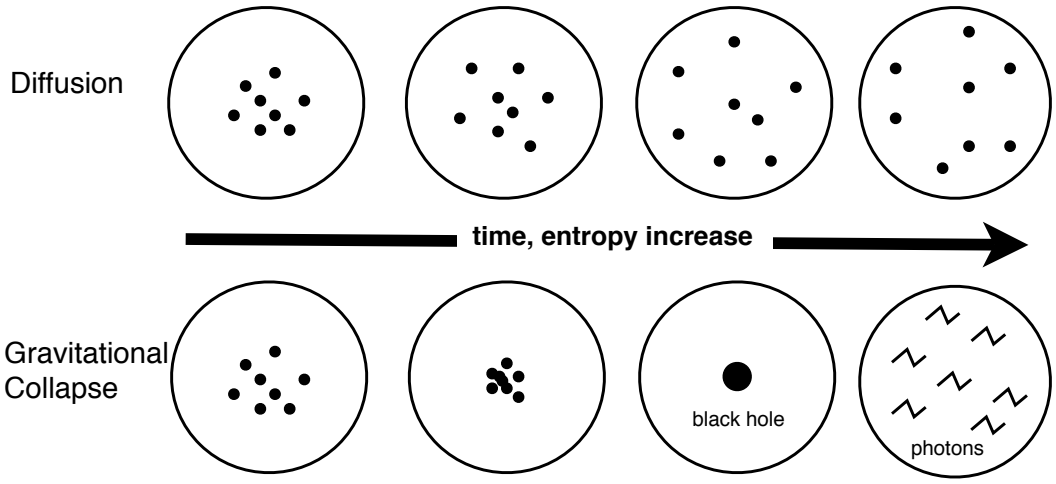

Figure A.7 Entropy increases during both diffusion (top) and gravitational clumping (bottom). If thermal energy dominates the gravitational binding energy (top), then entropy will increase as material diffuses and spreads out over the entire volume (think perfume diffusing in a room). If gravitational binding energy dominates thermal energy (bottom), then entropy will increase as some material and angular momentum is expelled to allow other matter to have lower angular momentum and gravitationally collapse into galaxies and stars, which eventually collapse/accrete into a black hole. If the temperature of the background photons is lower than the temperature of the black hole, the black hole will evaporate to produce the maximum entropy state of photons spread out over the entire volume (last circle in lower panel). Compare this figure to Fig. 27.10 of Penrose (2004).

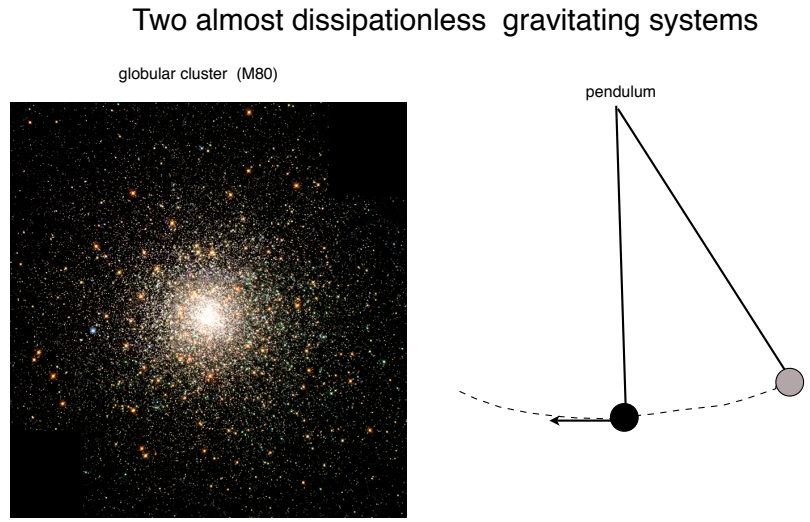

Figure A.8 Two almost dissipationless gravitating systems: a globular cluster and a pendulum. Globular clusters are some of the oldest structures in the universe ($\sim$ 12 billion years). If there were no friction we would have a Hamiltonian system in which energy inside the system is conserved as it sloshes back and forth between kinetic and potential energy. Such a system cannot collapse further. The resulting isothermal sphere is the maximum entropy solution (Binney & Tremaine 1987). Even nominally Hamiltonian systems such as galaxies and globular clusters, emit gravitational waves and collapse. These almost Hamiltonian systems should be contrasted with the large dissipation and entropy production of protoplanetary accretion disks that allow stars to form and the much larger accretion disks in active galactic nuclei (AGN) which feed black holes in the center of galaxies. (Image of M80 credit: Hubble Heritage Team, AURA/ STScI/ NASA)

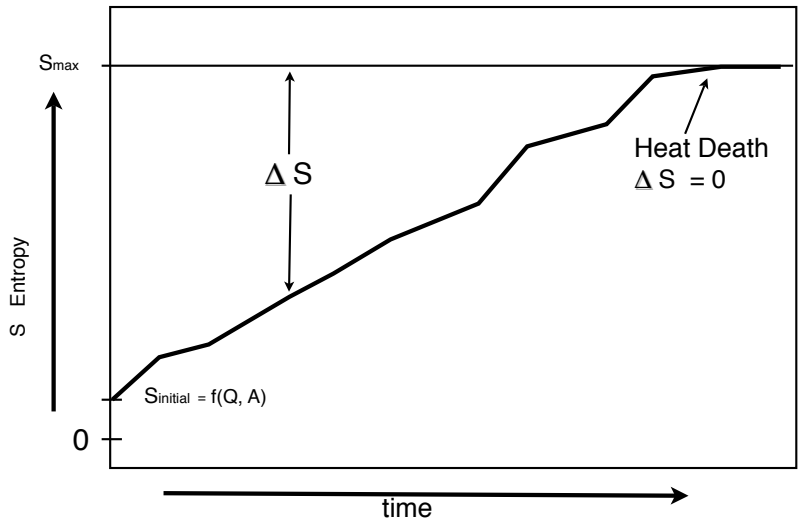

Figure A.9 The universe starts off at low entropy (not zero) due to the low level of density perturbations in the early universe – low Q and low A (e.g. Tegmark and Rees 1998) – where "low" means less than the maximum value S_{max}. At S_{max} all the energy density of the universe is in massless particles in equilibrium at a common temperature. Thus the universe starts off with a large entropy gap ΔS. The parameters Q and A are the observable normalizations of the primordial density fluctuations and set the initial gravitational entropy of the universe. There is no general agreement on the curve shown here. See for example Fig. 7.3 of Davies (1994) and Fig. 1.2 of Frautschi (1988).

A.5. The Entropy Gap and the Heat Death of the Universe

Is the entropy of the universe getting closer or further from its maximum value S_{max}? That is: Is the entropy gap, $\Delta S(t) = S_{max} - S(t)$, increasing or decreasing? Through gravitational collapse, and the irreversible, dissipative processes produced by the density and chemical gradients that result, the entropy of the universe increases, while S_{max} may be constant (Egan & Lineweaver 2009). Fig. A.9 shows a monotonically decreasing entropy gap leading to a heat death with no possibility for life thereafter. The concept of a heat death was introduced by Thomson (1851, 1862) and has dominated the discussion of the far future fate of the universe.

Tolman (1934) showed that if the universe could bounce back from a contraction into an expansion, a cyclic universe could not be one that is infinitely old, since with each cycle, the entropy of the material would increase, and the cycles would get longer and longer. Steinhardt and Turok (2007) have a model which gets around this entropy problem by reducing entropy with the free energy of a semi-infinite gravitational potential.

In a universe where the energy is conserved ($\Delta U = 0$), the free energy available to do work (to maintain far from equilibrium structures) is $\Delta F = -T\Delta S$ and this is plotted in Fig. A.10.

Entropy is the unifying concept of life because the second law is universal; it applies to everything (Schneider & Kay 1994). Man, machine, microbe or the entire cosmos – there is no scale or material to which the second law does not apply. However, the degree to which the equations of thermodynamics apply to near equilibrium situations, steady state situations and far from equilibrium situations is still problematic (see however, Dewar 2003, 2005).

If Darwin had read Carnot (1824), Prigogine (1978) and Penrose (1979, 2004) rather than Newton, Malthus and Lyell, the last paragraph of the Origin of Species would have read something like

> "There is grandeur in this view of life, with its dissipative powers, having been originally induced into many forms of far from equilibrium dissipative systems, and that, whilst irreversible processes on this planet have produced entropy according to the fixed second law of thermodynamics, from so simple a low gravitational entropic state, endless forms most beautiful and most wonderful have been and continue to increase the entropy of the universe as they destroy

the gradients which spawned them."

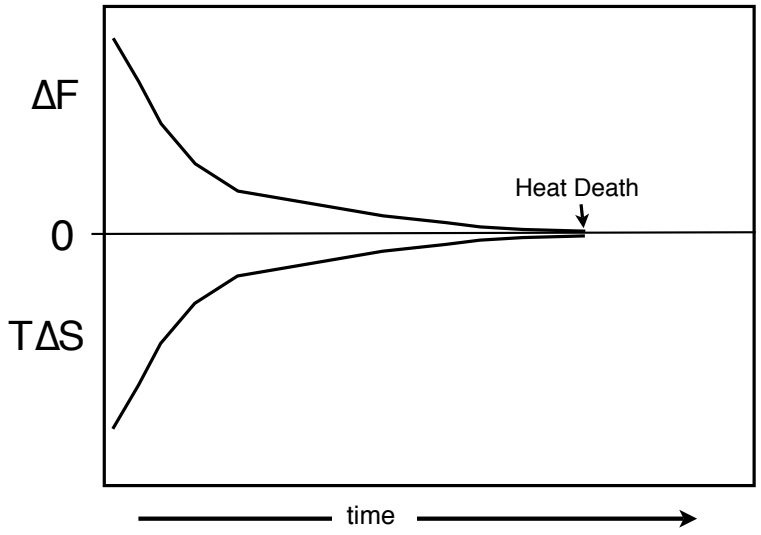

Figure A.10 The free energy in the Universe: $\Delta F = -T\Delta S$. As long as there is an entropy gap in the universe, i.e., as long as $\Delta S > 0$ (Fig. A.9), there will be a flow of free energy to make life possible. As $\Delta S \rightarrow 0$ and $T \rightarrow 0$ then $\Delta F \rightarrow 0$ and life can no longer survive.

Appendix A. Entropy of Blackbody Photons

Here we show that the entropy of a system of N particles is $S \sim N$. For reference, Boltzmann's constant is $k = 1.38066 \times 10^{-23} J/K$. The Stephn-Boltzmann constant $\sigma = \frac{\pi^2}{15}\frac{k^4}{\hbar^3 c^3} = 7.565 \times 10^{-16} Jm^{-3}K^{-4}$. Consider a photon gas at temperature T in a volume V (e.g. Sears & Salinger 1975). The internal energy is,

$$U = V\sigma T^4. \tag{A.22}$$

The entropy is

$$S = \frac{4}{3}\sigma V T^3. \tag{A.23}$$

The pressure is

$$p = \frac{1}{3}\sigma T^4, \tag{A.24}$$

and the number of photons is

$$\begin{aligned} N_\gamma &= \frac{36.06}{\pi^4 k}\sigma V T^3 && \text{(A.25)} \\ &= \frac{27.045}{k\pi^4} \times \frac{4}{3}\sigma V T^3 \\ &= \frac{27.045}{k\pi^4} S. && \text{(A.26)} \end{aligned}$$

Thus,

$$S = 0.2776\, k\, N_\gamma, \tag{A.27}$$

and to measure the entropy of the microwave background we just need to count photons. If the number of photons in a given volume of the universe is N, then the entropy of photons in that volume is $S \sim kN$. The photonic entropy of the universe is in the cosmic microwave background. Starlight cannot change that. If all the matter in the universe were transformed into 3 K blackbody radiation, the number of photons would add up to only ~ 1 % of the number of CMB photons. The entropy of the universe would increase by only ~ 1% (Frautschi 1982).

Appendix B. Which Free Energy is most useful F or G?

Thermodynamic equilibrium may be characterized by the minimization of the Helmholtz free energy (Eq. A.1) $F = U - TS$ (e.g. Prigogine 1978). When $U = TS$,

no free energy can be extracted from the system, but this is not the same as equilibrium. When there are pressure gradients that can do pdV work and drive organization, i.e., hurricanes, F is the most relevant free energy. When pressure cannot be used, i.e., life on Earth, or photon pressure of the cosmic microwave background, then G is more relevant.

Chemists are used to dealing with the Gibb's Free energy of a reaction G, where $G = U - TS - pV$ and G is the extractable energy, or free energy under constant pressure conditions (the usual conditions under our stable atmosphere and in the universe except at shock fronts and hurricanes). G does not include the pdV work that could be done by a pressure gradient of the atmosphere, while F does. We use the Helmholtz free energy because we are interested in the most generic situations. We want to know the extractable energy under any conditions.

Since the free energy can never be more than the internal energy, TS will always be positive, or $(TdS + SdT) > 0$. Using Eqs. Eq. A.1, A.22, A.23, the free energy of a photon gas is,

$$\begin{aligned} F &= U - TS && \text{(A.28)} \\ &= V\sigma T^4 - \frac{4}{3}\sigma V T^4 \\ &= -\frac{1}{3}\sigma V T^4. && \text{(A.29)} \end{aligned}$$

This is the work that the photon gas could do if it were surrounded by zero pressure. However the photon gas fills the universe, and can do no work on itself.

The Gibbs free energy of a photon gas in equilibrium does not include pdV work and is equal to zero:

$$\begin{aligned} G &= U - TS + pV && \text{(A.30)} \\ &= F + pV \\ &= -\frac{1}{3}\sigma V T^4 + \frac{1}{3}V\sigma T^4 \\ &= 0 && \text{(A.31)} \end{aligned}$$

No pdV work is used to drive the chemistry-based metabolisms of terrestrial life forms, however some dissipative structures are driven by pdV work and so here we use F in our computations. We interpret Eq. A.31 as "no Gibbs free energy can be extracted from a photon gas at equilibrium"

BIBLIOGRAPHY

Abe, S. et al.: 2008, *Phys. Rev. Lett.* **100**, 221803

Adams, F. C. and Laughlin, G.: 1997, *Reviews of Modern Physics* **69**, 337

Adamson, P. et al.: 2008, *Phys. Rev. Lett.* **101**, 131802

Aguirre, A., Gratton, S., and Johnson, M. C.: 2007, *Phys. Rev. D* **75(12)**, 123501

Aguirre, A. and Tegmark, M.: 2005, *Journal of Cosmology and Astro-Particle Physics* **1**, 3

Ahmed, M., Dodelson, S., Greene, P. B., and Sorkin, R.: 2004, *Phys. Rev. D* **69(10)**, 103523

Albrecht, A., Bernstein, G., Cahn, R., Freedman, W. L., Hewitt, J., Hu, W., Huth, J., Kamionkowski, M., Kolb, E. W., Knox, L., Mather, J. C., Staggs, S., and Suntzeff, N. B.: 2006, *ArXiv Astrophysics e-prints*

Allègre, C. J., Manhès, G., and Göpel, C.: 1995, *Geochim. Cosmochim. Acta* **59**, 1445

Allende Prieto, C.: 2006, *ArXiv Astrophysics e-prints*

Amendola, L.: 2000a, *Phys. Rev. D* **62(4)**, 043511

Amendola, L.: 2000b, *MNRAS* **312**, 521

Amendola, L., Campos, G. C., and Rosenfeld, R.: 2007, *Phys. Rev. D* **75(8)**, 083506

Amendola, L., Quartin, M., Tsujikawa, S., and Waga, I.: 2006, *Phys. Rev. D* **74(2)**, 023525

Amendola, L. and Quercellini, C.: 2003, *Phys. Rev. D* **68(2)**, 023514

Armendariz-Picon, C., Mukhanov, V., and Steinhardt, P. J.: 2000, *Physical Review Letters* **85**, 4438

Armendariz-Picon, C., Mukhanov, V., and Steinhardt, P. J.: 2001, *Phys. Rev. D* **63(10)**, 103510

Astier, P., Guy, J., Regnault, N., Pain, R., Aubourg, E., Balam, D., Basa, S., Carlberg, R. G., Fabbro, S., Fouchez, D., Hook, I. M., Howell, D. A., Lafoux, H., Neill, J. D., Palanque-Delabrouille, N., Perrett, K., Pritchet, C. J., Rich, J., Sullivan, M., Taillet, R., Aldering, G., Antilogus, P., Arsenijevic, V., Balland, C., Baumont, S., Bronder, J., Courtois, H., Ellis, R. S., Filiol, M., Gonçalves, A. C., Goobar, A., Guide, D., Hardin, D., Lusset, V., Lidman, C., McMahon, R., Mouchet, M., Mourao, A., Perlmutter, S., Ripoche, P., Tao, C., and Walton, N.: 2006, *A&A* **447**, 31

Bahcall, J. N. and Soneira, R. M.: 1980, *ApJS* **44**, 73

Balbus, S. A. and Hawley, J. F.: 2002, *ApJ* **573**, 749

Barrow, J. D.: 1994, *The origin of the universe*, New York : BasicBooks, c1994.

Barrow, J. D. and Tipler, F. J.: 1986, *Atmospheric Chemistry & Physics*

Basu, B. and Lynden-Bell, D.: 1990, *QJRAS* **31**, 359

Bean, R., Hansen, S. H., and Melchiorri, A.: 2001, *Phys. Rev. D* **64(10)**, 103508

Bekenstein, J. D.: 1973, *Phys. Rev. D* **7**, 2333

Bekenstein, J. D.: 1974, *Phys. Rev. D* **9**, 3292

Bekenstein, J. D.: 1981, *Phys. Rev. D* **23**, 287

Bekenstein, J. D.: 2005, *Foundations of Physics* **35**, 1805

Bell, E. F. and de Jong, R. S.: 2001, *ApJ* **550**, 212

Bensby, T. and Feltzing, S.: 2006, *MNRAS* **367**, 1181

Bensby, T., Feltzing, S., Lundström, I., and Ilyin, I.: 2005, *A&A* **433**, 185

Bento, M. C., Bertolami, O., and Sen, A. A.: 2002, *Phys. Rev. D* **66(4)**, 043507

Binney, J. and Tremaine, S.: 2008, *Galactic Dynamics: Second Edition*, Princeton University Press

Bludman, S.: 2004, *Phys. Rev. D* **69(12)**, 122002

Bludman, S. A. and Roos, M.: 2001, *ApJ* **547**, 77

Bostrom, N.: 2002, *Anthropic Bias: Observation Selection Effects in Science and Philosophy*, Routledge, London

Bousso, R.: 1999, *Journal of High Energy Physics* **7**, 4

Bousso, R.: 2001, *Journal of High Energy Physics* **4**, 35

Bousso, R.: 2002, *Reviews of Modern Physics* **74**, 825

Bousso, R., Harnik, R., Kribs, G. D., and Perez, G.: 2007, *Phys. Rev. D* **76(4)**, 043513

Caldwell, R. R.: 2002, *Physics Letters B* **545**, 23

Caldwell, R. R., Dave, R., and Steinhardt, P. J.: 1998, *Physical Review Letters* **80**, 1582

Caldwell, R. R., Kamionkowski, M., and Weinberg, N. N.: 2003, *Physical Review Letters* **91(7)**, 071301

Carroll, S. M.: 2001a, *SNAP (SuperNova Acceleration Probe) Yellow Book astro-ph/0107571*

Carroll, S. M.: 2001b, *Living Reviews in Relativity* **4**, 1

Carroll, S. M.: 2004, *Spacetime and geometry. An introduction to general relativity*, Spacetime and geometry / Sean Carroll. San Francisco, CA, USA: Addison Wesley, ISBN 0-8053-8732-3, 2004, XIV + 513 pp.

Carter, B.: 1974, in M. S. Longair (ed.), *IAU Symp. 63: Confrontation of Cosmological Theories with Observational Data*, pp 291–298

Carter, B.: 1983, *Philosophical Transactions of the Royal Society* **A 310**, 347

Chiba, T., Okabe, T., and Yamaguchi, M.: 2000, *Phys. Rev. D* **62(2)**, 023511

Chimento, L. P., Jakubi, A. S., and Pavón, D.: 2000, *Phys. Rev. D* **62(6)**, 063508

Chimento, L. P., Jakubi, A. S., and Pavón, D.: 2003, *Phys. Rev. D* **67(8)**, 087302

Chyba, C. F.: 1999, *AAS/Division for Planetary Sciences Meeting Abstracts* **31**, 66.09

Cleveland, B. T., Daily, T., Davis, R. J., Distel, J. R., Lande, K., Lee, C. K., Wildenhain, P. S., and Ullman, J.: 1998, *ApJ* **496**, 505

Cohn, J. D.: 1998, *Ap&SS* **259**, 213

Coleman, T. S. and Roos, M.: 2003, *Phys. Rev. D* **68(2)**, 027702

Copeland, E. J., Sami, M., and Tsujikawa, S.: 2006, *ArXiv e-prints hep-th/0603057*

Courteau, S. and van den Bergh, S.: 1999, *AJ* **118**, 337

Dalal, N., Abazajian, K., Jenkins, E., and Manohar, A. V.: 2001, *Physical Review Letters* **87(14)**, 141302

Davies, P. C. W.: 1987, *Classical and Quantum Gravity* **4**, L225

Davies, P. C. W.: 1994, in J. Halliwell, J. Pérez-Mercader, and W. Zurek (eds.), *Physical Origins of Time Asymmetry*, pp 119–130

Davis, T. M., Davies, P. C. W., and Lineweaver, C. H.: 2003, *Classical and Quantum Gravity* **20**, 2753

Davis, T. M., Mörtsell, E., Sollerman, J., Becker, A. C., Blondin, S., Challis, P., Clocchiatti, A., Filippenko, A. V., Foley, R. J., Garnavich, P. M., Jha, S., Krisciunas, K., Kirshner, R. P., Leibundgut, B., Li, W., Matheson, T., Miknaitis, G., Pignata, G., Rest, A., Riess, A. G., Schmidt, B. P., Smith, R. C., Spyromilio, J., Stubbs, C. W., Suntzeff, N. B., Tonry, J. L., Wood-Vasey, W. M., and Zenteno, A.: 2007, *ApJ* **666**, 716

Dehnen, W. and Binney, J. J.: 1998, *MNRAS* **298**, 387

del Campo, S., Herrera, R., Olivares, G., and Pavón, D.: 2006, *Phys. Rev. D* **74(2)**, 023501

del Campo, S., Herrera, R., and Pavón, D.: 2005, *Phys. Rev. D* **71(12)**, 123529

di Pietro, E. and Claeskens, J.-F.: 2003, *MNRAS* **341**, 1299

Dicke, R. H.: 1961, *Nature* **192**, 440

Dirac, P. A. M.: 1937, *Nature* **139**, 323

Dirac, P. A. M.: 1938, *Royal Society of London Proceedings Series A* **165**, 199

Dodelson, S., Kaplinghat, M., and Stewart, E.: 2000, *Physical Review Letters* **85**, 5276

Driver, S. P., Phillipps, S., Davies, J. I., Morgan, I., and Disney, M. J.: 1994, *MNRAS* **268**, 393

Durrer, R. and Maartens, R.: 2007, *ArXiv e-prints 0711.0077*

Eddington, A. S.: 1931, *Nature* **127**, 447

Efron, B.: 1979, *Ann. Statist.* 7(1)

Efstathiou, G.: 1995, *MNRAS* **274**, L73

Efstathiou, G. and Bond, J. R.: 1999, *MNRAS* **304**, 75

Egan, C. A. and Lineweaver, C. H.: 2008, *Phys. Rev. D* **78(8)**, 083528

Egan, C. A. and Lineweaver, C. H.: 2010a, *ApJ* **710**, 1825

Egan, C. A. and Lineweaver, C. H.: 2010b, *How High Could the Entropy be and will the Universe end in a Heat Death?*, in preparation

Eisenhauer, F., Genzel, R., Alexander, T., Abuter, R., Paumard, T., Ott, T., Gilbert, A., Gillessen, S., Horrobin, M., Trippe, S., Bonnet, H., Dumas, C., Hubin, N., Kaufer, A., Kissler-Patig, M., Monnet, G., Ströbele, S., Szeifert, T., Eckart, A., Schödel, R., and Zucker, S.: 2005, *ApJ* **628**, 246

Eisenstein, D. J. and Hu, W.: 1998, *ApJ* **496**, 605

Eisenstein, D. J., Zehavi, I., Hogg, D. W., Scoccimarro, R., Blanton, M. R., Nichol, R. C., Scranton, R., Seo, H.-J., Tegmark, M., Zheng, Z., Anderson, S. F., Annis, J., Bahcall, N., Brinkmann, J., Burles, S., Castander, F. J., Connolly, A., Csabai, I., Doi, M., Fukugita, M., Frieman, J. A., Glazebrook, K., Gunn, J. E., Hendry, J. S., Hennessy, G., Ivezić, Z., Kent, S., Knapp, G. R., Lin, H., Loh, Y.-S., Lupton, R. H., Margon, B., McKay, T. A., Meiksin, A., Munn, J. A., Pope, A., Richmond, M. W., Schlegel, D., Schneider, D. P., Shimasaku, K., Stoughton, C., Strauss, M. A., SubbaRao, M., Szalay, A. S., Szapudi, I., Tucker, D. L., Yanny, B., and York, D. G.: 2005, *ApJ* **633**, 560

Eke, V. R., Frenk, C. S., Baugh, C. M., Cole, S., Norberg, P., Peacock, J. A., Baldry, I. K., Bland-Hawthorn, J., Bridges, T., Cannon, R., Colless, M., Collins, C., Couch, W., Dalton, G., de Propris, R., Driver, S. P., Efstathiou, G., Ellis, R. S., Glazebrook, K., Jackson, C. A., Lahav, O., Lewis, I., Lumsden, S., Maddox, S. J., Madgwick, D., Peterson, B. A., Sutherland, W., and Taylor, K.: 2004, *MNRAS* **355**, 769

Elgarøy, O. and Multamäki, T.: 2007, *A&A* **471**, 65

Elmegreen, B. G.: 2007, in Y. W. Kang, H.-W. Lee, K.-C. Leung, and K.-S. Cheng (eds.), *The Seventh Pacific Rim Conference on Stellar Astrophysics*, Vol. 362 of *Astronomical Society of the Pacific Conference Series*, pp 269–+

Feng, B., Li, M., Piao, Y.-S., and Zhang, X.: 2006, *Physics Letters B* **634**, 101

Ferreira, P. G. and Joyce, M.: 1998, *Phys. Rev. D* **58(2)**, 023503

Frampton, P., Hsu, S. D. H., Kephart, T. W., and Reeb, D.: 2008, *ArXiv e-prints 0801.1847*

Frampton, P. H.: 2009a, *ArXiv e-prints 0904.2934*

Frampton, P. H.: 2009b, *Journal of Cosmology and Astro-Particle Physics* **10**, 16

Frampton, P. H. and Kephart, T. W.: 2008, *Journal of Cosmology and Astro-Particle Physics* **6**, 8

França, U.: 2006, *Physics Letters B* **641**, 351

França, U. and Rosenfeld, R.: 2004, *Phys. Rev. D* **69(6)**, 063517

Frautschi, S.: 1982, *Science* **217**, 593

Frautschi, S.: 1988, in D. J. Depew, B. H. Weber, and J. D. Smith (eds.), *Entropy, information, and evolution : new perspectives on physical and biological evolution*, MIT Press, Cambridge, Mass., California State University, Fullerton.

Fryer, C. L. and Kalogera, V.: 2001, *ApJ* **554**, 548

Fukugita, M. and Peebles, P. J. E.: 2004, *ApJ* **616**, 643

Garriga, J., Livio, M., and Vilenkin, A.: 1999, *Phys. Rev. D* **61(2)**, 023503

Garriga, J. and Vilenkin, A.: 2000, *Phys. Rev. D* **61(8)**, 083502

Garriga, J. and Vilenkin, A.: 2001, *Phys. Rev. D* **64(2)**, 023517

Gibbons, G. W. and Hawking, S. W.: 1977, *Phys. Rev. D* **15**, 2738

Glazebrook, K., Blake, C., Couch, W., Forbes, D., Drinkwater, M., Jurek, R., Pimbblet, K., Madore, B., Martin, C., Small, T., Forster, K., Colless, M., Sharp, R., Croom, S., Woods, D., Pracy, M., Gilbank, D., Yee, H., and Gladders, M.: 2007, *ArXiv Astrophysics e-prints*

Gnedin, N. Y. and Gnedin, O. Y.: 1998, *ApJ* **509**, 11

Gonzalez, G.: 1999a, *MNRAS* **308**, 447

Gonzalez, G.: 1999b, *Astronomy and Geophysics* **40**, 25

Gonzalez, G., Brownlee, D., and Ward, P.: 2001, *Icarus* **152**, 185

Gould, A., Bahcall, J. N., and Flynn, C.: 1996, *ApJ* **465**, 759

Graham, A. W., Driver, S. P., Allen, P. D., and Liske, J.: 2007, *MNRAS* **378**, 198

Grether, D. and Lineweaver, C. H.: 2006, *ApJ* **640**, 1051

Grether, D. and Lineweaver, C. H.: 2007, *ApJ* **669**, 1220

Gunn, J. E. and Gott, J. R. I.: 1972, *ApJ* **176**, 1

Guo, Z.-K. and Zhang, Y.-Z.: 2005, *Phys. Rev. D* **71(2)**, 023501

Gustafsson, B.: 1998, *Space Science Reviews* **85**, 419

Gustafsson, B., Karlsson, T., Olsson, E., Edvardsson, B., and Ryde, N.: 1999, *A&A* **342**, 426

Guth, A. H.: 1981, *Phys. Rev. D* **23**, 347

Hansen, B. M. S., Richer, H. B., Fahlman, G. G., Stetson, P. B., Brewer, J., Currie, T., Gibson, B. K., Ibata, R., Rich, R. M., and Shara, M. M.: 2004, *ApJS* **155**, 551

Harrison, E. R.: 1995, *ApJ* **446**, 63

Hawking, S. W.: 1976, *Phys. Rev. D* **13**, 191

Hebecker, A. and Wetterich, C.: 2001, *Physics Letters B* **497**, 281

Heger, A., Woosley, S. E., and Baraffe, I.: 2005, in R. Humphreys and K. Stanek (eds.), *The Fate of the Most Massive Stars*, Vol. 332 of *Astronomical Society of the Pacific Conference Series*, pp 339–+

Henry, T. J.: 2006, *RECONS database*

Hinshaw, G.: 2006, *Legacy Archive for Microwave Background Data Analaysis (LAMBDA)*, Online Archive: http://lambda.gsfc.nasa.gov/product/map/current/params/lcdm_wmap_sdss.cfm

Hopkins, A. M.: 2006, *ArXiv e-prints astro.ph/0611283*

Hulse, R. A. and Taylor, J. H.: 1975, *ApJ* **195**, L51

Huterer, D. and Cooray, A.: 2005, *Phys. Rev. D* **71(2)**, 023506

Ida, S. and Lin, D. N. C.: 2005, *ApJ* **626**, 1045

Jarrett, T. H., Chester, T., Cutri, R., Schneider, S. E., and Huchra, J. P.: 2003, *AJ* **125**, 525

Jaynes, E. T.: 1968, *IEEE Transactions on System Science and Cybernetics* **SSC-4**, 227

Jordan, P.: 1955, *Schwerkraft und Weltall*, Braunschweig, Germany

Kamenshchik, A., Moschella, U., and Pasquier, V.: 2001, *Physics Letters B* **511**, 265

Kolb, E. W. and Turner, M. S.: 1981, *Nature* **294**, 521

Kolb, E. W. and Turner, M. S.: 1990, *The early universe*, Frontiers in Physics, Reading, MA: Addison-Wesley, 1988, 1990

Kroupa, P.: 2002, *Science* **295**, 82

Kuchner, M. J. and Seager, S.: 2005, *ArXiv e-prints astro-ph/0504214*

Lanzetta, K. M., Yahata, N., Pascarelle, S., Chen, H.-W., and Fernández-Soto, A.: 2002, *ApJ* **570**, 492

Layzer, D.: 2009, *www.informationphilosopher.com*

Linde, A. D.: 1982, *Physics Letters B* **108**, 389

Linde, A. D.: 2009, *private communication*

Linder, E.: 1997, *First Principles of Cosmology*, First Principles of Cosmology, by E.V. Linder. Addison-Wesley, Harlow, England, 1997

Linder, E. V.: 2006a, *Astroparticle Physics* **26**, 102

Linder, E. V.: 2006b, *Phys. Rev. D* **73(6)**, 063010

Linder, E. V. and Huterer, D.: 2005, *Phys. Rev. D* **72(4)**, 043509

Lineweaver, C. H.: 1998, *ApJ* **505**, L69

Lineweaver, C. H.: 1999, *Science* **284**, 1503

Lineweaver, C. H.: 2001, *Icarus* **151**, 307

Lineweaver, C. H. and Davis, T. M.: 2002, *Astrobiology* **2**, 293

Lineweaver, C. H. and Davis, T. M.: 2003, *Astrobiology* **3**, 241

Lineweaver, C. H. and Egan, C. A.: 2007, *ApJ* **671**, 853

Lineweaver, C. H. and Egan, C. A.: 2008, *Physics of Life Reviews* **5**, 225

Lineweaver, C. H. and Grether, D.: 2003, *ApJ* **598**, 1350

Loveday, J.: 2000, *MNRAS* **312**, 557

Lynden-Bell, D.: 1967, *MNRAS* **136**, 101

Malquarti, M., Copeland, E. J., and Liddle, A. R.: 2003, *Phys. Rev. D* **68(2)**, 023512

Martel, H., Shapiro, P. R., and Weinberg, S.: 1998, *ApJ* **492**, 29

Mather, J. C., Cheng, E. S., Cottingham, D. A., Eplee, Jr., R. E., Fixsen, D. J., Hewagama, T., Isaacman, R. B., Jensen, K. A., Meyer, S. S., Noerdlinger, P. D., Read, S. M., Rosen, L. P., Shafer, R. A., Wright, E. L., Bennett, C. L., Boggess, N. W., Hauser, M. G., Kelsall, T., Moseley, Jr., S. H., Silverberg, R. F., Smoot, G. F., Weiss, R., and Wilkinson, D. T.: 1994, *ApJ* **420**, 439

Mather, J. C., Fixsen, D. J., Shafer, R. A., Mosier, C., and Wilkinson, D. T.: 1999, *ApJ* **512**, 511

Mbonye, M. R.: 2004, *Modern Physics Letters A* **19**, 117

Mersini-Houghton, L. and Adams, F. C.: 2008, *Classical and Quantum Gravity* **25(16)**, 165002

Metropolis, N. and Ulam, S.: 1949, *Journal of the American Statistical Association* **44(247)**, 335

Nagamine, K., Ostriker, J. P., Fukugita, M., and Cen, R.: 2006, *ApJ* **653**, 881

Nojiri, S. and Odintsov, S. D.: 2006, *Physics Letters B* **637**, 139

Nordström, B., Mayor, M., Andersen, J., Holmberg, J., Pont, F., Jørgensen, B. R., Olsen, E. H., Udry, S., and Mowlavi, N.: 2004, *A&A* **418**, 989

Olivares, G., Atrio-Barandela, F., and Pavón, D.: 2005, *Phys. Rev. D* **71(6)**, 063523

Olivares, G., Atrio-Barandela, F., and Pavon, D.: 2007, *ArXiv e-prints 0706.3860* 706

Özer, M. and Taha, M. O.: 1987, *Nuclear Physics B* **287**, 776

Page, D. N.: 1981, *General Relativity and Gravitation* **13**, 1117

Page, D. N. and McKee, M. R.: 1981, *Nature* **291**, 44

Pagel, B. E. J.: 1997, *Nucleosynthesis and Chemical Evolution of Galaxies*, Nucleosynthesis and Chemical Evolution of Galaxies, by Bernard E. J. Pagel, pp. 392. ISBN 0521550610. Cambridge, UK: Cambridge University Press, October 1997.

Pavón, D. and Zimdahl, W.: 2005, *Physics Letters B* **628**, 206

Peacock, J. A.: 1999, *Cosmological Physics*, Cosmological Physics, by John A. Peacock, pp. 704. ISBN 052141072X. Cambridge, UK: Cambridge University Press, January 1999.

Peebles, P. J. E. and Vilenkin, A.: 1999, *Phys. Rev. D* **59(6)**, 063505

Penrose, R.: 1979, in S. W. Hawking and W. Israel (eds.), *General Relativity: An Einstein centenary survey*, pp 581–638

Penrose, R.: 1987, *Newton, quantum theory and reality.*, pp 17–49, Three hundred years of gravitation, p. 17 - 49

Penrose, R.: 2004, *The road to reality : a complete guide to the laws of the universe*, The road to reality : a complete guide to the laws of the universe, by Roger Penrose. London: Jonathan Cape, 2004

Perlmutter, S., Aldering, G., Goldhaber, G., Knop, R. A., Nugent, P., Castro, P. G., Deustua, S., Fabbro, S., Goobar, A., Groom, D. E., Hook, I. M., Kim, A. G., Kim, M. Y., Lee, J. C., Nunes, N. J., Pain, R., Pennypacker, C. R., Quimby, R., Lidman, C., Ellis, R. S., Irwin, M., McMahon, R. G., Ruiz-Lapuente, P., Walton, N., Schaefer, B., Boyle, B. J., Filippenko, A. V., Matheson, T., Fruchter, A. S., Panagia, N., Newberg, H. J. M., Couch, W. J., and The Supernova Cosmology Project: 1999, *ApJ* **517**, 565

Pogosian, L. and Vilenkin, A.: 2007, *Journal of Cosmology and Astro-Particle Physics* **1**, 25

Press, W. H. and Schechter, P.: 1974, *ApJ* **187**, 425

Ratra, B. and Peebles, P. J. E.: 1988, *Phys. Rev. D* **37**, 3406

Reddy, B. E., Tomkin, J., Lambert, D. L., and Allende Prieto, C.: 2003, *MNRAS* **340**, 304

Reid, I. N.: 2002, *PASP* **114**, 306

Riess, A. G., Filippenko, A. V., Challis, P., Clocchiatti, A., Diercks, A., Garnavich, P. M., Gilliland, R. L., Hogan, C. J., Jha, S., Kirshner, R. P., Leibundgut, B., Phillips, M. M., Reiss, D., Schmidt, B. P., Schommer, R. A., Smith, R. C., Spyromilio, J., Stubbs, C., Suntzeff, N. B., and Tonry, J.: 1998, *AJ* **116**, 1009

Riess, A. G., Strolger, L.-G., Casertano, S., Ferguson, H. C., Mobasher, B., Gold, B., Challis, P. J., Filippenko, A. V., Jha, S., Li, W., Tonry, J., Foley, R., Kirshner, R. P., Dickinson, M., MacDonald, E., Eisenstein, D., Livio, M., Younger, J., Xu, C., Dahlén, T., and Stern, D.: 2007, *ApJ* **659**, 98

Riess, A. G., Strolger, L.-G., Tonry, J., Casertano, S., Ferguson, H. C., Mobasher, B., Challis, P., Filippenko, A. V., Jha, S., Li, W., Chornock, R., Kirshner, R. P., Leibundgut, B., Dickinson, M., Livio, M., Giavalisco, M., Steidel, C. C., Benítez, T., and Tsvetanov, Z.: 2004, *ApJ* **607**, 665

Robles, J. A., Egan, C. A., and Lineweaver, C. H.: 2008a, in *Australian Space Science Conference Series: 8th Conference Proceedings*

Robles, J. A., Lineweaver, C. H., Grether, D., Flynn, C., Egan, C. A., Pracy, M. B., Holmberg, J., and Gardner, E.: 2008b, *ApJ* **684**, 691

Robles, J. A., Lineweaver, C. H., Grether, D., Flynn, C., Egan, C. A., Pracy, M. B., Holmberg, J., and Gardner, E.: 2008c, *ApJ* **689**, 1457

Rocha-Pinto, H. J., Scalo, J., Maciel, W. J., and Flynn, C.: 2000, *A&A* **358**, 869

Sahni, V.: 2002, *Classical and Quantum Gravity* **19**, 3435

Sahni, V. and Wang, L.: 2000, *Phys. Rev. D* **62(10)**, 103517

Sassi, G. and Bonometto, S. A.: 2007, *New Astronomy* **12**, 353

Scherrer, R. J.: 2005, *Phys. Rev. D* **71(6)**, 063519

Seljak, U., Slosar, A., and McDonald, P.: 2006, *Journal of Cosmology and Astro-Particle Physics* **10**, 14

Soderblom, D. R.: 1983, *ApJS* **53**, 1

Spergel, D. N., Bean, R., Doré, O., Nolta, M. R., Bennett, C. L., Dunkley, J., Hinshaw, G., Jarosik, N., Komatsu, E., Page, L., Peiris, H. V., Verde, L., Halpern, M., Hill, R. S., Kogut, A., Limon, M., Meyer, S. S., Odegard, N., Tucker, G. S., Weiland, J. L., Wollack, E., and Wright, E. L.: 2007, *ApJS* **170**, 377

Spergel, D. N., Bean, R., Dore', O., Nolta, M. R., Bennett, C. L., Hinshaw, G., Jarosik, N., Komatsu, E., Page, L., Peiris, H. V., Verde, L., Barnes, C., Halpern, M., Hill, R. S., Kogut, A., Limon, M., Meyer, S. S., Odegard, N., Tucker, G. S., Weiland, J. L., Wollack, E., and Wright, E. L.: 2006, *astro-ph/0603449 http://lambda.gsfc.nasa.gov/product/map/dr2/params/lcdm-all.cfm*

Steinhardt, P.: 2008, *private communication*

Steinhardt, P. J.: 2003, *Royal Society of London Philosophical Transactions Series A* **361**, 2497

Steinhardt, P. J., Wang, L., and Zlatev, I.: 1999, *Phys. Rev. D* **59(12)**, 123504

Strominger, A. and Vafa, C.: 1996, *Physics Letters B* **379**, 99

Susskind, L.: 1995, *Journal of Mathematical Physics* **36**, 6377

Szydłowski, M., Kurek, A., and Krawiec, A.: 2006, *Physics Letters B* **642**, 171

't Hooft, G.: 1993, *ArXiv General Relativity and Quantum Cosmology e-prints*

Thomas, A.: 2009, *www.ipod.org.uk*

Thompson, R. I., Eisenstein, D., Fan, X., Dickinson, M., Illingworth, G., and Kennicutt, Jr., R. C.: 2006, *ApJ* **647**, 787

Thomson, W.: 1852, *Philosophical Magazine* **4**, 304

Turner, M. S.: 2001, *Nuclear Physics B Proceedings Supplements* **91**, 405

Valenti, J. A. and Fischer, D. A.: 2005, *ApJS* **159**, 141

Vilenkin, A.: 1995a, *Phys. Rev. D* **52**, 3365

Vilenkin, A.: 1995b, *Physical Review Letters* **74**, 846

Vilenkin, A.: 1996a, in N. Sanchez and A. Zichichi (eds.), *String Gravity and Physics at the Planck Energy Scale*, pp 345–367

Vilenkin, A.: 1996b, in K. Sato, T. Suginohara, and N. Sugiyama (eds.), *Cosmological Constant and the Evolution of the Universe*, pp 161–+

Wang, L., Caldwell, R. R., Ostriker, J. P., and Steinhardt, P. J.: 2000, *ApJ* **530**, 17

Wang, Y. and Mukherjee, P.: 2006, *ApJ* **650**, 1

Wang, Y. and Tegmark, M.: 2004, *Physical Review Letters* **92(24)**, 241302

Wang, Y. and Tegmark, M.: 2005, *Phys. Rev. D* **71(10)**, 103513

Weinberg, S.: 1987, *Physical Review Letters* **59**, 2607

Weinberg, S.: 1989, *Reviews of Modern Physics* **61**, 1

Weinberg, S.: 2000a, *Phys. Rev. D* **61(10)**, 103505

Weinberg, S.: 2000b, *ArXiv e-prints astro-ph/0005265*

Weisberg, J. M. and Taylor, J. H.: 2005, in F. A. Rasio and I. H. Stairs (eds.), *Binary Radio Pulsars*, Vol. 328 of *Astronomical Society of the Pacific Conference Series*, pp 25–+

Wetherill, G. W.: 1996, in L. R. Doyle (ed.), *Circumstellar Habitable Zones*, p. 193

Wood-Vasey, W. M., Miknaitis, G., Stubbs, C. W., Jha, S., Riess, A. G., Garnavich, P. M., Kirshner, R. P., Aguilera, C., Becker, A. C., Blackman, J. W., Blondin, S., Challis, P., Clocchiatti, A., Conley, A., Covarrubias, R., Davis, T. M., Filippenko, A. V., Foley, R. J., Garg, A., Hicken, M., Krisciunas, K., Leibundgut, B., Li, W., Matheson, T., Miceli, A., Narayan, G., Pignata, G., Prieto, J. L., Rest, A., Salvo, M. E., Schmidt, B. P., Smith, R. C., Sollerman, J., Spyromilio, J., Tonry, J. L., Suntzeff, N. B., and Zenteno, A.: 2007, *ArXiv Astrophysics e-prints*

Wright, J. T., Marcy, G. W., Butler, R. P., and Vogt, S. S.: 2004, *ApJS* **152**, 261

Yang, G. and Wang, A.: 2005, *General Relativity and Gravitation* **37**, 2201

Zel'Dovich, Y. B.: 1967, *Soviet Journal of Experimental and Theoretical Physics Letters* **6**, 316

Zhang, X.: 2005, *Modern Physics Letters A* **20**, 2575

Zimdahl, W., Pavón, D., and Chimento, L. P.: 2001, *Physics Letters B* **521**, 133

Zlatev, I., Wang, L., and Steinhardt, P. J.: 1999, *Physical Review Letters* **82**, 896